UNIVERSITA' DEGLI STUDI DI MILANO-BICOCCA

Facoltà di Scienze MM. FF. NN

Corso di Dottorato in Scienze Chimiche-XXVIII ciclo

Synthesis of glycoconjugates and their analogs for the study of biological systems

Davide Bini

UNIVERSITA' DEGLI STUDI DI MILANO-BICOCCA

Facoltà di Scienze MM. FF. NN

Corso di Dottorato in Scienze Chimiche-XXVIII ciclo

Synthesis of glycoconjugates and their analogs for the study of biological systems

PhD Student: Davide Bini

Supervisor: Prof. Laura Cipolla

PhD Coordinator: Prof. Giorgio Moro

Milan, 2016

“And those who were seen dancing were thought to be insane by those who could not hear the music.”

CONTENTS

1. Introduction: Glycans Key Role in Life Evolution 8

2. Aim of the work 18

3.1. Trehalose mimics as trehalase inhibitors: Introduction 21

3.2. Trehalose mimics as trehalase inhibitors: Results and discussion 34

4.1. Synthesis of multivalent glycoconjugates: Introduction 51

4.2. Synthesis of multivalent glycoconjugates: Results and discussion 61

5.1. Synthesis of glycosylated Pluronic block copolymers as antitumor drugs carriers: Introduction 85

5.2. Synthesis of glycosylated Pluronic block copolymers as antitumor drugs carriers: Results and discussion 98

6.1. Trehalose mimics as trehalase inhibitors: Conclusion 107

6.2. Synthesis of multivalent glycoconjugates: Conclusion 111

6.3. Synthesis of glycosylated Pluronic block copolymers as antitumor drugs carriers: Conclusion 115

7. Experimental Part 118

7.1. Trehalose mimics as trehalase inhibitors 118

7.2. Synthesis of multivalent glycoconjugates 130

7.3. Synthesis of glycosylated Pluronic block copolymers as antitumor drugs carriers 146

References 159

1. Introduction: Glycans Key Role in Life Evolution

Carbohydrates are one of four major groups of biologically relevant macromolecules that can be found in all forms of life. They possess many biochemical, structural, and functional features that could provide a number of evolutionary benefits or even stimulate or enhance some evolutionary events. During evolution, carbohydrates acted as a source of food and energy, provided protection against UV radiation and oxygen free radicals and participated in molecular structure of complex organisms. Through the process of polymerization, simple carbohydrates became then more complex and developed novel functions. According to the one origin of life theory, called glyco-world, carbohydrates are thought to be the original molecules of life, which supplied molecular basis for the evolution of all living things[1]. Ribose and deoxyribose are integral parts of RNA and DNA molecules and cellulose (glucose polymer) is the most abundant molecule on the planet. There is also evidence for catalytic properties of some carbohydrates[2], which further support the theory about the capacity of glycans to enable evolution of life.

Carbohydrates are essential for all forms of life, but the wider variety of their functions is now found in higher eukaryotes. The majority of eukaryotic proteins are modified by cotranslational and posttranslational attachment of complex oligosaccharides (glycans) to generate the most complex epiproteomic

modification: protein glycosylation. Varying the number, order and type of monosaccharide units, it's possible to obtain a multitudinous of different glycans. The most abundant monosaccharides that can be found in animal glycan are: fucose (Fuc), galactose (Gal), glucose (Glu), mannose (Man), *N*-acetylgalactosamine (GalNAc), *N*-acetylglucosamine (GlcNAc), sialic acid (Sia) and xylose (Xyl). There are two main ways for protein modification with glycans: *O*-glycosylation and *N*-glycosylation. The glycan can be bound to the oxygen (O) atom of serine or threonine amino acid (*O*-glycosylation) or to the nitrogen (N) atom of asparagine amino acid in the protein (*N*-glycosylation). Surfaces of all eukaryotic cells are covered with a dense layer of complex glycans attached to proteins or lipids. Many cells in our organism can function without the nuclei, but there is no known living cell that can function without glycans on its surface. Everything approaching the cell, being it a protein, another cell, or a microorganism, has to interface with the cellular glycan coat[3, 4, 5].

Even in sponges, which are the simplest multicellular organisms formed by more or less independent cells, the recognition between cells is based on glycans[6]. The formation of extracellular matrix (ECM)[7, 8] was surely one of the critical steps in the evolution of multicellularity. Multicellular life evolved independently multiple times during evolution and there are two main theories that try to explain how the initial multicellular group of cells was made. The first theory affirms that individual

cell came together to create symbiotic colonies, while another theory says that cells stayed together after cell division[7]. The appearance of extracellular matrix enabled this initial group of cells to start function as a coordinated unit. Extracellular matrix has great relevance for multicellular organisms[9]: it has role in cell signaling, communication between cells, cell adhesion and transmission of signal from the environment. It also provides structural support for cells, tissues and organs. Extracellular matrix plays essential role in numerous fundamental processes such as differentiation, proliferation, survival and migration of cells.

Glycoproteins and proteoglycans are the main components of ECM and are responsible for its functional properties[10]. Extracellular matrix evolved in parallel with first multicellular organisms[8]; therefore, glycans of the early ECM probably participated in evolution of multicellular organisms by enabling communication between cells and thus providing signals for cooperation and differentiation. In addition to ECM, glycans also supply other important properties and functions for the development of multicellular organisms. For example, in some fungal species *N*-acetylglucosamine (GlcNAc) acts as a signal that stimulates unicellular fungi to start to grow in a multicellular filamentous form[11, 12]. The same sugar modifies proteins in multicellular organisms and some of these modifications are responsible for the regulation of signaling (for example signaling through Notch protein)[13].

Glycans functions in complex organisms

In complex organisms like humans, glycans play an important role in almost all processes that involve more than one cell[14]. Covalent addition of glycans modifies nearly all membrane and secreted proteins, with very high site occupancy[15]. Absence of glycosylation is embryonically lethal[16] and mutations which impede proper glycosylation cause debilitating diseases[17]. Glycan parts of (glyco) proteins are integral elements of the final molecular structure and, together with amino acids in the polypeptide backbone, they form a single molecular entity that performs biological functions. The main two obstacles in the study of glycans are their non-linear complex chemical structure and the absence of a direct genetic template. In fact, glycans are encoded in a complex dynamic network comprising hundreds of genes[18, 19, 20]. However, despite the absence of a direct genetic template, heritability of glycome composition was reported to be high[21, 22], even over 80% for some of the glycans in the IgG glycome[23]. Very large interindividual differences in glycome composition were reported in recent population studies of the human plasma glycome[21]. Interestingly, the variability in composition of the glycome attached to immunoglobulin G (IgG) was almost three times larger than the variability of the total plasma glycome[22], suggesting that the variation in concentration of different plasma proteins is blurring the intricate regulation of glycosylation of an individual protein. Genome wide association studies (GWAS) performed in the same populations revealed a similar trend. GWAS of the

plasma glycome in 2705 individuals identified three genetic loci associated with variation in glycosylation[19, 20], while GWAS of the IgG glycome in 2247 individuals identified 16 genetic loci correlated with variations in the composition of the IgG glycome[24]. This denotes that at least three to four times more than currently estimated 750 genes[18], or at least 10% of the genome participates in glycosylation.

Glycans as defense weapons in higher eukaryotes

Glycosylation, as the most complex epiproteomic modification, gives higher organisms some distinctive advantages. For example, IgG is one of the most important weapons in our "arsenal," which allows us to successfully contrast microorganisms, despite their high mutation and reproduction rates. Evolution has invented elaborate genetic mechanisms to create variability in the Fab regions of immunoglobulins, but even more elaborate physiological mechanism of the immune system are activated downstream from the antigen-antibody recognition event[25]. Since genes for the variable regions of immunoglobulins are defined before the first encounter with their target, the polypeptide part of the antibody cannot be tuned to the type of antigen it will recognize. However, different invaders (toxins, viruses, bacteria, fungi, parasites) require activation of different effector mechanisms, and protein glycosylation seems to be essential in this process[26, 27]. Each heavy chain of IgG carries a single covalently attached bi-antennary *N*-glycan at the highly conserved

asparagine 297 residue. The attached glycans are essential structural components of the Fc region and minute changes in glycan composition can significantly change its conformation with dramatic consequences for IgG effector functions. For example, the addition of a fucose residue to the first *N*-acetylglucosamine in the core of the glycan (core-fucose) modifies the conformation of the Fc region, dramatically reducing its ability to bind to FcγRIIIa[28, 29]. FcγRIIIa (CD16) is an activating Fc receptor, mainly expressed on natural killer (NK) cells. IgG binding to FcγRIIIa initiates antibody-dependent cellular cytotoxicity (ADCC), resulting in the destruction of target cells. On average over 95% of circulating IgGs are core-fucosylated[22] and therefore contain a "safety switch" which prevents them from inducing potentially destructive ADCC[30]. The small fraction of IgG molecules which lack core-fucose are over 100 times more effective in initiating ADCC through FcγRIIIa binding and this also seems to be the primary mode of function of therapeutic anti-cancer monoclonal antibodies[31, 32]. Inappropriate regulation of this process could lead to either autoimmunity (too much ADCC) or cancer (inefficient ADCC). Another structural alteration of the IgG glycan, the addition of sialic acid to the ends of glycans, modifies the function of IgG and converts it from being pro-inflammatory into an anti-inflammatory agent[33]. Sialylation of IgG was found to be crucial for the function of intravenous immunoglobulin (IVIG): its anti-inflammatory activity is contained within the effector Fc portion, as Fc fragments alone were found to be sufficient to suppress

inflammation[34]. Fc with sialylated glycans seems to suppress inflammation through a novel TH2 pathway, which provides an intrinsic mechanism for maintaining immune homeostasis[35]. In addition to sialic acids, also galactosylation was shown to be significant for the anti-inflammatory activity of IgG[36]. A recent study reported by Ackerman et al.[37] presents just one of the examples about how variations in IgG glycosylation can provide new adaptive mechanism that allows fight against pathogens and assure survival. In this study it was shown that people called elite controllers, who are able to control HIV infection and therefore do not get sick, have glycosylation of HIV-specific antibody that promotes strong pro-inflammatory response against the virus[37]. Other glycoproteins were not studied in so much detail as IgG has been, but numerous examples confirm essential roles of alternative protein glycosylation in many biological processes[38]. Among others, binding of glycosylated ligands to selectins is the basis of lymphocyte homing[39, 40] and alternative glycosylation of Notch is essential for embryonic and adult development[41]. Notch signaling pathway is extremely relevant for proper development of multicellular organisms. Notch is a transmembrane receptor composed of extracellular, transmembrane and intracellular domains. The glycosylation of extracellular domain of Notch protein influences ligand recognition and activation of Notch signaling. Four different types of glycans have been reported to be present on Notch: *N*-glycans, *O*-fucose glycans, *O*-glucose glycans, and *O*-GlcNAc glycans, but just two of them are known to

significantly affect and modulate Notch activity: *O*-fucose glycans and *O*-glucose glycans. *O*-fucosylation of Notch extracellular domain is relevant in ligand recognition and binding[13, 41]. Further extension of *O*-fucose by the addition of *N*-acetylglucosamine, in a reaction catalyzed by glycosyltransferase called Fringe, also modulates Notch activity. Through the action of Fringe, Notch signaling pathway can be induced or inhibited depending on the ligand that interacts with Notch receptor[42]. Another example of role of glycosylation in signaling during the development of multicellular organisms is *O*-fucosylation of Crypto protein. Crypto protein is one of the proteins involved in Nodal signaling pathway and proper glycosylation of this protein is essential for its activity and binding properties[43, 44].

Glycans role in adaptation processes

The ability to create new structures without introducing changes into the precious genetic heritage is the biggest evolutionary advantage that glycans confer to higher eukaryotes[45, 46]. In principle all posttranslational modifications enable this to some extent, but most of them function as simple on/off molecular switches, while glycans represent prominent structural components contributing with up to 50% in mass[47] and even much more to the molecular volume of many proteins[48]. The fact that so large parts of the molecule are not hardwired in the genome supplies a rapid and extensive epiproteomic adaptation mechanism. One example of glycosylation role in the process of

adaptation is found in mammalian sperm cell, essential for the reproduction process itself. Mammalian sperm cells are masked with sialylated sugars in order to prevent recognition as foreign cells in the female reproductive system. After successful adaptation of sperm cell to the new environment, the removal of sialic acid residues is necessary in the process of sperm cell maturation and the establishment of interaction between sperm and egg cells[49]. Interactions established through glycans are not restricted just to cell-cell interactions and communication that could have played important role in the evolution of multicellular life forms. Glycans also play significant role in the interaction between different organisms, including host-pathogen interactions or interactions between symbionts. Effect of glycosylation on the composition of the human intestinal microbiota has been well studied[50]. Intestinal symbiotic bacteria are very important to humans as they help in food digestion, produce some vitamins and supply protection against pathogenic bacteria. In return, symbiotic bacteria use host glycan molecules as receptors for colonization of intestine and, also, both host and dietary glycans serve as energy source for symbiotic bacteria. It is reported that individuals who don't secrete blood group glycans into the intestinal mucosa have reduced number and diversity of probiotic bacteria in the intestine[51]. Except for food, symbiotic bacteria also employ sugars that are highly abundant in intestine for glycosylation of their surface in order to escape the human immune system[52]. Furthermore, digestion of sugars by symbiotic

bacteria enables activation of signaling system that control pathogenicity of some non-symbiotic bacteria[53]. Based on these facts, it can be safely assumed that glycans play important role in evolution of symbiotic relationship between humans and intestinal bacteria. In some biological systems, like for example AB0 blood groups, glycans behave as simple molecular switches that introduce interindividual variability of cellular surfaces. In other systems, like immunoglobulin glycosylation, they enable new physiological functions, which could not be accomplished without this complex posttranslational tool. Glycosylation is especially complex in human brain, but currently available technologies do not enable detailed study of this highly intricate system.

2. Aim of the work

My PhD project has been focused on the design, synthesis and biological activity studies of glycomimetics and glycoconjugates. During these three years I developed three different topics:

1. Trehalose mimics as trehalase inhibitors

Trehalase is a specific glycosidase that catalyzes the hydrolysis of trehalose (Figure 1) to the two constituent glucose units. This disaccharide is found in many organisms as diverse as bacteria, yeast, fungi, nematodes, plants, insects and some other invertebrates, but is absent in mammals. In insects, trehalose hydrolysis by trehalase is fundamental in various physiological processes (chitin synthesis, thermotolerance and flight metabolism). Hence, insect trehalases are attractive targets for the search of inhibitors as potential novel and selective insecticides. I have focused on the design and synthesis of iminosugar- and polyhydroxylated pyrrolizidine alkaloids-based glycomimetics, in order to inhibit insect trehalase, thus acting as potential non-toxic insecticides.

2. Synthesis of multivalent glycoconjugates

Recognition processes between glycans and their receptors are of paramount relevance in several biological phenomena, both in physiological and in pathological conditions. Moreover, most often these binding events occur in a multivalent and cooperative

manner. In order to better understand these phenomena, dendrimers and dendrons have been developed to provide multivalent glycoconjugates. I have worked on the design and synthesis of new hetrobifunctional dendrons for carbohydrates multivalent presentation and studied glycoconjugates interactions with specific proteins.

3. Synthesis of glycosylated Pluronic block copolymers as antitumor drugs carriers

Polymer-based nanotechnology became one of the most attractive and fast growing areas of pharmaceutical research. One promising example of such polymer nanomaterials is represented by a class of Pluronic block copolymers. In aqueous solutions, at concentrations above critical micelle concentration, these copolymers self-assemble into micelles. In application to anticancer chemotherapy, low molecular mass drugs encapsulation in micelles can diminish drug extravasation into normal tissues and provide for a passive drug targeting to tumors via the enhanced permeability and retention (EPR) effect. In order to gain also an active targeting effect on Pluronic micelless, I have been working on the design and synthesis of new glycosylated polymers for antitumor drug delivery.

Even if the topics and the target proteins (enzymes and receptors) are very different, these three arguments have a common element. In all cases, starting from the known mechanistic, structural and

biological information on the protein, I have designed glycomimetics or glycoconjugates that are potentially able to interact with the biological target. All the studied proteins are biologically relevant, so the final aim of the synthetic effort is always related to the biological properties of the newly synthesised molecules, in order to check the hypothesis done during the design step and to get further useful information about the biological system under study.

3.1. Trehalose mimics as trehalase inhibitors: Introduction

Trehalose (Figure 1) is a nonreducing disaccharide formed by an α,α-1,1-glycosidic bond between two glucose units. Chemically, three anomers of trehalose are possible (α,β-1,1-, β,β-1,1-, and α,α-1,1-), however only the α,α-trehalose has been detected in living organisms and is the isomer commonly referred to as trehalose.

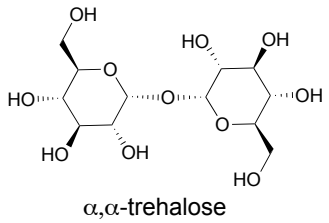

Figure 1. Chemical structure of the naturally occurring trehalose anomer.

The naturally occurring α,α-disaccharide is widespread throughout the biological world[54, 55, 56], and can be found in plant, insect, and microbial cells often linked to physiological stresses such as heat and osmotic shock, sporulation, and dehydration. It has exclusive water-retention properties, allowing plants to survive almost complete desiccation[57], which has led to its extensive use in the pharmaceutical and food industries[58, 59]. Trehalose holds several distinctive physical properties, including high hydrophilicity and chemical stability, non-hygroscopic glass formation and the lack of internal hydrogen bond. These features

account for the major role of trehalose as a stress metabolite. The widespread distribution of α,α-trehalose among different species suggests a relevant role of this molecule in the biology of such living organisms. A few decades ago trehalose was thought to represent a glucose stock to be used as energy source or for the synthesis of cellular components[59, 60]. Since then, the understanding of trehalose functions has expanded enormously, and it is now generally accepted that the role of trehalose goes much beyond the simple storage function. It surely behaves as energy source in some organisms, while it plays structural or transport roles in others[61]. It can be also found in signaling or regulation pathways, or as a protection for membranes and proteins during cellular stresses, such as cold, desiccation, heat, and anoxia[62]. For example, the resurrection plants *Selaginella lepidophylla* and *Craterostigma plantagineum*, that possess more than 10% dry weight of trehalose, can survive after heating to 100 °C without damage in the fully dried state, and they are able to recover their activity upon rehydration[63, 64]. Likewise, some mushrooms with up to 20% trehalose in the dry state are stable on storage at room temperature for many years, and rapidly produce a fresh product upon rehydration[64]. Therefore, depending on the specific biological system taken into consideration, a variety of functions have been proposed for trehalose. Usually, in prokaryotic organisms, this disaccharide is an external carbon source, stored as compatible solute by photosynthetic bacteria, or a structural component of the cord factor in mycobacteria[56, 65]. In

yeast and filamentous fungi, large amounts of trehalose are accumulated both as a reserve source and as protection against stress conditions. Several species of insects contain trehalose in the "fat body" and in the hemolymph, as energy source during flight. Trehalose studies in insects arose from its discovery in pupae of the silkmoth *Antheraea polyphemus*[66] and in the desert locust *Schistocerca gregaria*[67], in 1956. It is the main sugar circulating in the blood or haemolymph of most insects, vital for their flight since upon hydrolysis it generates glucose[68]. Trehalose rapidly exchanges between haemolymph and fat body and its amount in insect blood is in general ten fold higher than glucose levels detected in the blood of mammals and other vertebrates. Trehalose, however, is not the only metabolite occurring in high concentrations in insect blood; glucose is often present, together with amino acids, proteins and other biomolecules, sometimes in concentrations exceeding that of trehalose [69]. Trehalose concentration is extremely variable, usually between 5 and 50 mM, determined by environmental conditions, physiological state and nutrition. This variability is fundamental for trehalose to perform its different biological roles, as energy storage compound, as cryoprotectant in freeze-avoiding insects, as protein stabiliser during stress conditions (heat or osmotic), or as a component of a feedback mechanism regulating feeding behaviour and nutrient intake, modulating taste receptor responses and influencing food selection. The only known pathway of trehalose use is its hydrolysis to two glucose units,

catalyzed by the glycolytic enzyme trehalase (EC3.2.1.28). This enzyme was first observed in *Aspergillus niger*[70] and then by Fischer in 1895 from *S. cerevisiae*[54], and afterwards reported in several other organisms within the plant and animal kingdoms. Trehalases belong to the GH37 family of the Carbohydrate-Active Enzyme (CAZy) classification[71].

Despite the natural abundance of this enzyme, in most cases neither the function nor the properties have been studied in details yet. In contrast to other enzymes of trehalose metabolism that are not present in mammals, trehalase is also found in mammals both in the kidney brush border membranes[72] and in the intestinal villae membranes[73]. While trehalase role in the kidney has not been elucidated yet (trehalose is not found in the blood), in the intestine trehalases are devoted to the hydrolysis of ingested trehalose, as confirmed by the fact that humans defective in their intestinal trehalase suffer from diarrhea upon ingestion of food with high trehalose levels, such as mushrooms[74]. From a mechanistic point of view, it is an inverting glycosidase[75], hydrolysing the glycosidic bond with inversion of configuration at the anomeric center. Trehalose hydrolysis is a relevant, and somehow essential, process of several organisms; it is essential for insect flight[68], and growth resumption of resting cell or spore germination in fungi. The first 3D structure of a trehalase (Tre37A from *E.coli*) in complex with two known inhibitors (validoxylamine A and 1-thiatrehazolin, Figure 2) was solved only in 2007 (pdb entries 2JF4 and 2JG0)[76], despite the number of open

reading frames identified (around 130). The structure of Tre37A consists of an $(\alpha/\alpha)_6$ barrel, with the subsites +1 for the leaving-group and −1 as the "catalytic" site.

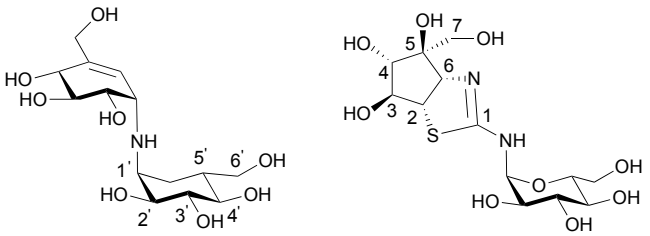

Validoxylamine A **1-Thiatrehazolin**

Figure 2. Structures of validoxylamine A and 1-thiatrehazolin.

The +1 subsite accomodates the "aglycon" moiety (pseudosugar ring of validoxylamine A and glucose ring of 1-thiatrehazolin) having the $^4C_1$ chair conformation; an extensive network of hydrogen bonds between the "aglycon" and several amino acid residues of the protein, together with the lack of hydrophobic stacking, affords the driving force for the accommodation of the α,α-1,1-linked disaccharide, as opposed to a-1,4-linked substrates. The exact transition state conformation for glycoside hydrolysis in the −1 subsite is still undefined, with both $^4H_3$ half-chair and $^{2,5}B$ boat conformations of the six-membered rings being possible. Asp312 and Glu496 are, respectively, the catalytic acid and base implicated in the inversion mechanism, where leaving-group departure is achieved by Brønsted base assistance to nucleophilic attack by a water molecule, in a single-displacement mechanism. In insect tissues the enzyme trehalase is mainly found in brain and

thoracic ganglia, asynchronous and synchronous flight muscle, midgut cells, midgut surrounding visceral muscle, follicle cells, spermatophore, and hemolymph. For its role in glucose metabolism insect trehalase has been regarded as an interesting target for the development of new and selective insecticides[77]. Inhibition studies revealed that several compounds are able to specifically block trehalase activity in a micromolar or submicromolar range. Among the most powerful compounds there are some natural pseudodisaccharides, such as validoxylamine A[76, 78] (Figure 2), trehazolin[79], casuarine-6-*O*-α-D-glucoside[80, 81] (**1**, Figure 3) and its analogues[82], together with synthetic trehalose analogues[76, 78, 83, 84, 85, 86].

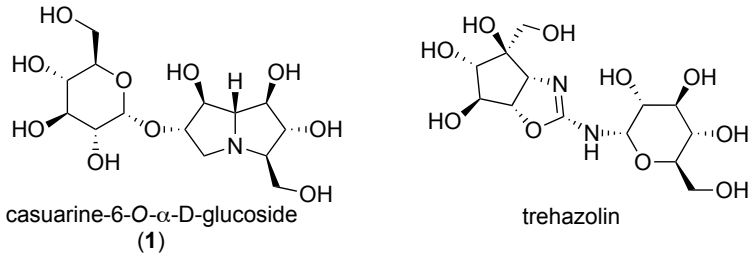

Figure 3. Structures of casuarine 6-*O*-α-D-glucoside (**1**) and trehazolin.

In addition, trehalase is inhibited by iminosugars that strongly inhibit other glycosidases[80, 87]. Most of what we know about insect trehalase derives from studies performed on terrestrial species such as Lepidoptera, Diptera, Blattaria, and Orthoptera, and recently, from aquatic insects, such as Chironomidae[83].

Iminosugar-based trehalase inhibitors

It is well known that polyhydroxy pyrrolidine and piperidine[80, 88], are potent glycosidases inhibitors due to the presence of the endocyclic nitrogen, which is able to mimic the transition state of the enzymatic reaction.

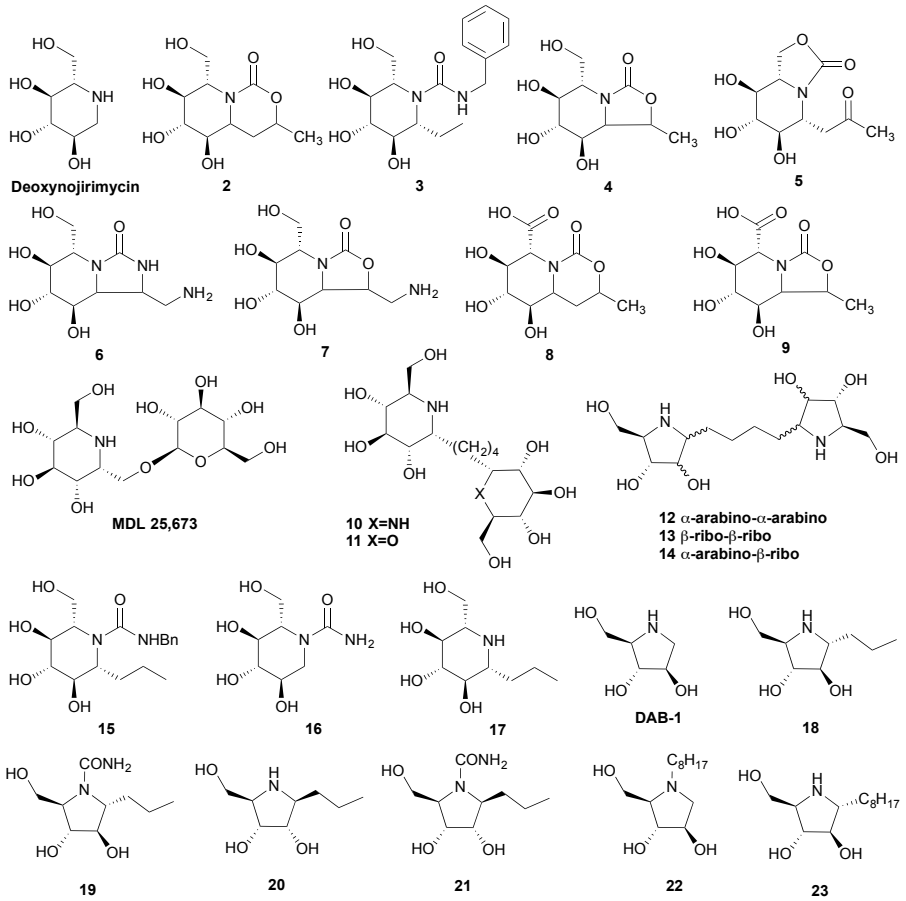

Figure 4. Structure of deoxynojirimycin, MDL 25,673, DAB-1 and others iminosugar-based trehalase inhibitors (**2**-**23**).

Monocyclic iminosugar alkaloids such as DAB-1 and deoxynojirimycin (Figure 4) have been recently found in the latex exuded from Mulberry leaves (*Morus spp*.) and their toxic effect towards Eri silkworm (*Samia ricini*) larvae has been evidenced. A series of inhibitors (**2**-**9**) were synthesized, introducing a substituent of the iminoglucitol ring of deoxynojirimycin[83], and assayed on *Chironomus riparius* trehalase activity. The most active molecule was compound **3**; inhibition kinetics confirmed competitive inhibition for this compound (K_i = 25 mM). For comparison, the same assay was carried out using porcine kidney trehalase; only compound **3** showed slight inhibitory activity. Moreover, the degree of inhibition of compound **3** on porcine trehalase was significantly lower than that on midge trehalase. MDL 25,637 that efficiently inhibits trehalase (IC_{50} = 140 nM on porcine kidney trehalase) and to a lesser extent isomaltase > sucrase > glucoamylase > maltase was used as reference compound[89]. Compounds **10**-**14** (Figure 4) were tested for their inhibitory activity against porcine trehalase. Compound **10**, which is the nojirimycin dimer, was the most active derivative of the series, showing 100% inhibition at a concentration of 1 mM. For this compound, a dose–response curve was performed, affording IC_{50} = 88 μM and K_i = 44 μM. Another set of compounds (**15-23**) has been synthesized and evaluated as potential inhibitors of both porcine and insect trehalase. Compounds **16**, **17** and **22** proved to be active against both enzymes with selectivity towards the insect glycosidase, while compounds **15**, **18** and **19** behaved as

inhibitors only of insect trehalase. The most active and specific inhibitor was compound **17** (IC_{50} = 9,7 μM on *C.riparius* and 109 μM on porcine kidney trehalase), characterized by a nojirimycin ring with a propyl group at C-1. Compared to lead 1-deoxynojirimycin, the presence of the propyl group in **17** causes a slight decrease of activity, but nevertheless imparting a ten-fold selectivity towards insect trehalase. In general, the collected data clearly indicate that the catalytic sites of trehalases from porcine kidney and insects have different recognition requirements, which can be exploited for the future design of specific inhibitors.

Casuarine derivatives as trehalase inhibitors

Casuarine (**24**) and its 6-*O*-α-D-glucopyranoside (**1**, Figure 5), have been isolated from *Casuarina equisetifolia* (Casuarinaceae)[80] and from the leaves of *Eugenia jambolana* Lam. (Myrtaceae)[80, 90], two plants well known for their therapeutic action against diarrhoea, dysentery and colic[91], breast cancer[80, 92], diabetes and bacterial infections[90, 93, 94]. These two compounds were also synthesized[81, 95, 96]; the first total synthesis of 6-*O*-α-D-glucopyranosyl casuarine was achieved by Cardona et al.[81] and allowed to perform more reliable biological tests on chemically pure compound. The most noteworthy inhibition activity was shown for compound **1** (IC_{50}= 0.34 mM against porcine kidney trehalase) that inhibited the enzyme in a competitive manner, with a K_i value of 0.18 mM. It is now well accepted that trehalase

catalytic site contains two subsites[76, 81, 97, 98], a catalytic site and a recognition site.

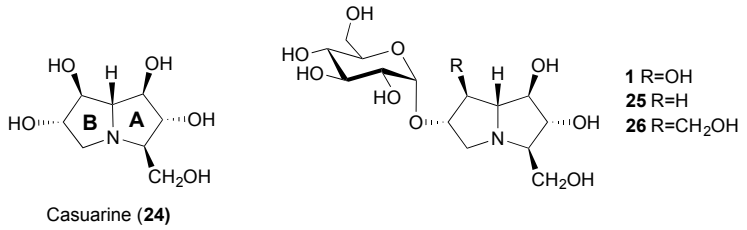

Figure 5. Structures of casuarine (**24**), casuarine-6-*O*-α-D-glucoside (**1**) and its analogues (**25**, **26**).

The extremely high affinity of a pseudodisaccharide inhibitor derives from the synergistic interactions of an alkaloid unit and a sugar (or cyclitol) unit with the two subsites[87]. Compounds **24** and **1** proved their strong and selective inhibitory properties also towards *E. coli* trehalase Tre37A[81]. Compound **1** (K_i = 12 nM) was shown to be around a thousand fold more potent than **24** (K_i = 17 μM), indicating that the glucose moiety contributes considerably to binding. In order to generate highly potent trehalase inhibitors with potential insecticidal activity, Cardona *et al.* undertook the total synthesis of two new casuarine-6-*O*-α-D-glucoside analogues **25** and **26** (Figure 5)[82]. Compounds **1**, **25** and **26** were tested against *C. riparius* trehalase, Tre37A and commercial porcine kidney trehalases (Table 1). The potency of **1**, **25** and **26** towards the three trehalases showed a similar trend, with the most potent inhibition obtained using compound **1**. The functional group at

the C7 position has a critical effect on the inhibitory activity of these analogues; the activity is decreasing in the order OH > H > CH_2OH.

Table 1. Inhibition of porcine kidney trehalase, Tre37A and *C. riparius* trehalase by compounds **1**, **25** and **26**.

	Porcine kidney, K_i	*E. coli* Tre 37A, K_i	*C. riparius*, K_i
1	11nM[a]	12 nM	0.66 nM
25	138 nM	86 nM	22 nM
26	>10 mM	2.8 mM	157 nM

[a] K_i = 18 nM for **1** isolated from natural source (purity about 60%)

It is interesting to observe, however, that compounds **1** and **26** are at least one order of magnitude more potent towards the *C. riparius* trehalase than the porcine trehalase. Compound **1** is the most potent trehalase inhibitor described to date with a K_i value against *C. riparius* lower than that displayed by validoxylamine A towards the porcine kidney trehalase (K_i = 2 nM)[79, 99] and an order of magnitude lower than that determined for trehazolin with other insect species (K_i = 10^{-8} M towards locust flight muscle trehalase)[77, 79]. However, in terms of selectivity, compound **26** is probably the most interesting one, displaying more than 60-fold selectivity between *C. riparius* and porcine kidney trehalase. To further explore the potentiality of the pyrrolizidine ring of casuarine, a number of derivatives were assayed as inhibitors of *C.*

riparius trehalase activity[83]. The structures included in this study are illustrated in Figure 6; none of the compounds tested resulted to be more effective than casuarine itself in inhibiting trehalase activity: thus, the hydroxyl group in position 7 of casuarine seems again to play a fundamental role in enhancing inhibitory activity.

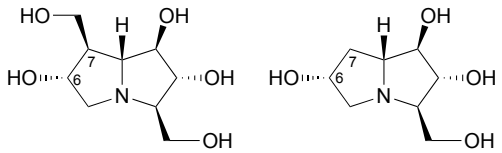

Figure 6. Structures of casuarine analogues used as inhibitors of trehalase.

Table 2. Inhibition by casuarine derivatives of membrane-bound trehalase from *C. riparius* larvae and trehalase from porcine kidney. Initial rate of trehalase activity was measured in the presence of 0.5 mM trehalose (*C. riparius*) and 5 mM trehalose (porcine kidney) and increasing concentrations of the indicated inhibitors ranging from 0.1 to 200 μM. Data are means ± SE of three independent experiments.

Compound	***C. riparius***		**Porcine kidney**	
	IC_{50}(μM)	**K_i**	**IC_{50}(μM)**	**K_i**
7-Deoxycasuarine (**28**)	1.2 ± 0.04	0.59 ± 0.02	21.5 ± 2.8	11.7 ± 1.4
7-Homocasuarine (**27**)	65.5 ± 1.5	33.0 ± 0.8	214.0 ± 28.8	107.0 ± 14.4
Casuarine (**24**)	0.25 ± 0.03	0.12 ± 0.01	12	-

In particular, substitution of the hydroxyl group with a hydroxy methyl group dramatically increased the K_i value (273-fold in *C. riparius*), whereas removing the hydroxyl group (7-deoxycasuarine) had a relatively slight effect with a 4.9-fold increase of the K_i value (see Table 2). Also, this latter compound had a K_i value 19.8-fold lower for trehalase from *C. riparius* larvae than that for trehalase from porcine kidney.

3.2. Trehalose mimics as trehalase inhibitors: Results and discussion

In the search for new inhibitors that might be specific towards insect trehalase, I studied two sets of trehalose mimics testing their biological activity against both insect and porcine trehalase, compared to the human α-amylase enzyme:

1) Iminosugar-based trehalose mimics: ***N*-bridged 1-deoxynojirimycin dimers**.
2) Polyhydroxylated pyrrolizidine alkaloids: **Casuarine derivatives.**

1) *N*-bridged 1-deoxynojirimycin dimers.

In the search for new inhibitors, based on 1-deoxynojirimycin and its *N*-acyl derivatives, that might be specific towards insect trehalase, I designed and synthetized a small set of *N*-bridged 1-deoxynojirimycin dimers (Figure 7, **29**-**31**).

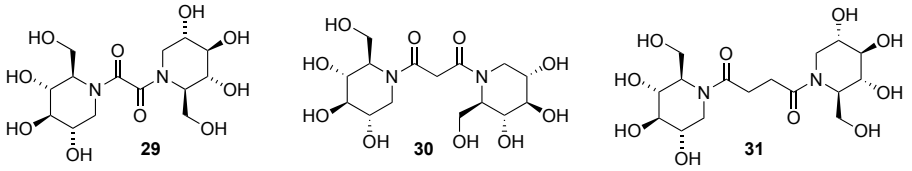

Figure 7. Structures of the synthesized dimers **29**-**31**.

The synthesis of compounds **29**-**31** was straightforward from protected 1-deoxynojirimycin (**32**), as outlined in Scheme 1.

Compound **32** was synthetized from tetra-benzyl-D-glucose, as already reported in literature[100] (see Experimental Part 7.1).

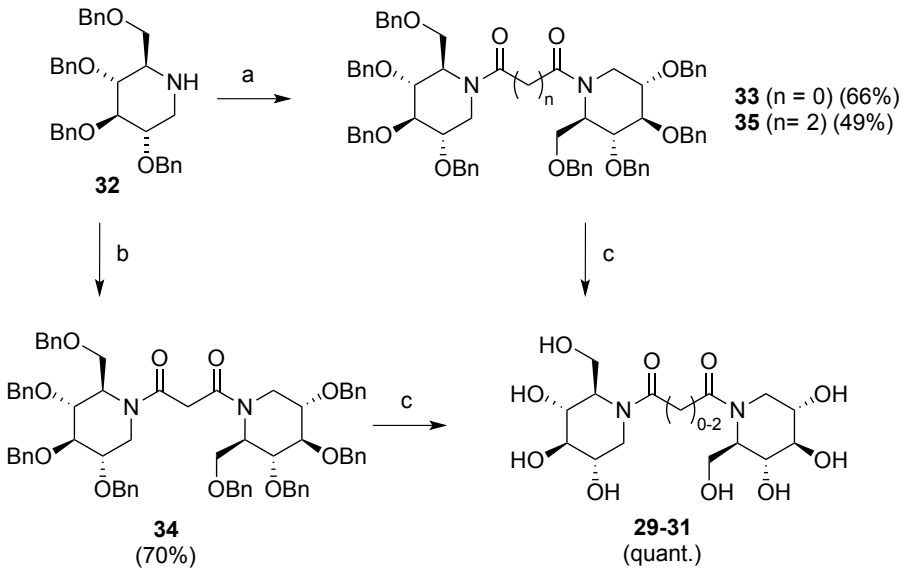

Scheme 1. Synthesis of nojirimycin dimers **29-31**. Reagents and conditions: (a) Oxalyl or succinyl chloride, pyridine, DCM, 0°C→r.t., 3 h; (b) Malonic acid, DCC, DMAP, p-TsOH, DCM, r.t., 30 min.; (c) $Pd(OH)_2/C$, H_2, EtOAc/EtOH = 1:1.

The reaction of compound **32** with oxalyl or succinyl chloride successfully afforded compounds **33** and **35** in 66% and 49% yields, respectively; in contrast, the reaction of **32** with malonyl chloride in the same reaction conditions gave compound **34** only in traces. The unexpected outcome of the reaction with malonyl chloride is probably due to by-products deriving from reaction of methylenic acidic protons of malonyl chloride with the basic

pyridine used in the procedure. Dimer **34** was obtained in 70% yield by reaction of **32** with malonic acid in the presence of DCC. Direct hydrogenolysis of **33-35** quantitatively afforded the compounds **29-31**. Compounds **29-31** were tested for their inhibitory activity against insect trehalase of midge larvae of *C. riparius*[101], porcine trehalase (purchased from Sigma-Aldrich) as the mammalian counterpart and α-amylase from human saliva (purchased from Sigma-Aldrich), as a relevant glycolytic enzyme. Midge larvae are widespread in freshwater ecosystems, are widely used in ecotoxicological studies and environmental biomonitoring programs as sentinel organisms and represent a good model for biochemical studies. To examine the potential of each 1-deoxynojirimycin dimer as trehalase inhibitor, preliminary screening assays at a fixed concentration (1 mM) of potential inhibitors were carried out, and dose-response curves were established for most active compounds in order to determine the IC_{50} values.

Experiments were performed at a fixed substrate concentration, in the presence of increasing inhibitor concentrations. The inhibitory activity is shown in Figure 8 as IC_{50} value. All the synthesized dimers resulted inactive against α-amylase, while they were similarly active against *C. riparius* trehalase (activity in the micromolar range). Compound **29** resulted to be the most active derivative of the series (IC_{50} = 6,1 μM); all dimers **29-31** showed a slight selectivity (from 4 to 7 fold) towards the insect glycosidase, resulting more selective between mammalian and

insect trehalase if compared to the parent compound 1-deoxynojirimycin (2 fold more selective toward *C. riparius* trehalase).

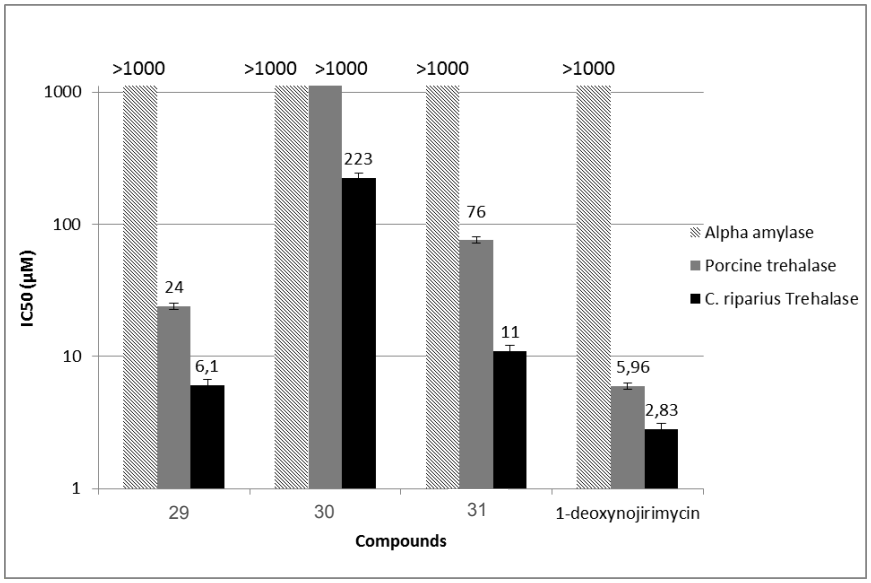

Figure 8. Inhibitory activity of compounds **29-31**, compared to 1-deoxynojirimycin.

2) Casuarine derivatives.

As discussed in the introduction of this section, simple modifications at the C-7 of the B ring of casuarine (OH, H, CH_2OH) are able to influence both potency and specificity of inhibition. It was therefore expected that also modifications at the C-6 of the B ring could disclose interesting results in terms of potency/specificity of trehalase inhibition and this was the aim of my work. Moreover, it is trivially of great importance the

obtainment of new inhibitors by simple, and low cost synthetic routes in order to investigate them in *in vivo* tests and, if effective, in agri-food industry. In order to briefly investigate modifications at position C-6 of the B ring pyrrolizidine nucleus, we proposed a novel synthetic approach to 7-deoxy-uniflorine A (**37**, Figure 9) and the biological evaluation of analogues **28**, **36-37** and of 7-deoxy-6-(α-glucopyranosyl)casuarine **25** as selective trehalase inhibitors.

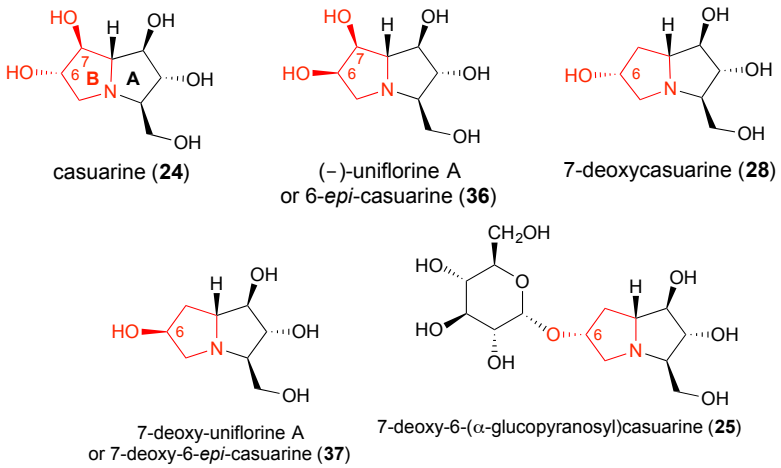

Figure 9. Chemical structure of casuarine (**24**) and compounds **25**, **28**, **36-37** used in the present study.

Derivatives **25**, **28** and **36** were synthesized as already described. Natural (-)-uniflorine A (**36**) was isolated in 2000 from the leaves of *E. uniflora* L. (Myrtaceae), an evergreen tree widely found in Paraguay, Uruguay, Argentina and Brazil. From such leaves a natural Paraguayan medicine named Nangapiry is produced and

used in folk medicine as antidiarrheic, diuretic, antirheumatic, antifebrile and antidiabetic agent. The activity of **36** as α-glucosidase, maltase and sucrose inhibitor was also reported[102]. Our total synthesis of **36** was accomplished in nine steps and 11% overall yield[103] from a carbohydrate based nitrone exploiting the nitrone cycloaddition chemistry[104]. The cycloaddition with a different dipolarophile on the same nitrone allowed the synthesis of 7-deoxycasuarine (**28**)[105]. A selective α-glucosylation on intermediate **38**[105] (Scheme 2) provided, after proper synthetic elaborations, 7-deoxy-6-(α-glucopyranosyl)casuarine (**25**)[82]. Derivative **37** was synthesized *ex novo*, as reported in Scheme 2, in order to test a non-natural derivative bearing the same configuration at C-6 of native (-)-uniflorine A but lacking the hydroxyl group at C-7. Our aim was to verify if:

1) stereochemistry at C-6 may have an effect on inhibition in terms of potency and selectivity;
2) the presence of a further hydroxyl group at C-7 is fundamental for activity;
3) an additional glucosyl moiety at C-6 is essential, considering that both introduction of an OH group at C-7 and a glucosyl moiety at C-6 considerably elongate the total synthesis requiring more synthetic steps and lowering the overall yield of the final compound.

In order to achieve the desired inversion of configuration at C-6, a Mitsunobu reaction on intermediate **38** appeared to be the best and simple straightforward strategy. *p*-Nitrobenzoic acid (3.2 equiv.) was used as the nucleophile for the Mitsunobu reaction, in THF as solvent and in the presence of triphenylphosphine (3 equiv.) and diisopropylazodicarboxylate (3.2 equiv.) (Scheme 2).

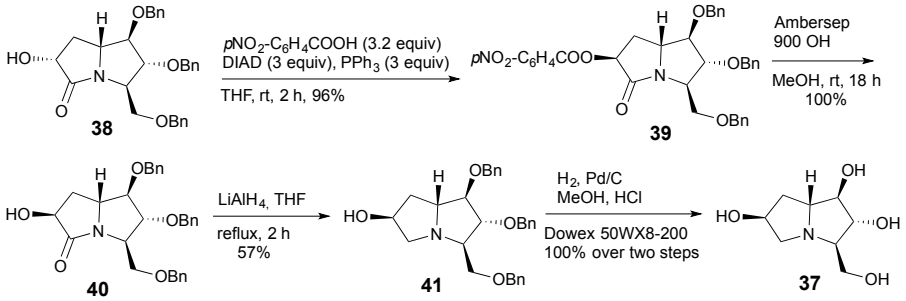

Scheme 2. Synthesis of 7-deoxy-uniflorine A (**37**).

After 2 hours at room temperature, lactam **38** was converted into ester **39** in 96% yield. Treatment with the strongly basic resin Ambersep 900 OH provided lactam **40** in quantitative yield, with the opposite configuration at C-6 with respect to **38**. Reduction of the C=O bond with $LiAlH_4$ in refluxing THF gave pyrrolizidine **41** in 57% yield [106]. Final catalytic hydrogenation followed by treatment with ion exchange resin afforded 7-deoxy-6-*epi*-casuarine (**37**) quantitatively (Scheme 2). The synthesis of **37** had been previously reported by Behr and co-workers with a different synthetic strategy that also yielded 7-deoxycasuarine (**28**) in

approximately 1:1 ratio[107, 108]. The synthetic strategy reported herein afforded **37** in 54% yield over 4 steps from lactam **38**, thus allowing the production of this compound on a much larger scale as required for *in vivo* tests. In order to evaluate the specific inhibition of the synthesized compounds against insect trehalases and to briefly explore the importance of the configuration at C-6 in the selectivity, a set of different α-glucosidases were chosen for comparison. Derivatives **25**, **28**, **36-37** were then assayed for their activity against α-amylase from human saliva, trehalase from porcine kidney, purified *C. riparius* trehalase[101] and trehalases present in different tissue homogenates from *S. littoralis* larvae (*S. littoralis* is a serious lepidopteran pest responsible for significant crop losses worldwide). The biological activity is resumed in Table 3[109].

Table 3. IC_{50} of compounds **25**, **28**, **36-37**.

Compd.	α-amylase	Porcine trehalase	*C. riparius* trehalase	*S.littoralis* Midgut trehalase	*S.littoralis* Malpighian tubule trehalase
36	>1 mM	>1 mM	177 ± 18 nM	261 ± 24 nM	43 ± 10 nM
28	>1 mM	20.6 ± 2.2 µM	1.22 ± 0.08 µM	9.84 ± 0.49 µM	1.34 ± 0.27 µM
37	>1 mM	>1 mM	175 ± 12 nM	560 ± 40 nM	330 ± 90 nM
25	>1 mM	479 ± 45 nM	44 ± 1.0 nM	96 ± 15 nM	49.7± 6.8 nM

Results obtained on trehalases from *S. littoralis* confirmed effects on *C. riparius* trehalase, suggesting *C. riparius* as a good model for biochemical studies. For a given compound IC_{50} values of the same order of magnitude are obtained in the two insect species, even though a marked albeit small difference was detected between trehalase from midgut and Malpighian tubules of *S. littoralis*, probably due to enzyme isoforms. None of the tested compounds inhibited α-amylase from human saliva, suggesting the possibility to find non-toxic insecticides/fungicides within these compounds. Casuarine derivatives **25** and **28,** possessing the stereochemistry at carbon 6 corresponding to native casuarine, did not show inhibition of α-amylase even at the highest concentration tested (1 mM), while they were active on both porcine and insect trehalases. In particular, the glucosylated derivative **25** showed IC_{50} values in the nanomolar range, while 7-deoxy-casuarine (**28**) was able to inhibit both trehalases only in the low micromolar range, indicating the important role exerted by the glucosyl moiety in terms of potency of inhibition. Anyway, a considerable activity towards the mammalian enzyme was maintained for both compounds and only a slight selectivity toward insect trehalases could be observed. Much more interestingly, uniflorine derivatives (or 6-*epi*-casuarines **36** and **37**) showed total selectivity against insect trehalases, being completely inactive toward α-amylase and porcine trehalase at 1 mM concentration. In both cases, IC_{50} was in the high nanomolar range, independently of the substituent (7-hydroxyl or 7-deoxy) at position 7 and even

if both these compounds lack an additional glucosyl moiety at C-6. The observed trend in the inhibitory activity of the compounds against the mammalian and insect trehalase suggests that the stereochemistry at position 6 is a key issue in discriminating the two enzymes and that the presence of an additional glucosyl moiety at C-6, which considerably elongates the total synthesis of the compounds, is not essential. Inhibition kinetics revealed that all the compounds tested interact with the active site of the insect trehalase. To evaluate the inhibitory pattern produced by the compounds studied, kinetics experiments, as a function of trehalose concentration at different inhibitor concentrations, were performed for each of them. Results showed different inhibitory pattern by the compounds, compounds **28** and **36** being hyperbolic mixed-type, compound **37** pure competitive and compound **25** linear mixed-type (see Figure 10-13). To simplify diagnosis of the inhibition type, data were plotted according to the Lineweaver-Burk plot and replots were built to calculate inhibition constants and additional kinetic parameters (Table 4). Kinetic analysis revealed that compounds **28** and **36** produce hyperbolic mixed-type inhibition. Hyperbolic mixed-type is quite rare, however it can be overlooked if a sufficient inhibition concentration range is not explored[110]. Detailed kinetic analysis performed in structure-activity relationships studies may disclose such behavior[110]. This type of inhibition occurs when both E and EI complex bind S, but with different affinities and both ES and ESI complexes are productive, but with different rates.

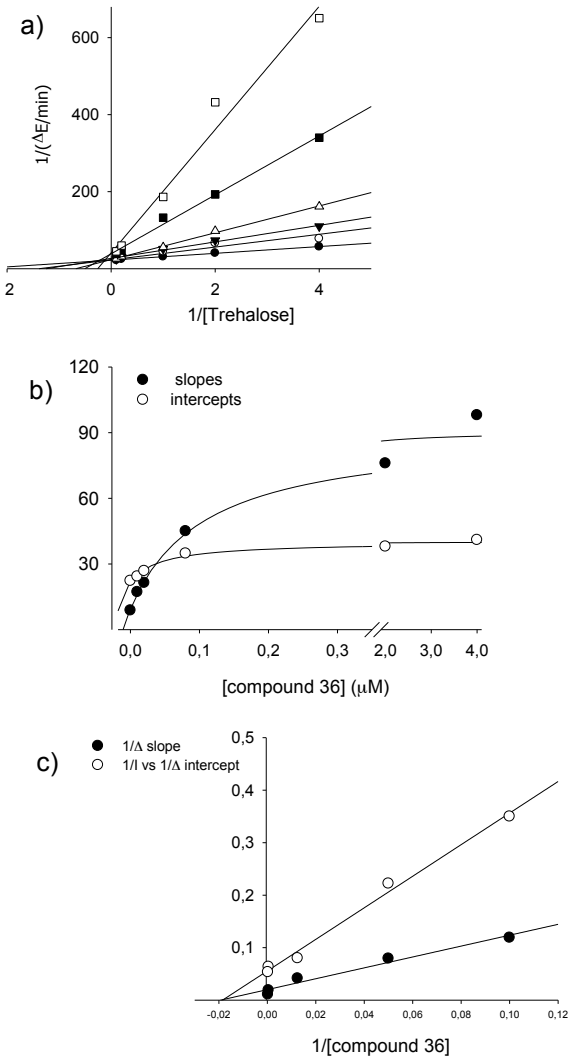

Figure 10. Inhibition kinetics of midge trehalase in the presence of compound **36**. a) double reciprocal plot in the presence of different fixed inhibitor concentrations (10, 20, 80, 2000 and 4000 nM); b) replot of the slopes and the intercepts of each reciprocal plot versus the corresponding inhibitor concentration; c) secondary replot of 1/Δ slope and 1/Δ intercept versus the reciprocal inhibitor concentration.

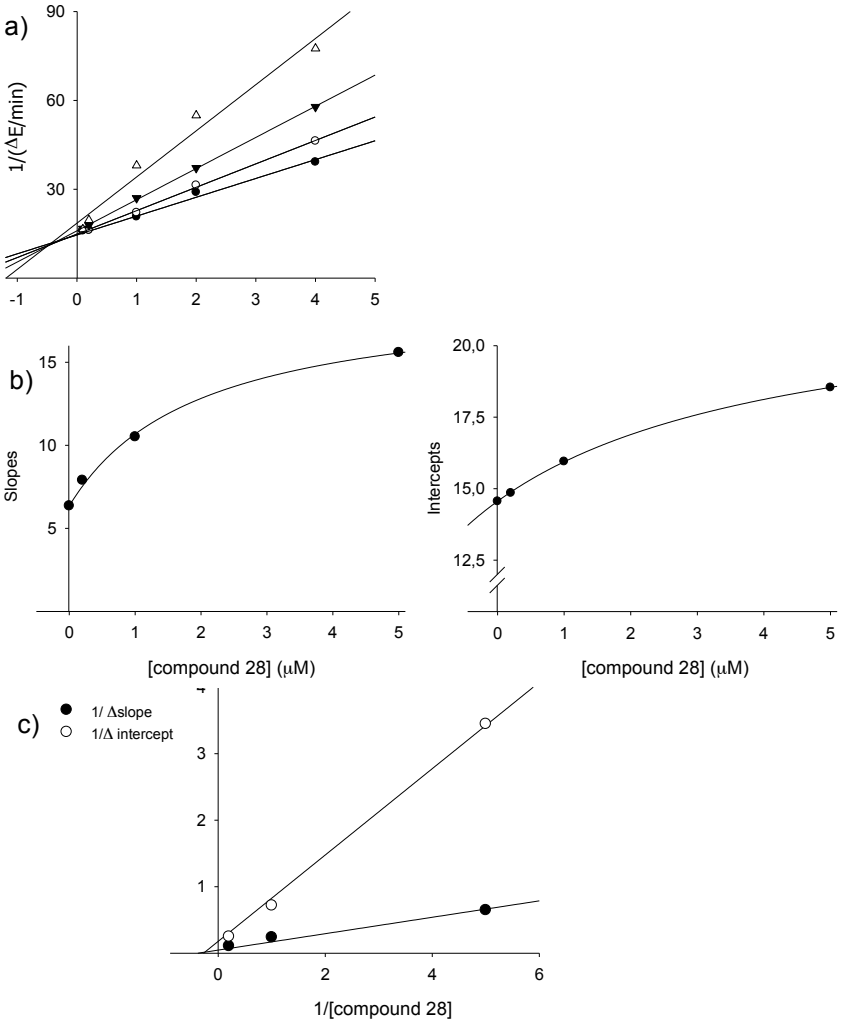

Figure 11. Inhibition kinetics of midge trehalase in the presence of compound **28**. a) double reciprocal plot in the presence of different fixed inhibitor concentrations (0.2, 1, 5 μM); b) replot of the slopes and the intercepts of each reciprocal plot versus the corresponding inhibitor concentration; c) secondary replot of 1/Δ slope and 1/Δ intercept versus the reciprocal inhibitor concentration.

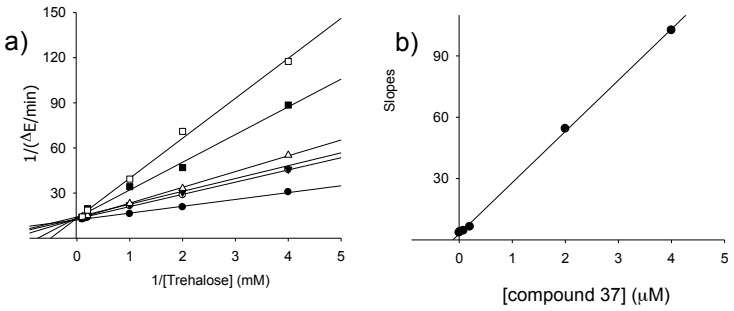

Figure 12. Inhibition kinetics of midge trehalase in the presence of compound **37**. a) double reciprocal plot in the presence of different fixed inhibitor concentrations (20, 80, 200, 2000 and 4000 nM); b) replot of the slopes of each reciprocal plot versus the corresponding inhibitor concentration.

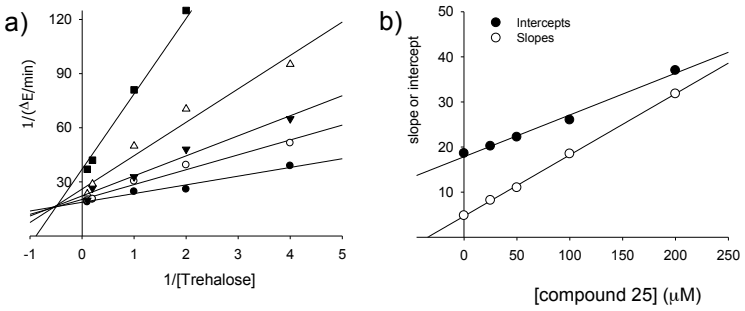

Figure 13. Inhibition kinetics of midge trehalase in the presence of compound **25**. a) double reciprocal plot in the presence of different fixed inhibitor concentrations (20, 50, 100, and 200 nM); b) replot of the slopes and the intercepts of each reciprocal plot versus the corresponding inhibitor concentration.

Table 4. Kinetic parameters of the inhibition of *C. riparius* trehalase.

The factors α is the factor by which K_S changes when the inhibitor occupies the enzyme and the factor β is the factor by which the rate constant for the breakdown of enzyme-substrate complex changes when the inhibitor is bound. The factor β is determined from 1/Δ intercept replot. The replot has an intercept on the 1/Δ intercept-axis of $\beta V_{max}/(1-\beta)$. The factor α is determined from 1/Δ slope replot: this replot has an intercept on the 1/Δ slope-axis of $\beta V_{max}/K_m(\alpha-\beta)$. When 1/Δ intercept = 0, the intercept on the 1/[I]-axis gives $-\beta/\alpha K_i$. With α and β known K_i can be calculated (see Figure 10-13).

Inhibitor	K_i (nM)	α factor	β factor
compound **36**	48 ± 4	4.8	0.4
compound **28**	810 ± 16	2.5	0.5
compound **37**	118 ± 12	-	−
compound **25**	34 ± 2	5.8	−

The primary plot of the hyperbolic mixed-type inhibition is not different from that of classical mixed-type, i.e. the family curves pivot above the 1/[S] axis. However, secondary plots are hyperbolic instead of linear type. The system states that at any inhibitor concentration, an infinitely high [S] will drive all the enzyme to a mixture of EI and ESI. Because ESI is less productive by a factor β the V_{max} decreases. The value of β ranges from 0 to less than 1. At any infinitely high [I] again all the enzyme is driven to EI and ESI. As EI has a lower affinity to [S] K_S is increased by factor $\alpha > 1$. Because ESI is productive, the velocity cannot be driven to zero by increasing [I]. To calculate residual activity in the presence of hyperbolic mixed-type inhibitor appropriate rate

equations have been developed[111]. Applying these equations to compounds **28** and **36,** at a concentration 20-fold higher than the K_i value the enzyme still retains 12% and 19% residual activity, respectively. Considering the data obtained on *C. riparius* trehalase, the stereochemistry of the pyrrolizidine ring around carbon 6 appears to be crucial for inhibition, suggesting a more precise fitting of the inhibitor when the stereochemistry of compound **37** is adopted, as testified by the K_i being 6.8-fold higher for compound **28** compared to compound **37**. This is also true for *S. littoralis* enzyme. However if a hydroxyl group is present on carbon 7 as in compound **36** the inhibition becomes mixed-type even though a slight decrease of the K_i value is observed. The addition of a glucosyl moiety produces a stronger inhibitor in terms of potency of inhibition, due to a much closer structural similarity with the natural substrate. However compound **25** was able to inhibit porcine trehalase while compounds **36** and **37** did not, thus revealing that in terms of selectivity towards the insect trehalases the presence of an additional glucosyl moiety is not essential. Due to the promising activity and selectivity detected by *in vitro* assays on insect trehalases, we decided to test the *in vivo* activity of casuarine derivative **37**. Different doses of the inhibitor were intra-hemocoelically injected in sixth instar *S. littoralis* larvae. Inhibitor concentrations were chosen according to similar experiments reported in literature on insecticidal activity of trehalase inhibitors[78, 112]. Effects on larval and pupal weight, larval, pupal

and adult morphology and adult emergence, longevity and fertility were monitored. Contrary to what expected, in these preliminary experiments no effects on the parameters analyzed were detected (Figure 14). The treatment of fifth instar larvae with the higher doses applied for sixth instar bioassay also failed to impair *S. littoralis* development.

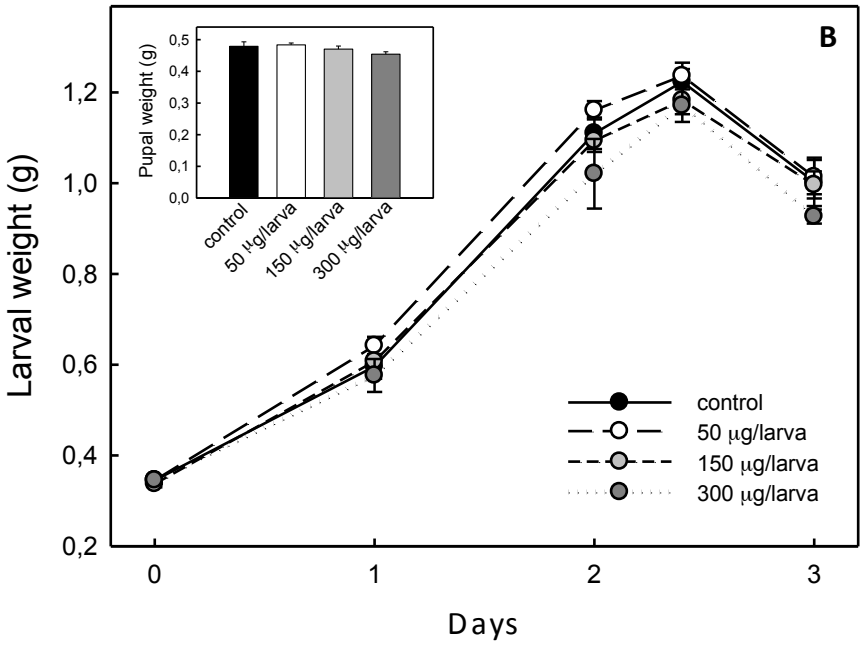

Figure 14. *S. littoralis* larval and pupal weight after intra-hemocoelical injection of derivative **37**. Each experimental group consisted of 16 animals.

Preliminary and promising *in vitro* responses of putative bioinsecticides may go against *in vivo* effectiveness, both in qualitative and quantitative terms, due to the complexity of the *in*

vivo context[113]. Having made that preliminary remark, the lack of effects at this point could be due to both low inhibition of *S. littoralis* trehalases in the *in vivo* conditions (e.g. high hemolymphatic trehalose concentration) and/or rapid degradation of the derivative in the hemolymph. It is thus pivotal to take into account these hypotheses for the improvement in the design of the inhibitors, including effective delivery vectors that preserve their activity in the *in vitro* context[114].

4.1. Synthesis of multivalent glycoconjugates: Introduction

Carbohydrates constitute the most abundant class of biomolecules on Earth. They play different roles in the natural world as energy storage, molecular recognition for intracellular trafficking or interactions between pathogenic microorganisms and viruses and the surfaces of mammalian cells[115]. The carbohydrates present inside and at the surface of cells mediate many biological processes that are fundamentally important for both physiological and pathological states of living organisms [116, 117]. Usually carbohydrates are covalently linked to other biomolecules like proteins or lipids. The molecular and supramolecular scaffolds of such glycoconjugates provide them with a very important property: multivalency[118, 119, 120, 121]. Multivalency is a powerful strategy for achieving high-affinity molecular recognition in biological systems; it is postulated that multivalent interactions between endogenous proteins and glycans can act as tuners that can adjust thresholds of cellular activation, differentiation, and survival and critically influence functional outputs by modulating signaling of canonical receptors[117, 122, 123, 124]. Individual interactions between sugars and proteins are very weak; however, multiple simultaneous interactions between carbohydrate ligands and their receptors reinforce one-another like molecular velcro to achieve functionally useful avidities. Recent advances in carbohydrate microarray technologies [125, 126, 127, 128, 129, 130, 131] combined with the utilization of freely accessible resources of the

Consortium for Functional Glycomics (http://www.functionalglycomics.org/) have considerably expanded our knowledge of carbohydrate-binding proteins, and reinforced the importance of multivalent interactions[132, 133, 134, 135, 136, 137, 138]. It has become clear that the avidities and selectivities of specific interactions are very dependent on the density of the sugar groups and also on the chemical structure of the linker group to the underlying multivalent scaffold. Translating this knowledge for the design and preparation of multivalent glycoconjugates remains a significant challenge to diagnose and treat diseases[139, 140, 141, 142]. Protein–carbohydrate interactions often mediate the first step of the infection process for many pathogens including viruses, fungi, bacteria, and bacterial toxins[143, 144, 145, 146]. Therefore, a vast array of unnatural glycoconjugates (neoglycoconjugates) with various valencies and spatial arrangement of the ligands have been constructed to prevent or treat diseases caused by pathogens. Scaffolds based on proteins[147, 148, 149], polymers[150, 151, 152, 153], calixarenes[154, 155, 156, 157], dendrimers[158, 159, 160, 161, 162], cyclodextrins[163, 164], cyclopeptides[165, 166, 167], fullerenes[168, 169], gold nanoparticles[170, 171], and quantum dots[172, 173, 174] supply nanoscale materials with anti-adhesive and cell targeting properties. Such structures, that can competitively interfere with the recognition processes between host cells and pathogens, have the potential to prevent colonisation or even reverse the formation of biofilms. Another alternative to fight pathogens involves glycoconjugates that can act as vaccines and

immunomodulators. Vaccines have long relied on attenuated strains of microorganisms as a means of delivering the extracellular carbohydrate antigens. As the cell surface of pathogenic bacteria and viruses is often covered with unusual carbohydrates, structurally defined glycoconjugates displaying these structures are beginning to emerge as vaccines for the future [175, 176]. Following a lectin-mediated cellular uptake mechanism, such carbohydrate-based vaccines can prepare the immune defence mechanisms in advance of an infection, or stimulate the body to protect itself against an existing chronic infection.

Smart biomaterials

Smart biomaterials, in which the structural scaffold is functionalized with biomolecules in order to promote desired biological responses, strongly increase the chances of local tissue regeneration[177, 178]. Different biomolecules have been exploited to produce bio-active materials, including the adhesive cue Arg-Gly-Asp, and growth factors. Carbohydrates, one of the most relevant classes of biomolecules, have been neglected in this scenario and only a few examples have been described[179]. A biomaterial particularly suitable for tissue engineering is collagen, since it can be prepared in a number of different forms including strips, sheets, sponges, hydrogels and beads depending on the final applications[180, 181]. The term collagen usually refers to a group of well-known proteins widespread in vertebrates, representing the

chief structural protein accounting for approximately 30% of all vertebrate body protein. More than 90% of all extracellular proteins in the tendon, cartilage and bone, and more than 50% in the skin, consist of collagen[182, 183]. Collagen is nowadays widely used as a biomaterial for several tissue engineering applications[184, 185] due to its biocompatibility[186, 187, 188], to the expanding medical applications of biomaterials and connective tissue research, together with the effective production of medical-grade collagen, that allows collagen products to be successfully placed on the market. Many efforts are devoted to the improvement of the physical, chemical and biological features of collagen devices. For example, collagen has been engineered by adding other proteins, such as elastin, fibronectin or glycosaminoglycans or combining it with other molecules[189, 190, 191, 192, 193], such as liposomes[194], to enhance the mechanical strength of the medical devices. In addition, collagen glycosylation has emerged as a regulatory process with several implications in healthy and pathological states[195].

Ligands of P. aeruginosa LecB

Pseudomonas aeruginosa is an opportunistic pathogen associated with chronic airway infections, especially in cystic fibrosis patients. This strain synthesizes two lectins, LecA and LecB[196], which play a significant role in human infections. It was demonstrated that solutions of galactose and fucose, that respectively bind to LecA and LecB, have a therapeutic effect

against *P. aeruginosa* pneumonia in mice models[197] and cystic fibrosis patients[198]. Glycomimetic peptides that had a high affinity for binding to both LecA and LecB and could inhibit their ciliotoxic activity[199], were recently identified. LecB (also called PA-IIL) is a tetramer consisting of four 11.73 kDa subunits with high specificity for L-fucose and a weaker one for D-mannose[196, 200]. The LecB crystal structure denoted the occurrence of two bridging calcium ions in the binding site. This unique mode of binding is not observed in other lectins[201], but explains the very high affinity for fucosides and Lewis a. Although most of the LecB is cytoplasmic, it could also be found in the outer membrane, including on the surface of biofilm cells, from which it can be released by application of L-fucose[202]. Recently, it has been hypothesized that LecB undergoes transient N-glycosylation that could play a role in the secretion mechanism[203]. The search for a putative binding partner led to the proposal of outer membrane protein OprF which is a nonspecific, weakly cation-selective porin channel protein. LecB may mediate the adhesion of *P. aeruginosa* cells to receptors that are located on its surface and facilitate biofilm formation, thereby promoting colonization of host tissues. The search for high affinity ligands for LecB led to the synthesis of several classes of fucose-containing compounds (Figure 15 and Table 5) based on calixarene **42**[204], pentaerythritol **46**[205], peptide dendrimer **43–45** or glycoclusters scaffolds **49**. Compounds have also been designed for bivalent presentation of αFuc(1-4)GlcNAc **47**[206], and *N*-fucosyl amides **48**[207].

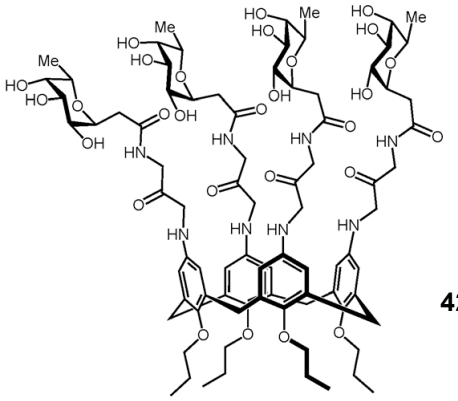

42

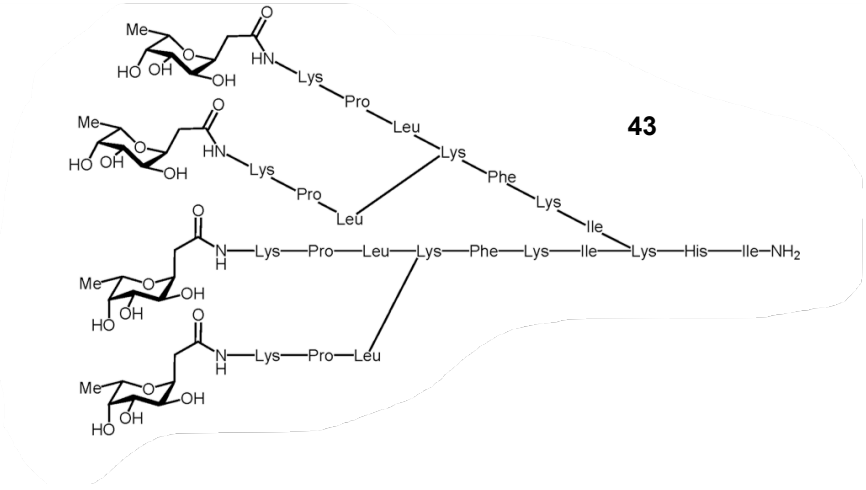
Lys—Pro—Leu—Lys—Phe—Lys—Ile—Lys—His—Ile—NH2
Lys—Pro—Leu

43

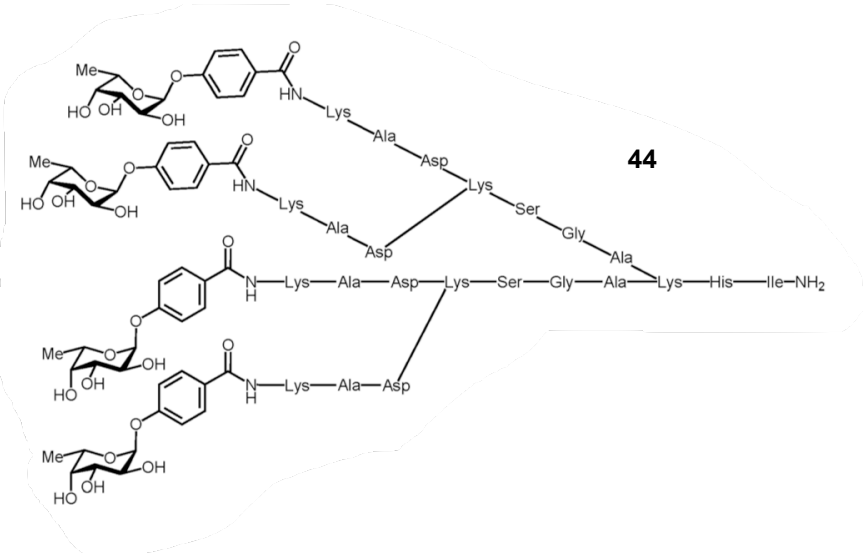
Lys—Ala—Asp—Lys—Ser—Gly—Ala—Lys—His—Ile—NH2
Lys—Ala—Asp

44

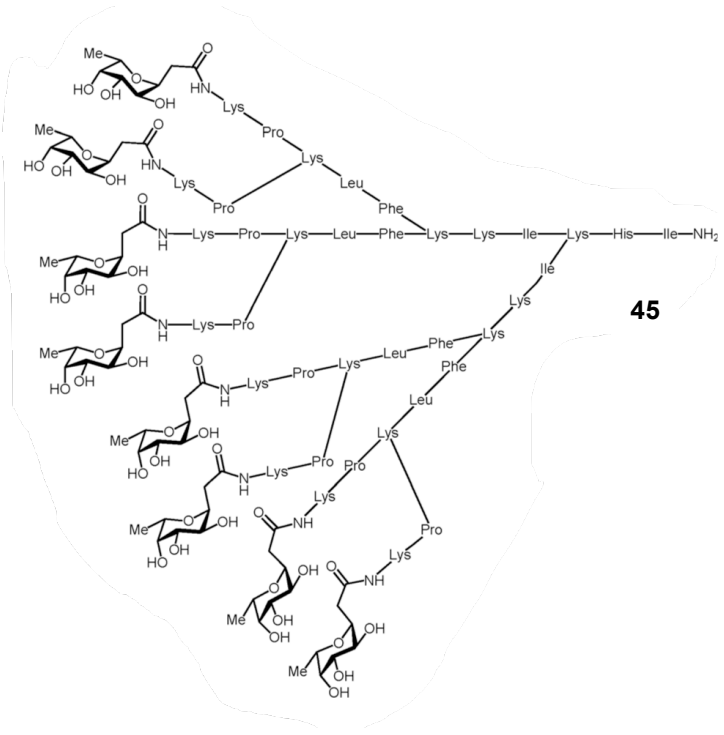

45

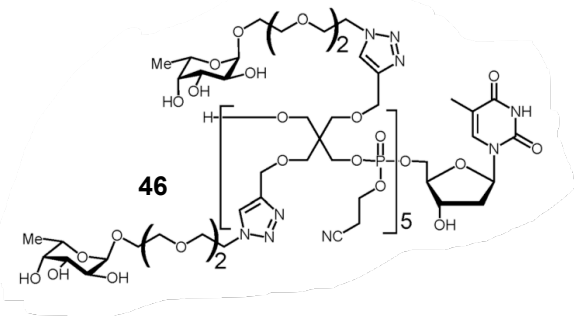

46

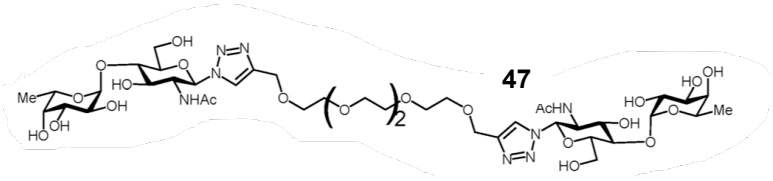

47

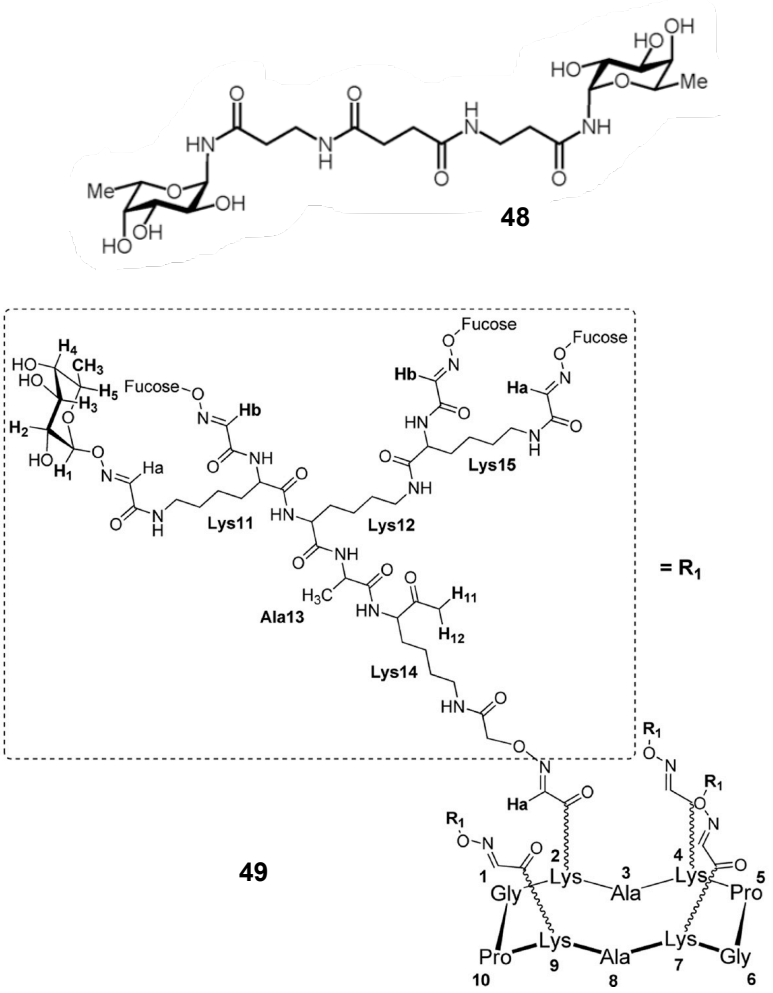

Figure 15. Multivalent glycoconjugates **42–49** as LecB high affinity ligands.

Glycopeptide dendrimer ligands for LecB were identified by screening combinatorial libraries of peptide dendrimers[208, 209, 210] functionalized with *N*-terminal *C*-fucoside residues at the end of the dendrimer branches. FD2 **43** and PA8 **44** (Figure 15) proved

to be potent ligands for LecB[211, 212]. Structure–activity relationship studies showed that multivalency was significant for activity; in particular divalent and linear peptide analogs of the dendrimers showed strongly reduced binding at the level of monosaccharides (Table 5).

Table 5. Multivalent compounds targeted to LecB: ELLA and ITC data expressed as IC_{50} and K_d respectively.

Comp.	Val.	ELLA	ITC	Ref.
αMeFuc	1		0.47 μM	213
42	4	Test biofilm 80% inhibition at 200 μM		204
43	4	0.14 μM	—/—	214
44	4	0.11 μM	—/—	215
45	8	0.025 μM	—/—	216
46	10	0.25 μM	—/—	205
47	2	—/—	0.09 μM	206
48	2	—/—	0.62 μM	207
49	16	0.6 nM	0.028 μM	217

These studies led to the identification of dendrimer 2G3 **45** with 8 fucosyl endgroups as the most potent glycopeptide dendrimer ligand to LecB. The diastereoisomer D-36, prepared from D-amino acids, also proved to be a similarly potent ligand to LecB[214]. Finally, hexadecavalent glycocluster **49** was synthetized by Renaudet and co-workers and reported a dissociation constant of 28 nM, measured by isothermal titration micorcalorimetry (ITC),

which represents the highest affinity ligand ever reported for LecB.

4.2. Synthesis of multivalent glycoconjugates: Results and discussion

My work on the synthesis of new multivalent glycoconjugates focused on two different main topics:

1) **Multivalent carbohydrates immobilisation on a biomaterial surface.**
2) **Synthesis of multiglycosylated dendrons as ligands of *P. aeruginosa* LecB.**

1) Multivalent carbohydrates immobilisation on a biomaterial surface.

As previously discussed in the introduction of this section, glycan interactions with their receptors play fundamental roles in a plethora of intra- and intercellular events[218, 219, 220, 221]. Moreover, binding events between glycans and their complementary receptors (i.e. lectins)[124, 222] occur in a multivalent and cooperative manner[223]. Investigations focusing on the design of artificial multivalent systems are attracting considerable attention[224], and multivalent glyco-materials have been shown to be powerful tools for biomedical research[131, 138, 141, 154, 175, 225]. In this context, we proposed an innovative methodology for the preparation of advanced functional materials exposing on their surface multivalent glycosylated patterns, that can be of wide applicability, including the development of "smart" biomaterials

for tissue engineering. As a model system for the present study, collagen patches were used. We developed a widely applicable chemoselective functionalization method, using a thiol-ene photoclick reaction, wich allows the introduction of a multi-antennary glycidic structure on the material surface. The proposed strategy includes thiolation of collagen, chemoselective thiol-ene photoclick-reaction with a double-bond terminated heterobifunctional dendron[226] and finally glycan conjugation by a second chemoselective reaction (Scheme 3).

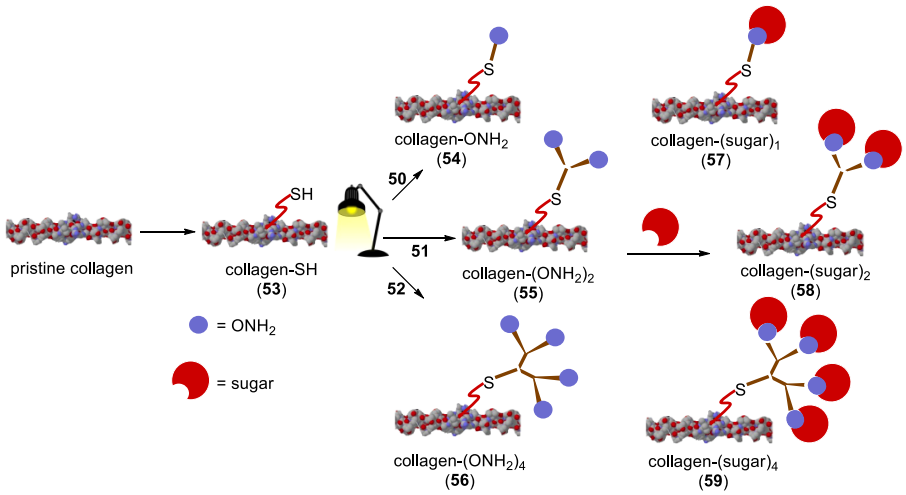

Scheme 3. General scheme for the generation of multivalent biomaterial surfaces.

Since collagen contains few or no cysteine residues[227], thiol functional groups must be suitably introduced. This goal was achieved reacting lysine side-chain amino groups with γ-

thiobutyrolactone (0.02 M in 1:1 v/v EtOH:PBS). To label and quantify -SH groups inserted with γ-thiobutyrolactone, derivatization of the thiolated and non-thiolated samples with 5,5'-Dithiobis-(2-Nitrobenzoic Acid) (DTNB, Figure 16) was performed.

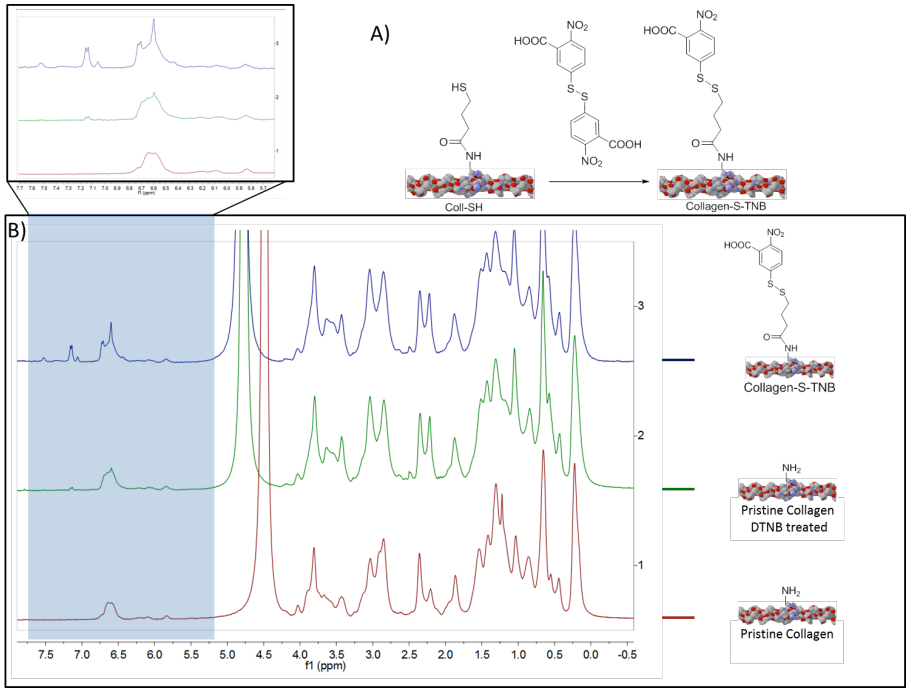

Figure 16. Thiol group quantification via NMR. A) Reaction between collagen-SH and DTNB; B) ^{1}H NMR spectra of pristine collagen, pristine collagen treated with DTNB and collagen-S-TNB.

If compared to pristine collagen distinguished by a low number of aromatic amino acids (Phe, Tyr and His), the resulting collagen-S-TNB patch should display additional protons resonating in the

characteristic aromatic region (6.4-7.5 ppm) coming from the TNB moiety. In order to exclude the presence of adsorbed DTNB, pristine collagen (non-thiolated) was also reacted with DTNB and ^{1}H-NMR recorded as well. Given the collagen amino acid composition, in particular the amount of aromatic amino acids and lysine, we can estimate that approximately 60% of total lysines bears the thiol group needed for the subsequent thiol-ene photoclick-reaction with double-bond terminated heterobifunctional dendrons. The heterobifunctional dendrons with orthogonal functional groups, a double bond at the focal point and multiple alkoxyamino termini (Scheme 4), have been synthesized therein for the first time. Zero, first and second generation heterobifunctional dendrons (**50-52**) were synthesized starting from (Boc-aminooxy) acetic acid (**60**) and selected building blocks (**61-63**, Scheme 4) through esterification and protection/deprotection steps (Scheme 5). Reaction of (Boc-aminooxy) acetic acid (**60**) with 9-decen-1-ol (**61**), in the presence of DPTS (4-(dimethylamino)pyridinium *p*-toluenesulfonate) and DCC, afforded compound **64** that was deprotected in acidic conditions to give G0 dendron (**50**) with 42% overall yield. To obtain G1 dendron (**51**), Bis-MPA (**62**) was reacted with Bromo-1-pentene (**63**) in the presence of caesium carbonate.

The obtained intermediate (**65**) was used for coupling reaction with (Boc-aminooxy) acetic acid (**60**) in the same conditions previously discussed.

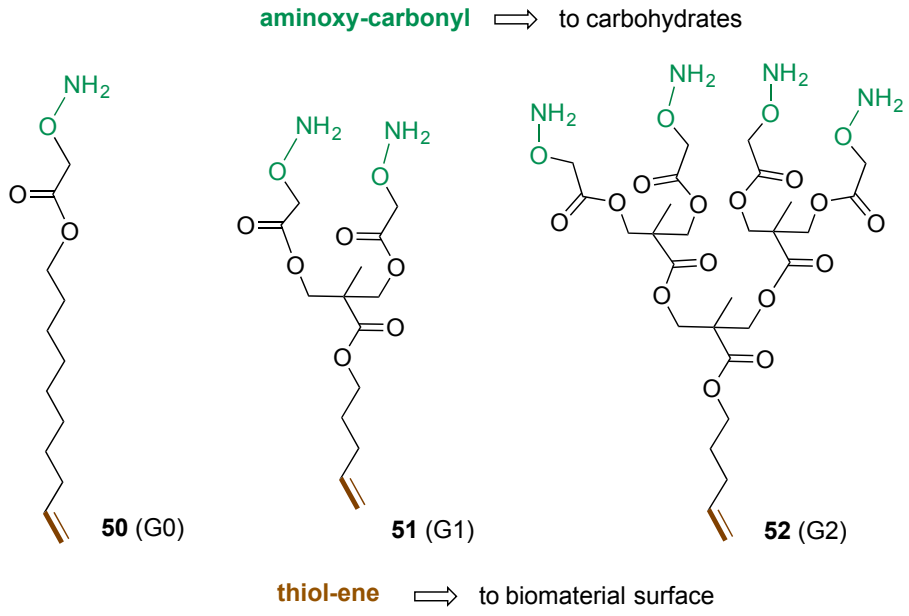

Building Blocks

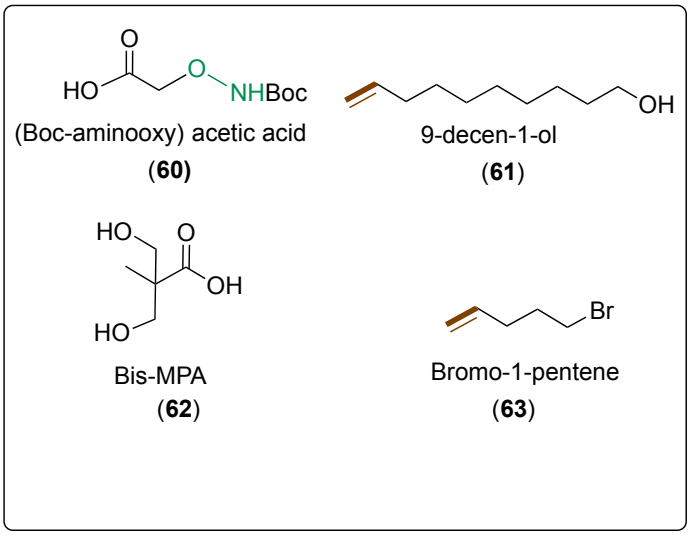

Scheme 4. Structure of G0-G2 dendrons **50**-**52** and building blocks **60**-**63** used for their synthesis.

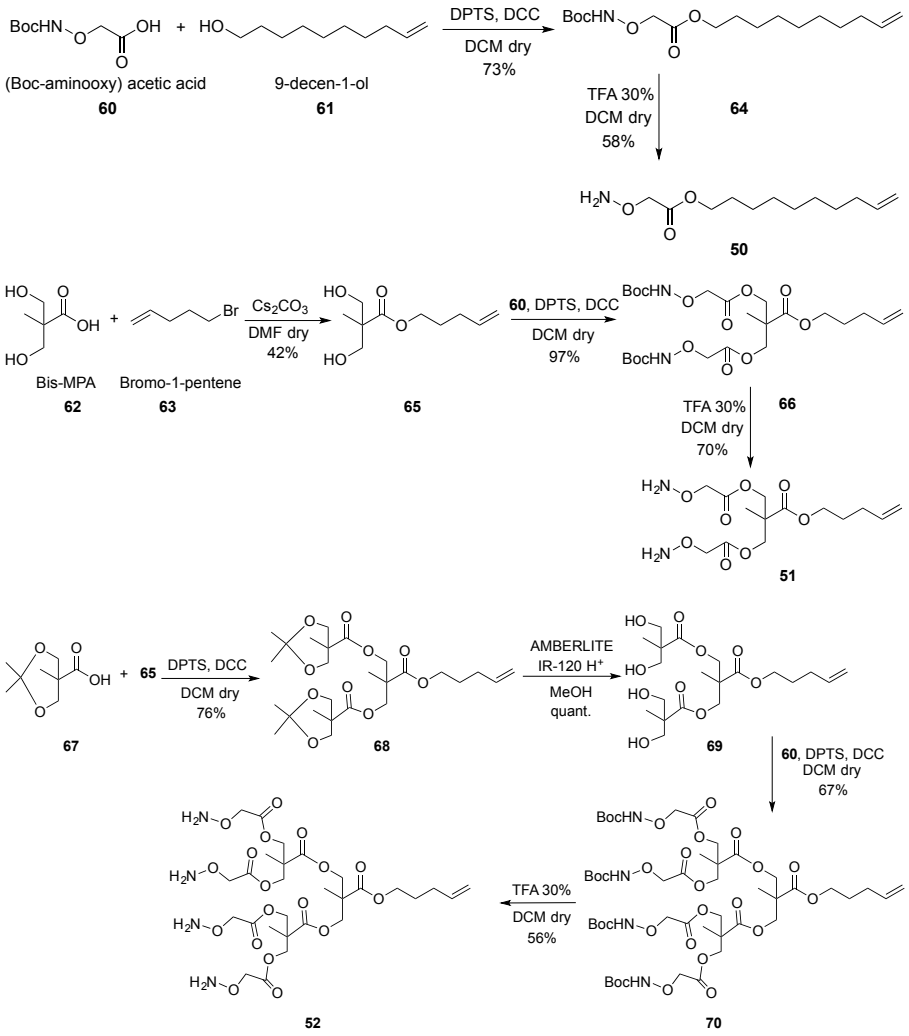

Scheme 5. Synthesis of dendrons **50**–**52**.

Final deprotection of compound (**66**) with TFA (30% in DCM) afforded first generation heterobifunctional dendron (**51**) with 29% overall yield. Finally, second generation heterobifunctional dendron (**52**) was synthetized starting from protected Bis-MPA (acetonide derivative **67**) that was used for coupling with 1,3 diol

65. Deprotection of the acetonide group in the presence of an acidic resin (AMBERLITE IR-120 H^+) afforded tetra-hydroxy intermediate **69** that was used for the subsequent coupling reaction with (Boc-aminooxy) acetic acid (**60**). Final Boc deprotection of **70** in acidic conditions provided G2 dendron (**52**) with 12% overall yield. The subsequent photo-click reaction of thiolated collagen (collagen-SH) with dendrons **50**-**52** was carried out at room temperature for 1 h in a MeOH:H_2O (1:2) solution by irradiation with a UV-lamp @ 365 nm (Raionet®) using 2,2-dimethoxy-2-phenylacetophenone (DPAP) as the radical photoinitiator (Scheme 6) in a 2:1 dendron-DPAP ratio.

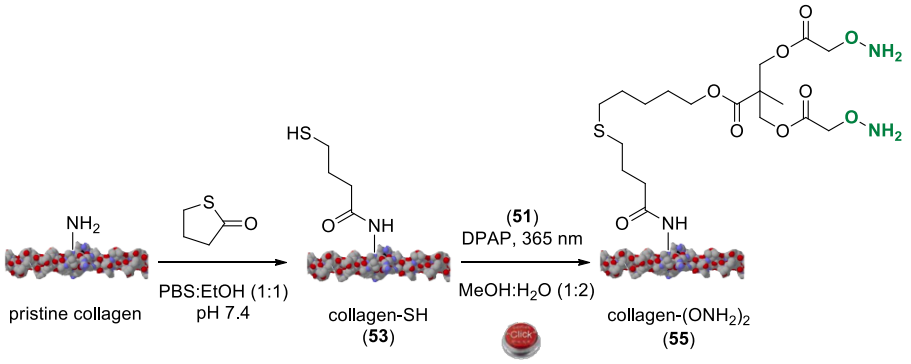

Scheme 6. Synthetic scheme for collagen neoglycosylation exemplified for the G1 dendron (**51**).

Final chemoselective neoglycosylation of the multifunctional collagen patches **54**-**56** was performed using lactose as model saccharide for multivalent functionalization. Given the

equilibrium between the hemiacetal and carbonyl forms of reducing carbohydrates, the alkoxyamino group is able to react with lactose, forming a hydrolitically stable oxime bond[228]. The reaction was carried out at r. t. for 15 h in acetate buffer (pH 4). The effectiveness of the chemical steps and collagen multivalent neoglycosylation was determined by NMR, FTIR spectroscopy and XPS.

Quantification of collagen thiolation was determined by ^{1}H NMR spectroscopy as previously described (Figure 16): 60% of total lysines bears the thiol group needed for the subsequent coupling to heterobifunctional dendrons **50-52**.

XPS (X-ray Photoelectron Spectroscopy) measurements were carried out on collagen patches before and after the neoglycosylation reaction, namely from samples **54** to **57** (1 saccharide), **55** to **58** (2 saccharides) and **56** to **59** (4 saccharides). C1s, O1s, N1s and S2p core level regions were probed, with the aim of investigating the spectral evolution associated with glycosylation. Complete XPS data (Binding Energy, BE, Full Width Half Maximum, FWHM, atomic percents) collected on all samples are reported in Table 6. The most significant signals probing the neoglycosylation reaction effectiveness are C1s and O1s and specifically the peak contributions, identified by curve fitting[229], associated with C-O and C=O functional groups. Therefore, the C1s and O1s core levels data will be discussed here in detail. In Figure 17A and 17B are reported the C1s spectra for the conversion **54→57** and **56→59**.

Table 6: XPS data collected on collagen-$(ONH_2)_n$ and collagen-$(sugar)_n$ samples; core level binding energy (BE), full width at half-maxima (FWHM) and atomic ratio $N_{i(tot)}/N_{N(tot)}$ % values are reported, together with the proposed signal assignments.

Sample	Signal	BE (eV)	FWHM (eV)	Atomic percent [a] (%)	Attribution
#54	C1s	285.00	2.02	64.0	C-C
		286.61	2.02	23.6	C-O, C-N, C-S
		288.81	2.02	12.4	C=O
	O1s	531.00	2.63	38.2	C=O
		532.79	2.63	58.8	C-O
		534.64	2.63	3.0	H_2O
	N1s	400.60	2.21		-NHCO (amide-like) + $-NH_2$
		402.79	2.21		$-NH_3^+$ + O-NH_2
	$S2p_{3/2}$	164.30	3.04		C-S-C (thiol-like)
#55	C1s	285.00	1.78	63.8	C-C
		286.56	1.78	21.4	C-O, C-N, C-S
		288.24	1.78	14.8	C=O
	O1s	530.09	2.05	28.4	C=O
		531.75	2.05	51.0	C-O
		533.28	2.05	20.6	H_2O
	N1s	399.90	1.71		-NHCO (amide-like) + $-NH_2$
		401.05	1.71		$-NH_3^+$ + O-NH_2
	$S2p_{3/2}$	163.31	3.04		C-S-C (thiol-like)
#56	C1s	285.00	1.90	63.3	C-C
		286.68	1.90	21.6	C-O, C-N, C-S
		288.19	1.90	15.4	C=O
	O1s	529.9	2.29	27.4	C=O
		531.55	2.29	53.8	C-O
		233.09	2.29	18.8	H_2O
	N1s	399.79	2.06		-NHCO (amide-like) + $-NH_2$
		401.25	2.06		$-NH_3^+$ + O-NH_2
	$S2p_{3/2}$	163.85	3.22		C-S-C (thiol-like)
#57	C1s	285.00	1.93	53.0	C-C
		286.70	1.93	30.4	C-O, C-N, C-S
		288.85	1.93	16.6	C=O
	O1s	530.37	2.76	24.3	C=O
		531.85	2.76	73.5	C-O
		534.14	2.76	2.2	H_2O
	N1s	400.10	1.75		-NHCO (amide-like) + $-NH_2$ + O-N=C
		402.03	1.75		$-NH_3^+$
	$S2p_{3/2}$	163.83	3.39		C-S-C (thiol-like)
#58	C1s	285.00	1.94	53.0	C-C
		286.70	1.94	30.5	C-O, C-N, C-S
		288.87	1.94	16.5	C=O
	O1s	530.97	2.19	40.1	C=O
		532.55	2.19	51.2	C-O
		534.16	2.19	8.7	H_2O
	N1s	400.75	1.71		-NHCO (amide-like) + $-NH_2$ + O-N=C
		401.89	1.71		$-NH_3^+$

	$S2p_{3/2}$	163.69	2.96		C-S-C (thiol-like)
#59	C1s	285.00	1.93	52.6	C-C
		286.50	1.93	27.9	C-O, C-N, C-S
		288.26	1.93	19.5	C=O
	O1s	530.16	2.06	31.7	C=O
		531.83	2.06	61.7	C-O
		533.30	2.06	6.6	H_2O
	N1s	400.07	1.77		-NHCO (amide-like) + $-NH_2$ + O-N=C
		401.66	1.77		$-NH_3^+$
	$S2p_{3/2}$	163.80	3.20		C-S-C (thiol-like)

[a] atomic percent of spectral components were calculated for C1s and O1s signals only. The intensity of N1s signals arising by thio-ene spacers is too low in comparison with collagen N1s signal to be distinguishable.

In C1s spectra three main spectral components were individuated: the peak at 285.00 eV BE, attributed to aliphatic carbon atoms, was taken as reference for the energy scale; the feature at about 286.5 eV BE is diagnostic for C atoms bonded to more electronegative atoms, as O, N, S: due to the energy resolution of about 1eV, photoelectrons arising by carbon atoms belonging to C-O, C-S and C-N groups contribute to this same feature. The third component (the pronounced shoulder at high BE values - around 288.3 eV), is assigned to C=O or C=N functionalities[230]. It is noteworthy that for all samples the three C1s components appear at the same BE values, with nevertheless different relative intensities. Spectral modifications are evidenced in Figure 17A and 17B (colored arrows); as expected, the intensity of C-O (C-OH or C-O-C) and C=O (or C=N) components increases after glycosylation. The intensity of the feature attributed to C-C, arising mainly by the collagen substrate, slightly decreases due to signal attenuation. As a result, C1s spectra of collagen-$(sugar)_n$ appear larger than the collagen-$(ONH_2)_n$. The composition of each

signal, expressed as atomic percent of signal components, was also calculated.

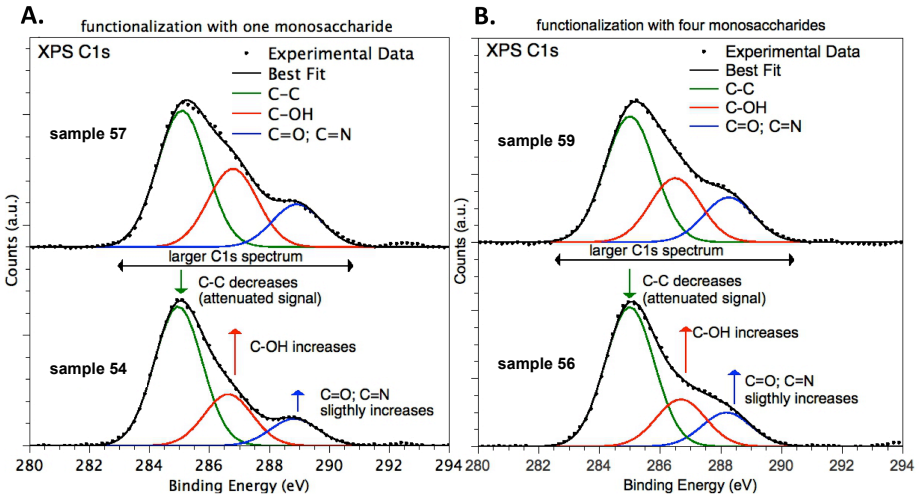

Figure 17. (A) C1s XPS spectra of samples **54** and **57**, showing intensities variation of C1s components upon functionalization with 1 monosaccharide. (B) Same as (A), upon glycosylation with 4 monosaccharides (samples **56** and **59**).

The estimated values resulted in a trend associated with the glycan insertion: for all couples of collagen-$(ONH_2)_n$ – collagen-$(sugar)_n$ samples, the C-O component intensity increases more than C=O (C=N) upon monosaccharides insertion. For example, from sample **54** to sample **57** C-C% goes from 64.0% to 53.0%, C-O% from 23.6% to 30.4%, (C=O + C=N)% from 12.4% to 16.6%. For the couple **56→59**, C-C% goes from 63.3% to 52.6%, C-O% from 21.3% to 37.9%, (C=O + C=N)% from 15.4% to 19.5%. XPS

O1s data analysis is in excellent agreement with this finding (O1s spectra of samples **56** and **59** are reported in Figure 18).

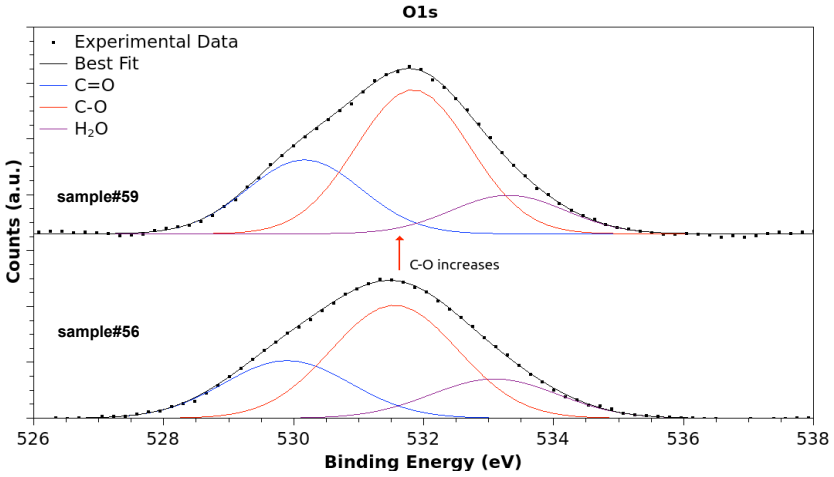

Figure 18. XPS O1s spectra of samples #**56** and #**59**; the intensity of the spectral component attributed to C-O groups increases with glycosylation. The same trend is observed for all samples.

For all samples, three O1s spectral components were identified, and respectively ascribed to C=O (BE ≈ 530 eV), C-O-like oxygen (nearly 532 eV BE) and physisorbed water (≈ 533.5 eV BE)[231]. The semiquantitative analysis confirms the increase of C-O groups amount with respect to carbonyl-like ones[232] going from collagen-$(ONH_2)_n$ to collagen-$(sugar)_n$ samples. For example, for sample **56** C=O% = 63.3%, C-OH% = 21.6%, whereas for sample **59** C=O% = 52.6%, C-OH% = 27.9%. Collagen patches have been investigated also by FTIR spectroscopy in attenuated total reflection (Figure 19).

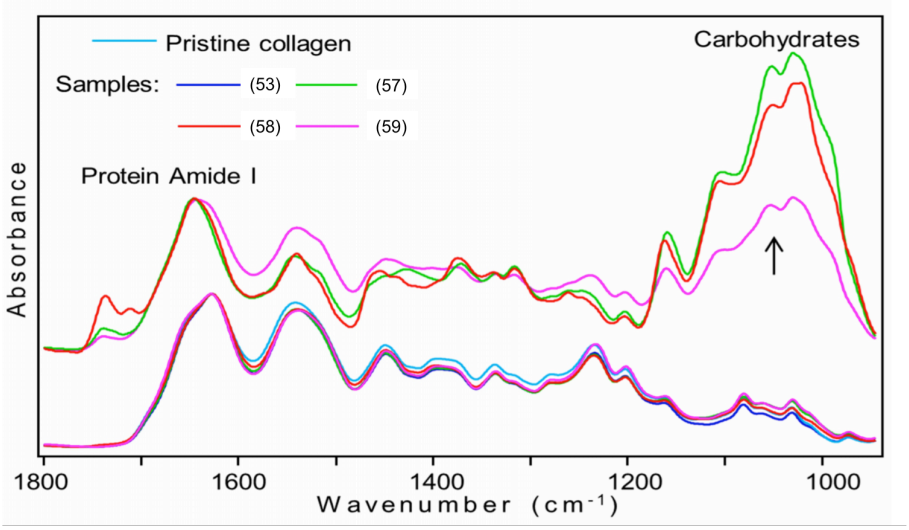

Figure 19. FTIR absorption spectra of intact collagen patches (bottom spectra) and of the sample external layers (upper spectra), reported after normalization at the maximum of the Amide I band.

FTIR spectroscopy has been widely employed for the study of protein secondary structures, glycosylation, and glycation. In particular, protein secondary structures can be studied through the analysis of the Amide I band (due to the C=O stretching vibrations of the peptide bonds) that occurs in the 1700-1600 cm^{-1} spectral region [233]. Noteworthily we found that the IR spectra of the external layers from samples (**57**), (**58**), and (**59**) displayed a higher absorption in the 1200-900 cm-1 spectral region, where the carbohydrate marker band of glycosylated and glycated proteins occurs[234], compared to the pristine collagen and to the intact patches of treated collagen. These results clearly indicate that the neoglycosylation of collagen successfully took place, even

if this FTIR approach allowed only a qualitative evaluation of the carbohydrate content. Moreover, the FTIR spectra of intact collagen patches displayed almost over-imposable Amide I band, suggesting that the overall protein secondary structures were mostly maintained after the sample treatments. Absorption spectra were baseline corrected between 1800 cm^{-1} and 900 cm^{-1} and normalized at the Amide I band maximum to compensate for the different protein content. In order to exclude chemisorption of lactose to the material surface we report here the FTIR spectra of pristine and thiolated (**53**) collagen reacted with lactose in the absence of the alkoxyamino dendron (Figure 20).

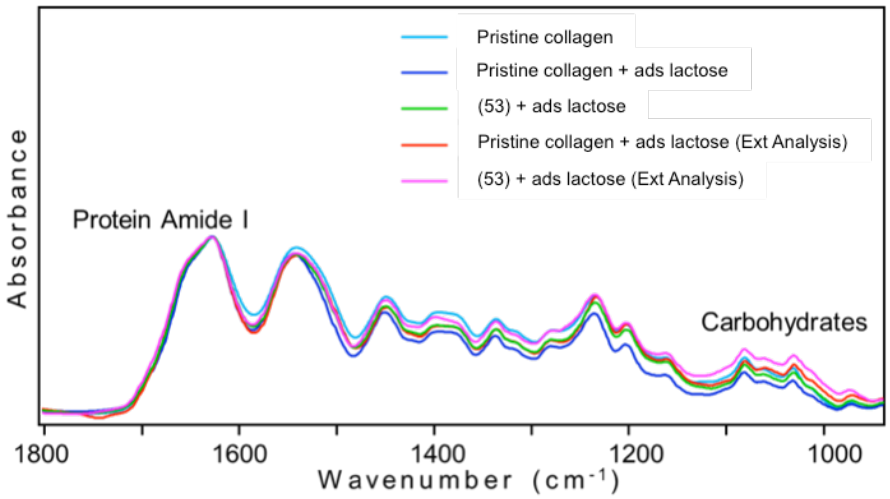

Figure 20. FTIR spectra of collagen and thiolated collagen (**53**) treated with lactose.

ATR/FTIR analyses were performed on all the samples both on intact collagen patches and on their external layers. As shown in Figure 20, no significant increase of the absorption bands in the 1200-900 cm^{-1} spectral region is evident in the recorded spectra. This result clearly indicated the absence of adsorbed carbohydrates. Furthermore, in order to demonstrate both the functionalization and at the same time suitable exposition of the galactose unit, Enzyme-Linked Lectin Assay (ELLA)[179e] was performed, using peroxidase labelled lectin from peanut (*Arachis hypogaea*). Absorbance values at 450 nm confirmed the presence and correct exposition of galactose units (Figure 21).

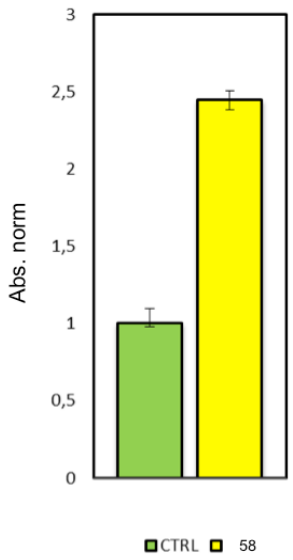

Figure 21. ELLA assay on sample **58** with Arachys hypogaea (PNA) lectin conjugated with horse radish peroxidase (PNA-HRP) (abs. at 450 nm).

2) Synthesis of multiglycosylated dendrons as ligands of *P. aeruginosa* LecB.

In the search of new high affinity ligands of *P. aeruginosa* LecB, I designed and synthetized three new dendrons of generation 0, 1 and 2 possessing a double bond at the focal point and a carbonyl group at the termini. The heterobifunctional dendrons were designed in order to have bio-orthogonal functional groups: in particular, a double bond was placed as the focal point, for further conjugation by thiol-ene chemistry to the desired matrix, whereas carbonyl groups at their termini can be exploited for multivalent carbohydrate functionalization[226] through reductive amination, oxime or hydrazone formation to properly functionalized saccharides (Figure 22). In order to evaluate our glycoconjugate dendrons interactions with LecB, and given the relevance of L-fucose in mammal oligosaccharides, α-L-(2-aminoethyl) fucoside (**74**)[235] and α-*O*-L-fucopyranosyl oxyamine (**75**)[236] were used as sample monosaccharides for dendron conjugation (Scheme 7). Zero, first and second generation heterobifunctional dendrons (**71-73**) were synthesized starting from 9-decen-1-ol (**61**) or selected building blocks **65** and **69** through esterification reactions with levulinic acid (**82**) (Scheme 8). Building blocks (**65** and **69**) were synthesized respectively in 1 and 3 steps starting from bis-(hydroxymethyl)propionic acid (bis-MPA) and bromo-1-pentene, as previously reported in Scheme 5. G0, G1 and G2 heterobifunctional dendrons (**71-73**) were obtained in 99%, 35% and 18% overall yields, respectively.

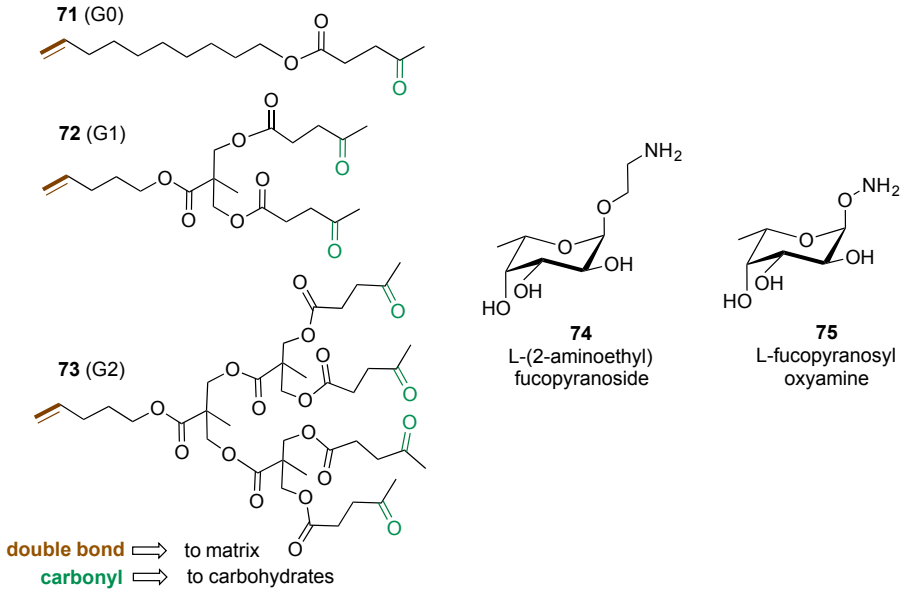

Figure 22. Synthesized G0, G1 and G2 dendrons and functionalized saccharides (**74**-**75**) used for carbonyl conjugation.

α-L-(2-aminoethyl) fucopyranoside (**74**) and α-*O*-L-fucopyranosyl oxyamine (**75**) were synthesized, respectively in 4 and 5 steps from commercial L-fucopyranose, following the procedures already reported by Flitsch and co-workers[235] and Dumy and co-workers[236] (see Experimental Part 7.2). Derivative **74** and **75** were obtained in 31% and 14% overall yield respectively. α-L-(2-aminoethyl) fucopyranoside (**74**) was first conjugated to G0 dendron (**71**) by reductive amination in the presence of $NaCNBH_3$ (Scheme 9).

The reaction afforded the desired glycosylated dendron (**76**) in 27% yield.

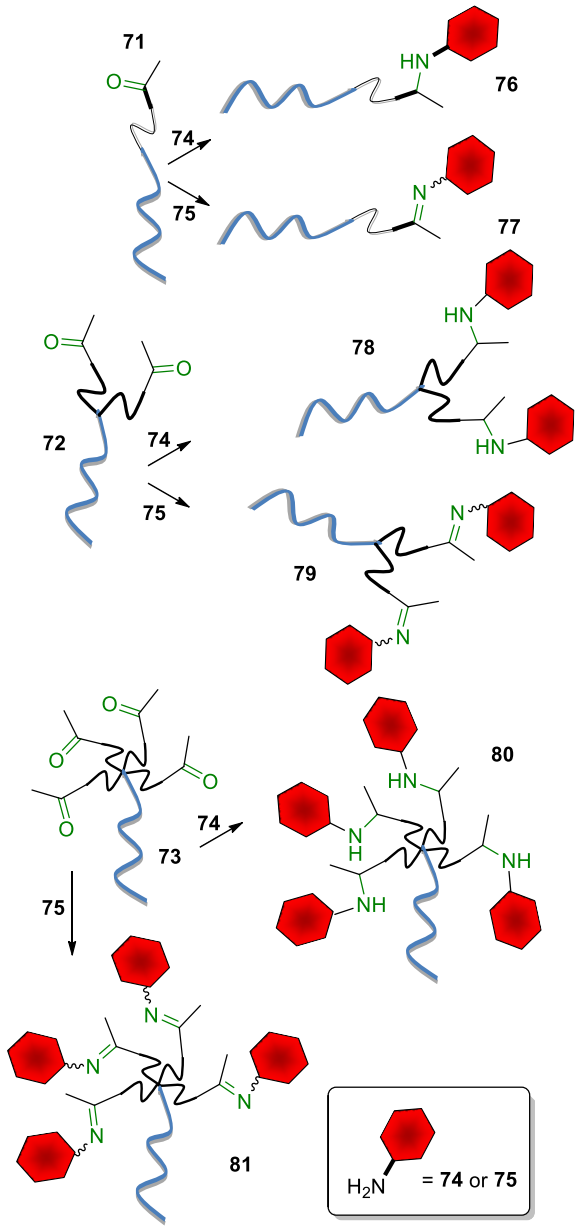

Scheme 7. Schematic depiction of dendron conjugation to saccharides via carbonyl chemistry.

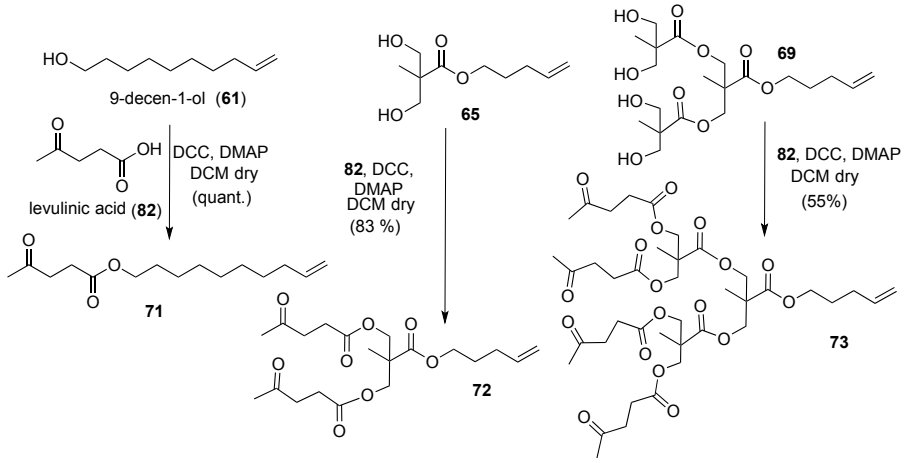

Scheme 8. Synthesis of heterobifunctional dendrons (**71-73**).

The very low yield was attributed to the competing carbonyl reduction to the corresponding alcohol **83**, as byproduct. The same reaction on the G1 dendron (**72**) gave an even more complex mixture of products, that were identified by mass spectroscopy (System Applied Biosystems MDS SCIEX instruments: Q TRAP, LC/MS/MS, turbo ion spray and Q STAR elite nano spray) performed directly on the TLC spots following literature procedures [237]. By mass values, the mixture was composed by the desired fucosylated dendron **78**, together with monoglycosylated derivatives **84** and **85** and alcohol **86** and **87**. In order to reduce the formation of alcohol byproducts, a "milder" reducing agent as $Na(AcO)_3BH$ was employed, without any success. Given the large extent of by-products formation and the low efficiency of glycoconjugation to G0 and G1 dendrons by reductive amination, we decided to evaluate the possibility to

obtain better conjugation yields by oxime ligation.

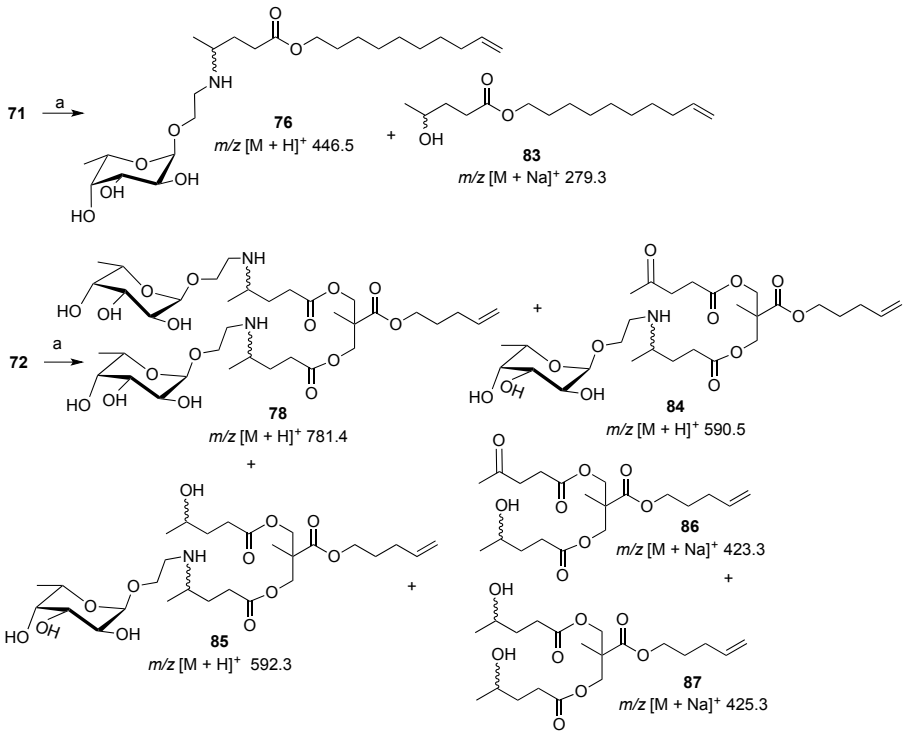

Scheme 9. Dendron conjugation to fucose moieties by reductive amination. Reagents and conditions: (a) **74**, Na_2SO_4 3 M, AcOH, $NaCNBH_3$, EtOH, 80°C, 6h.

Thus, G0, G1 and G2 dendrons (**71**-**73**) were reacted with α-*O*-L-fucopyranosyl oxyamine (**75**) in citrate buffer at pH = 3.5[238] (Scheme 10).

Initially, due to their partial hydrophobic nature, dendrons **71**-**73** do not fully dissolve in the buffer, and the solution is not completely clear till the reaction is over.

All of the dendrons **71**-**73** were reacted overnight at room temperature with α-*O*-L-fucopyranosyl oxyamine (**75**), affording the desired glycoconjugates **77**, **79** and **81** in quantitative yields.

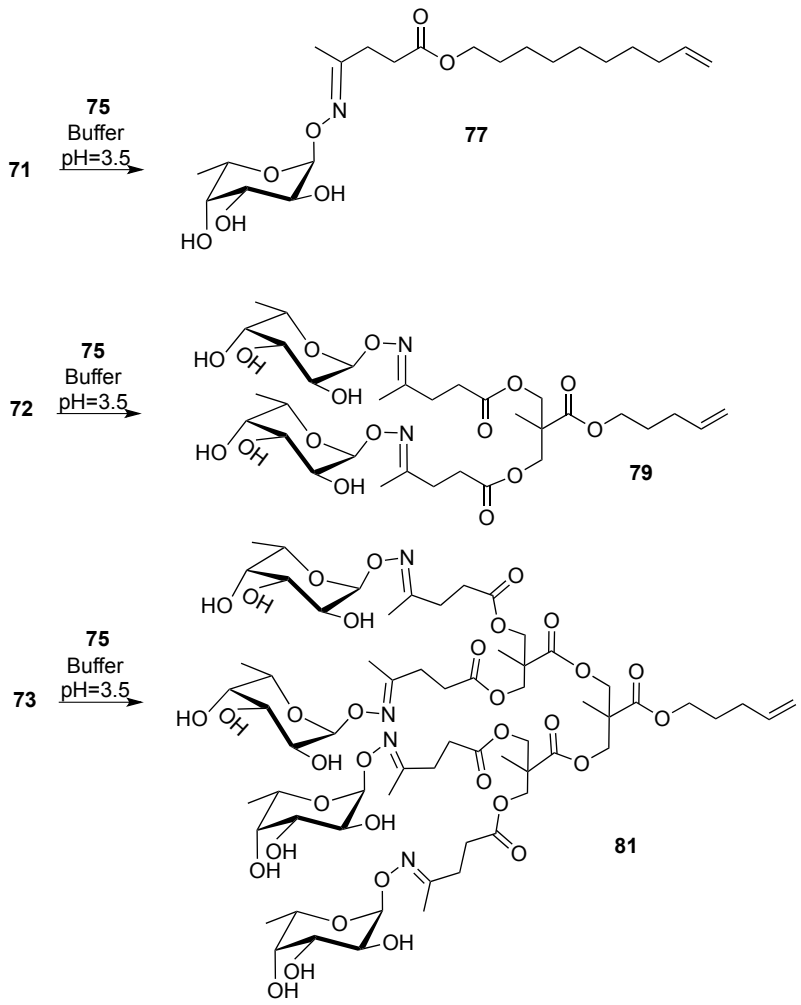

Scheme 10. Dendron conjugation to fucose via oxime ligation (Buffer = Citrate Buffer).

Once obtained our glycosylated dendrons **77**, **79** and **81** we evaluate their affinity as ligands of *P.aeruginosa* LecB, studying their binding properties by isothermal titration calorimetry (ITC). Compounds **77**, **79** and **81** were used for titration microcalorimetry in order to determine the stoichiometry and thermodynamic contribution of the binding in solution. Typical thermograms obtained with the three compounds are displayed in Figure 23. All three compounds displayed low- or sub-micromolar affinities. Analysis of the thermodynamic contributions (Table 7) indicates that the divalent compound behaves very well with a stoichiometry of 0.5 (compound/lectin monomer) and an affinity 10 times better than the monomeric compound (K_d = 0,128 μM for **79** and 1,18 μM for **77**). The affinity is not huge (Renaudet and co-workers reported a dissociation constant of 28 nM for hexadecavalent glycocluster **49**, see Table 5) but still very good. The enthalpy of binding is twice the one for the monovalent compound, indicating that both fucose are efficiently recognized; the entropy cost is high but does not compensate fully. There is some visible aggregation so the compound is bridging tetramers in solution. As for the tetravalent compound **81**, it resulted less efficient. The stoichiometry indicates that all fucose are reaching lectin binding sites, but clearly not very efficiently since the enthalpy is not four times the one of the monovalent compound. It is probable that the molecule is a little bit crowdy and some steric hindrance/constrains prevent all of 4 fucose to be in perfect orientation in binding site.

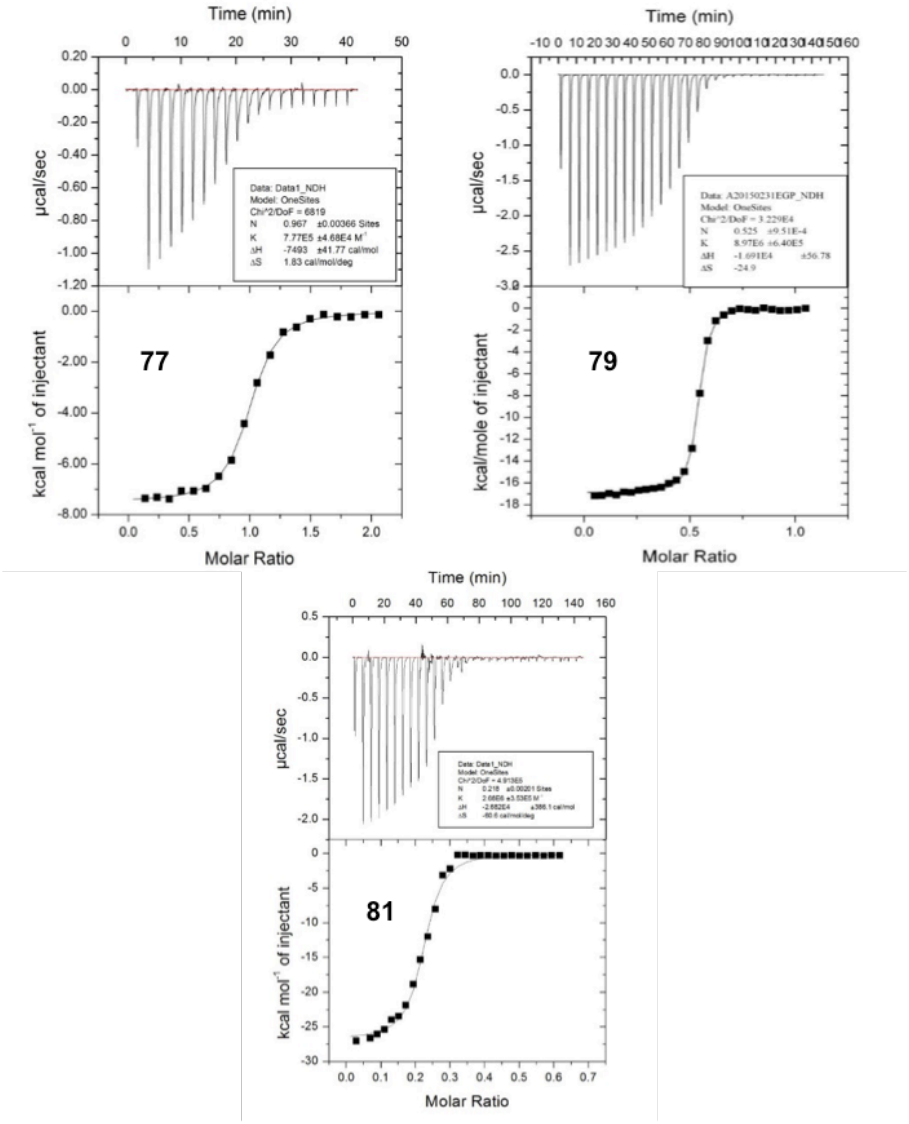

Figure 23. Three selected thermograms for compounds **77**, **79** and **81** with integration of peaks and fit with one–site model. Top: thermograms obtained by injections of lectin LecB (0.1 mM) in solution of compounds **77**, **79** and **81**. Bottom: corresponding integrated titration curves.

On top, entropy takes its part, so finally the tetravalent has lower affinity than the divalent (K_d = 0,279 μM for compound **81**).

Table 7. Isothermal Titration Microcalorimetry data for glycoconjugates binding to LecB. Each measure has been done in duplicate and deviations are given for the data directly fitted from the curve.

comp.	val.	n	K_d (mM)	ΔG (KJ/mol)	ΔH (KJ/mol)	-TΔS (KJ/mol)
77 (1mM)	1	0.94±0.02	1.18±0.10	-33.8	-31.6±0.2	-2.2
79 (0.5mM)	2	0.51±0.02	0.128±0.016	-39.4	-71.2±0.4	-31.8
81 (0.3mM)	4	0.23±0.02	0.279±0.094	37.5	-109±3	-71.5

5.1. Synthesis of glycosylated Pluronic block copolymers as antitumor drugs carriers: Introduction

Cisplatin (*cis*-diamminodichloroplatinum(II), Figure 24), accidentally discovered in the late 1960s, is one of the first anticancer metallopharmaceuticals and its clinical introduction represented a major landmark in the history of successful anticancer drugs[239]. At present, it is one of the most largely employed anticancer drugs as it is effective in the treatment of 70-90% of testicular and, in combination with other drugs, of ovarian, small cell lung, bladder, brain, and breast tumors. The attainment of cisplatin led to the synthesis and biological evaluation of many thousands of platinum- and non-platinum-based compounds. Nevertheless, almost forty years after the first report on the biological activity of cisplatin, only its two additional analogues, carboplatin and oxaliplatin (Figure 24), are in routine clinical use worldwide [240] with a leading role in contemporary medical oncology as the best-selling anticancer drugs of the world[241].

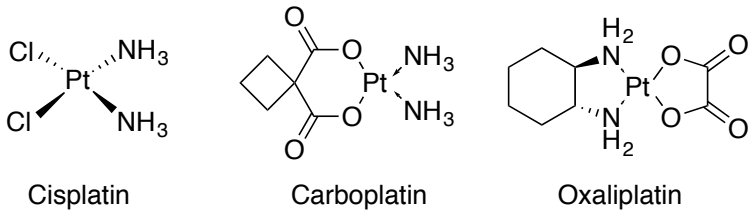

Cisplatin Carboplatin Oxaliplatin

Figure 24. Structures of cisplatin, carboplatin and oxaliplatin.

On the other hand, the use of cisplatin in the curative therapy is often associated with some severe clinical problems, such as serious normal tissue toxicity (in particular oto- and nephrotoxicity), neuropathy, myelosuppression, alopecia, nausea and vomit, and with the frequent occurrence of either intrinsic or acquired resistance to the treatment[240]. The most relevant adverse side effect is nephrotoxicity correlated to platinum binding and inactivation of renal thiol-containing enzymes[239, 242]. Moreover, the activity of the anticancer agents is mainly limited by the development of drug resistance, as tumour cells are a rapidly changing target because of their genetic instability, heterogeneity and high rate of mutation, leading to selection and overgrowth of a drug-resistance tumour cell population[243]. Anyway, the success of cisplatin in anticancer chemotherapy has raised great interest in the study of metal complexes as antitumor agents, prompting the ongoing investigation of alternative metal-based drugs[243, 244, 245, 246]. Therefore, the main aims of the development of novel metal-based drugs are the reduction of the side effects of cisplatin, and the enhancement of their effectiveness against cisplatin-resistant tumors[247].

Gold compounds as antitumor agents

Gold complexes have recently gained increasing attention among the non-platinum antitumor agents, because of their strong inhibitory effects on tumor cell growth, generally achieved by exploiting non-cisplatin-like pharmacodynamics and

pharmacokinetic properties and mechanisms of action[248, 249]. Owing to their traditional use in medicine for the treatment of rheumatoid arthritis, gold derivatives are suitable candidates as potential alternatives to platinum drugs. In fact, the investigation of the efficacy of anticancer drugs, e.g. 6-mercaptopurine and cyclophosphamide, in the treatment of rheumatoid arthritis arose from their known immunosuppressive and antiinflammatory actions, thus establishing, at least in principle, a connection between the two therapies[250]. Many studies have been performed onto the antitumor activity of (phosphine)gold(I) thiolates, such as the well-known antiarthritic drug Auranofin, and most of them have been shown to have useful antitumor activity *in vitro* but, unfortunately, very limited efficacy *in vivo*[251]. Certainly, there are other reasons for the study of the antitumor activity of gold compounds. A commonly cited reason relates to the fact that gold(III) complexes show chemical features that are very close to those of clinically established platinum(II) derivatives; gold in the + 3 oxidation state is isoelectronic with platinum(II), possessing the typical d8-electronic configuration, and tetracoordinate gold-(III) complexes are found in square-planar geometries[252, 253, 254, 255] resembling, in this regard, the situation found for cisplatin itself. Surprisingly, despite the strict similarity, few literature data exist on the use of gold(III) complexes as anticancer agents[256, 257, 258], probably because of their high redox potential and relatively poor stability, which make their use rather problematic under physiological conditions. Screening for cytotoxicity/antitumor

activity of gold(III) complexes dates back to the mid-1970s, but a renewed interest is evident, judging from the number of recent papers on the subject. For example, four complexes, namely trichloro-(2-pyridylmethanol)gold(III), dichloro(2-pyridylmethanol)-gold(III), dichloro(*N*-methylsalicylaldiminate)gold(III), and dichloro(*N*-ethylsalicylaldiminate)gold(III), have showed an interesting cytotoxicity level toward a series of established human tumor cell lines tested and only minimal crossresistance with cisplatin has been observed[259]. Also some gold(III) complexes with multidentate ligands (that is, 1,2-ethylendiamine, diethylentriamine, 1,4,8,-11-tetraazacyclotetradecane, terpyridine, phenanthroline, and bipyridyl) have displayed relevant cytotoxic effects toward a panel of established human cell lines, either cisplatin-sensitive or -resistant, allowing further investigation, such as solution chemistry and DNA binding properties[260, 261].

Ruthenium compounds as antitumor agents

In latest years, ruthenium compounds have attracted much attention as promising antitumor and antimetastatic drugs[262]. Although it belongs to the same group, ruthenium shows a number of differences with platinum[263]. In fact, several ruthenium compounds are active against cisplatin-resistant tumours[264], probably due to a different mechanism of action To date, two ruthenium-based complexes have successfully completed phase I clinical trials and entered phase II[265]: NAMI-A (imidazolium-*trans*-

[tetrachloro-(*S*-dimethyl-sulfoxide)(1H-imidazole)-ruthenate(III)]) [266] and KP1019 (indazolium[*trans*-tetrachlorobis(1H-indazole)ruthenate(III)])[267]. NAMI-A took part in clinical trials for the treatment of non-small-cell lung cancer (NSCLC) [268] . NSCLC includes squamous cell carcinoma, adenocarcinoma and large cell-undifferentiated carcinoma, and accounts for about 80–85% of all cases of lung cancer, representing the most common cause of death in men and second, after breast cancer, in women[269]. The prognosis for patients with advanced NSCLC is extremely poor and up to platinum-based combination chemotherapy[270], no single drug or drug combination proved to enhance survival or quality of life[271]. NAMI-A lacks of direct cytotoxicity on tumour cells and of significant effect in reduction of primary tumour mass growth. Nevertheless, it is effective on lung metastasis. The mechanism of action, not yet completely elucidated, seems to be correlated with an anti-angiogenic activity that was proven both *in vitro* on endothelial cell functions and *in vivo* with the chorioallantoic membrane (CAM) model[272]. Unlike NAMI-A, KP1019 is significantly cytotoxic *in vitro* and it was proven to induce apoptosis mainly through an intrinsic mitochondria pathway[273]. The activity of KP1019 seems to be partially due to a transferrin-mediated drug transport mechanism, having KP1019 a strong affinity for the transferrin iron-binding pockets[274]. Ruthenium-based chemotherapeutics are making important progresses in clinical trials because of their high delivery in cancer cells, as well as their low systemic toxicity.

Ruthenium is capable to mimic iron in binding to different serum proteins, such as transferrin and albumin[262]. Cancer cells have a greater requirement for iron compared to healthy ones, because they are rapidly dividing cells. This condition promotes the up-regulation of the number of transferrin receptors on cell surface. Accordingly, an important increase of the ruthenium concentration in cancer cells has been demonstrated by *in vivo* studies [275] . Furthermore, under physiological conditions, ruthenium offers a wide range of oxidation states stabilized by different coordination spheres. For example, the antitumor activity of ruthenium(III) species for both NAMI-A and KP1019 is triggered by the reduction to the corresponding ruthenium(II) counterparts *in vivo*[262]. Cancer cells have a lower oxygen concentration, a higher level of glutathione and a lower pH value than normal tissues; this creates a strongly reducing environment, that allows to modify the redox potential of ruthenium, reducing the inactive Ru^{III} species to Ru^{II}[263, 276]. This redox process could involve the oxidation of some biomolecules generating the apoptotic cascade. Sulfur-containing biomolecules, such as cysteine, methionine, glutathione, metallothionein and albumin, play an important role in platinum anticancer chemotherapy because of their high affinity to the soft metal ion. These interactions are commonly believed to have negative effects on the therapeutic efficacy, cause strong and irreversible binding of the metal to intracellular thiolato ligands is considered as a major inactivation step[277]. Furthermore, they have also been related to

drug detoxification, nephrotoxicity and resistance. In this regard, a number of thiol-based and sulfur-containing nucleophiles have been tested as chemoprotectants to modulate cisplatin nephrotoxicity and some of them seem promising for clinical use[242]. Positive outcomes were obtained with sodium diethyldithiocarbamate that was shown to provide protection against renal, gastrointestinal and bone marrow toxicity induced by cisplatin, without decreasing the antitumor activity[278]. Anyway, the selective protection of normal tissues with no inhibition of the drug anticancer activity was proven to be challenging.

Pluronic block copolymers as micellar nanocarriers for drug delivery

Polymer-based nanotechnology became one of the most interesting and fast growing areas of pharmaceutical research. Materials currently being researched include polymer micelles, polymer-DNA complexes ("polyplexes"), nanogels, liposomes, and other nanoscale sized materials for medical use that are collectively called nanomedicines. Specific arrangements of polymeric molecules at the nanoscale achieved within such materials constitute unique opportunities for safe and efficient delivery of drugs, genes, and imaging molecules[279, 280, 281, 282, 283, 284, 285, 286, 287, 288, 289, 290, 291]. One promising example of such polymer nanomaterials is represented by a class of Pluronic block copolymers (also known as "poloxamers"). These block copolymers consist of hydrophilic poly(ethylene oxide) (PEO) and

hydrophobic poly(propylene oxide) (PPO) blocks disposed in A-B-A tri-block structure: PEO-PPO-PEO (Figure 25). The block copolymers are characterized by different hydrophilic-lipophilic balance (HLB), depending on the different numbers of hydrophilic ethylene oxide and hydrophobic propylene oxide units. Due to their amphiphilic character these copolymers exhibit surfactant properties as the ability to interact with hydrophobic surfaces and biological membranes. At concentrations above critical micelle concentration (CMC) in aqueous solutions, these copolymers self-assemble into micelles whose diameters usually vary from ca. 10 nm to 100 nm[292].

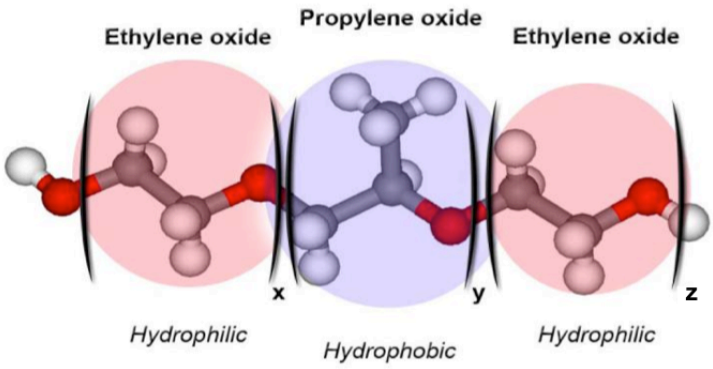

Figure 25. General structure of Pluronic block copolymer.

The core of the micelles, consisting of hydrophobic PPO blocks, is separated from the aqueous exterior by the shell hydrated of hydrophilic PEO chains. By itself the core represents a "cargo hold" for incorporation of different therapeutic or diagnostic

reagents (Figure 26), being able to incorporate considerable amounts (up to 20-30 % wt.) of water-insoluble drugs[293]. The PEO shell decreases undesirable drug interactions with cells and proteins and ensures that the micelles remain in a dispersed state. Incorporation of low molecular mass drugs into Pluronic micelles can enhance drug solubility and drug stability, and improve drug pharmacokinetics and biodistribution. Polymeric micelles were exploited for delivery of CNS drugs across the blood brain barrier (BBB)[294, 295], oral delivery of drugs[296, 297, 298] and tumor-specific delivery of antineoplastic agents[299, 300, 301].

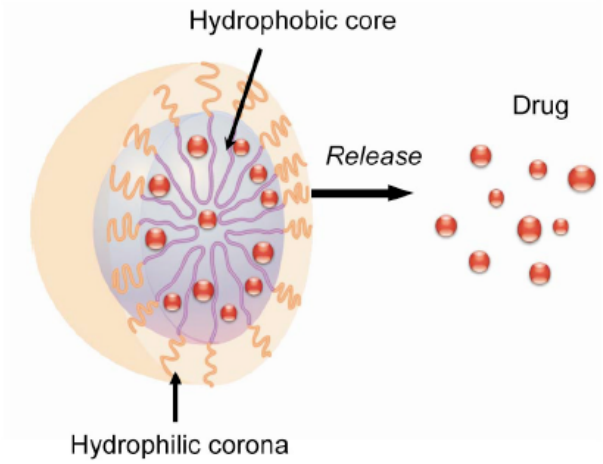

Figure 26. Micelle with a solubilized drug.

In one early study, for example, neuroleptic drug loaded Pluronic P85 micelles were targeted to the brain by conjugating the micelles with neurospecific antibodies or insulin as targeting

moieties[302]. An improvement of oral bioavailability of a poorly water-soluble phytoestrogen, like genistein, was achieved by encapsulation of this drug into Pluronic F127 micelles[298]. Pluronic block copolymers were also reported to notably improve the bioavailability of various antibacterial and antifungal drugs and to enhance the activity of these drugs with respect to many microorganisms [303, 304, 305, 306]. In application to anticancer chemotherapy, drug incorporation in micelles can diminish drug extravasation into normal tissues and provide for a passive drug targeting to tumors via the enhanced permeability and retention (EPR) effect. The abnormally high permeability of tumor blood vessels, combined with prolonged circulation of the micelles due to their decreased extravasation in normal vessels and lack of renal clearance, are at the basis of EPR effect. The first anti-cancer micellar formulation to reach clinical evaluation was SP1049C containing doxorubicin (Dox) in the mixed micelles of Pluronics L61 and F127[307]. More efficient accumulation of micellar drug in the tumors, compared to the free drug, was demonstrated by the analysis of pharmacokinetics and biodistribution of Dox incorporated into these micelles. Moreover, this study indicated that the peak levels of Dox formulated with SP1049C in the tumor were delayed and the drug residence time was increased in comparison with the free Dox[299]. Enhancement of drug anticancer effect in *in vivo* tumor models was also observed for formulation of Dox, paclitaxel or other drugs with Pluronic micelles[299, 308, 309, 310]. Results obtained in these studies showed that the tumors were

more responsive to Pluronic/Dox than to Dox alone. Another study reported that micellar solutions of Pluronic P85 and L61 enhanced carboplatin (CPt) toxicity in the experimental colorectal carcinoma *in vivo*[301, 311]. The polymers used for drug delivery were considered as biologically inert components that prevent drugs degradation, prolong exposure of drugs to tissues, and increase transport of drugs into cells. However, this paradigm is undergoing substantial evolution due to growing evidence that select synthetic polymers can drastically modify specific cellular responses[312, 313, 314]. In fact, Pluronic block copolymers were shown to be potent biological response modifiers able of sensitizing multidrug resistant (MDR) cancer cells and enhancing drug transport across cellular barriers, such as polarized intestinal epithelial cells, Caco-2, and brain endothelium[315, 316]. The intricate mechanisms of Pluronic effects in MDR cells were closely studied. It was demonstrated that Pluronic block copolymers were able to:

1) Incorporate into membranes changing its microviscosity;
2) Induce a strong reduction in ATP levels in cancer and barrier cells;
3) Inhibit drug efflux transporters, such as Pgp[315, 317, 318, 319, 320], multidrug resistance proteins (MRPs)[321], and breast cancer resistance protein (BCRP)[322, 323];
4) Induce release of cytochrome C and enhancement of reactive oxygen species (ROS) levels in the cytoplasm;
5) Increase proapoptotic signaling and decreasing anti-apoptotic defense in MDR cells[324];

6) Inhibit the glutathione/glutathione S-transferase detoxification system[318, 321];
7) Abolish drug sequestration within cytoplasmic vesicles[309] (Figure 27).

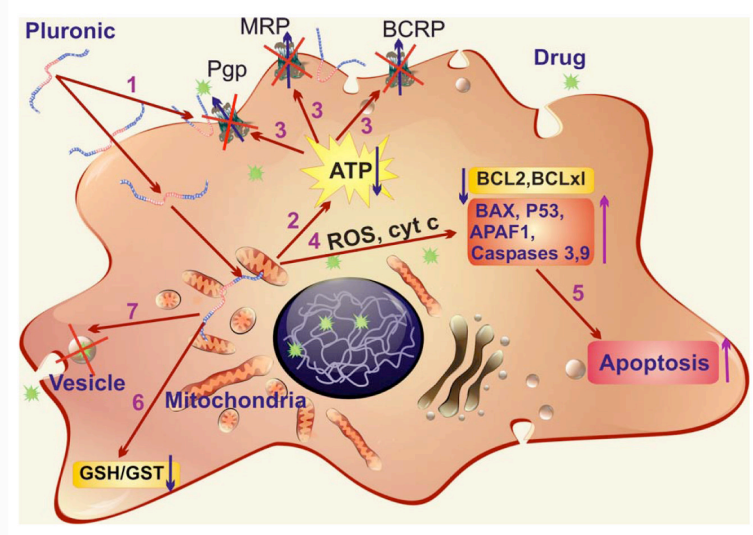

Figure 27. Multiple effects of Pluronic block copolymers in MDR cells: 1) incorporation of Pluronic molecules into membranes and decrease of the membrane microviscosity; 2) induction of ATP depletion; 3) inhibition of drug efflux transporters; 4) release of cytochrome C from mitochondria and increase in ROS levels in cytoplasm; 5) increase of pro-apoptotic signaling and decrease of anti-apoptotic defense in MDR cells; 6) inhibition of the glutathione/glutathione S-transferase detoxification system; and 7) abolishment of drug sequestration within cytoplasmic vesicles.

Remarkably, these effects were most apparent at polymer concentrations below the critical micellization concentration CMC[325, 326] suggesting that unimers, i.e. single block copolymer molecules, are responsible for biological modifying properties (CMC for Pluronic P85 is 0.03%wt). The crucial role of unimers (but not micelles) is determined by their ability to incorporate and translocate across the cellular membranes[318, 327] . The hydrophobic PPO chains of Pluronic immerse into the membrane hydrophobic areas, inducing alterations of the membrane structure, and decreasing its microviscosity ("membrane fluidization"). Contrarily, formation of micelles at high concentrations of the block copolymer results in hiding these hydrophobic PPO chains in the micellar core and decreases Pluronics availability to affect the cellular membranes. Recently, it was also shown that Pluronic block copolymers can prevent the development of MDR in the cancer cells exposed to the drug[328]. This further increases the potential benefits of using such formulations for chemotherapy of cancer tumors; if resistance is intrinsic, Pluronic sensitizes the tumor, whereas if resistance is acquired, MDR cells no longer have a selective advantage.

5.2. Synthesis of glycosylated Pluronic block copolymers as antitumor drugs carriers: Results and discussion

As just described in the introduction of this section, encapsulation of antitumor drugs into Pluronic micelles constitutes a smart strategy to increase drug solubility and stability and improve drug pharmacokinetics, biodistribution and bioavailability. In addiction, in application to anticancer chemotherapy, it can diminish drug extravasation into normal tissues and provide for a passive drug targeting to tumors via the enhanced permeability and retention (EPR) effect: in this way, it's possible to obtain a more efficient accumulation of micellar drug in the tumors compared to the free drug. Finally, the use of Pluronic block copolymers can sensitize multidrug resistant (MDR) tumor (if the resistance is intrinsic) and prevent the development of MDR in the cancer cells exposed to the drug (if the resistance is acquired). The aim of my work was to synthetized new functionalised Pluronic block copolymers in order to introduce also an active targeting on the polymeric carriers. The synthetic strategy involved the introduction of an appropriate linker on the polymer that could be conjugate to the biomolecule of interest (Figure 28). Pluronic F127 was the block coploymer choosen for this project while glucose was the selected biomolecule for polymer functionalization. In fact, it's now well known that glucose is transported into the cell via facilitative glucose transporters (GLUT) present in all cell types. Due to the ubiquity of these

transporters, their differential expression is involved in various disease states such as diabetes, ischemia and cancer.

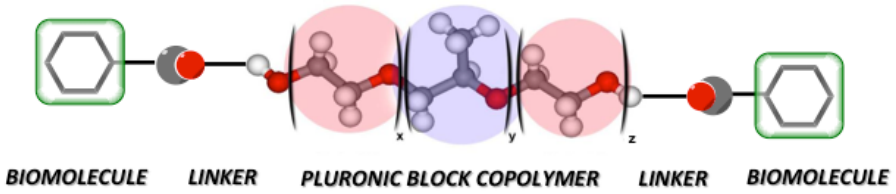

Figure 28. General structure of a functionalized Pluronic block copolymer.

Most of cancers and isolated cancer cell lines over-express the GLUT family members that are present in the respective tissue of origin under non-cancerous conditions. Furthermore, due to the requirement of energy to feed uncontrolled proliferation, cancer cells often express GLUTs, which under normal conditions would not be present in these tissues[329]. Therefore, the introduction of a glucose moiety on the Pluronic block copolymers could potentially confer active targeting properties to the polymer micelles and increase the tumor cells uptake improving chemoterapic drug cytotoxic activity. The selected synthetic strategy involved the use of aminooxyacetic acid as the linker. Therefore, the idea was to exploit the aminooxy functionality by reaction with the carbonyl group of a suitable disaccharide. In particular, D-cellobiose and D-maltose were choosen in order to expose respectively β- and α-glucose on the Pluronic block copolymer (Figure 29).

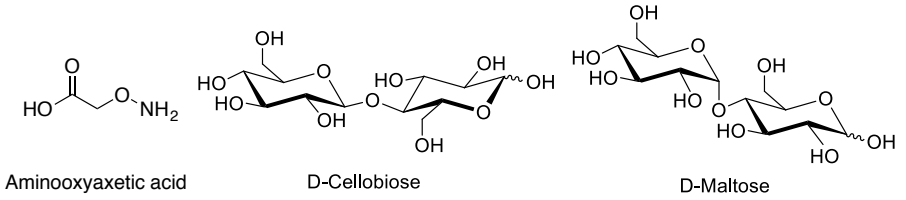

Figure 29. Structures of aminooxyacetic acid, D-cellobiose and D-maltose.

Pluronic F127 was treated with Boc-aminooxyacetic acid (**60**) in the presence of DCC and DPTS (4-(dimethylamino)pyridinium *p*-toluenesulfonate) obtaining derivative **88** (Scheme 11).

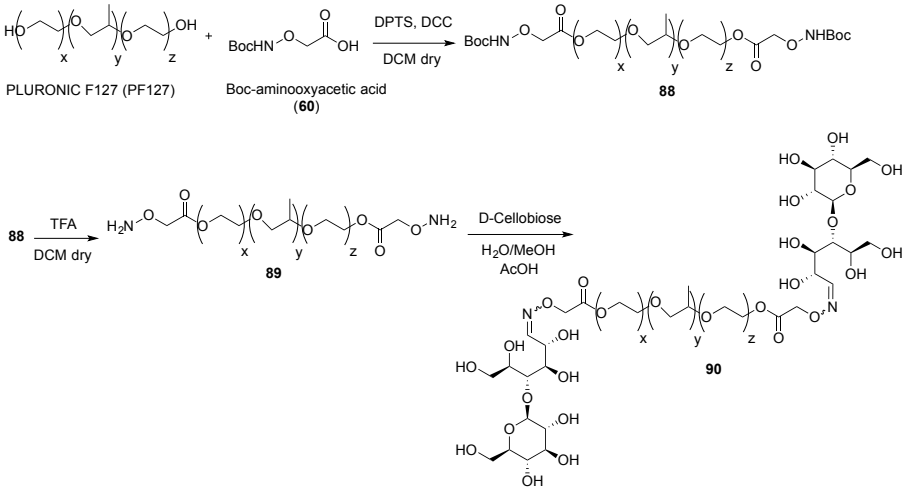

Scheme 11. Synthesis of glycosylated Pluronic block copolymer **90**.

The product was purified by chromatography and the amount of the functionalization was calculated by ^{1}H NMR performed using

methyl groups of the polymer as internal standard; it resulted to be around 74%. Compound **88** was then deprotected in acidic conditions to free the aminooxy functionalities that were exploited for conjugation with D-cellobiose to get glycosylated Pluronic block copolymer **90** (Scheme 11) that was purified by chromatography. Unfortunately, the amount of glycosylated polymer found by ^{1}H NMR resulted really low (around 12%, using both internal and external standards), probably due to the equilibrium between the hemiacetal and carbonyl forms of D-cellobiose that make its carbonyl group scarcely available for the reaction. Given the low efficiency of this reaction, we decided to change our synthetic strategy using levulinic acid (**82**) as the linker instead of aminooxyacetic acid. In this way we could use the inserted carbonyl group on the polymer for conjugation with properly functionalized carbohydrates. For this purpose I synthetized β-aminooxy-D-glucose (**91**) and *O*-β-D-maltosylhydroxylamine (**92**) (Figure 30) following the procedures already reported in the literature[330, 331].

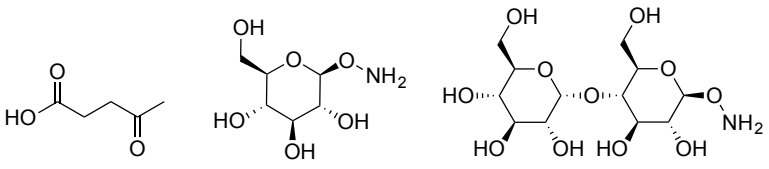

82 Levulinic acid

91 (β-Aminooxy-D-glucose)

92 (O-β-Maltosylhydroxylamine)

Figure 30. Structures of levulinic acid (**82**), β-aminooxy-D-glucose (**91**) and *O*-β-D-maltosylhydroxylamine (**92**).

Compounds **91** and **92** were synthetized in 4 steps starting from D-glucose and D-maltose, respectively. The aminooxy functionality on the sugars could be exploited for the formation of a stable oxime bond for reaction with the carbonyl group of levulinic acid. In this way we could expose β- and α-glucose on the polymer, in the presence or not of a further spacer (the glucose moiety of maltose). Reaction of Pluronic F127 with levulinic acid in the presence of DCC and DMAP afforded derivative **93** that was treated with **91** in citrate buffer (pH = 3.5) to obtain glycosylated Pluronic block copolymer **94** (Scheme 12).

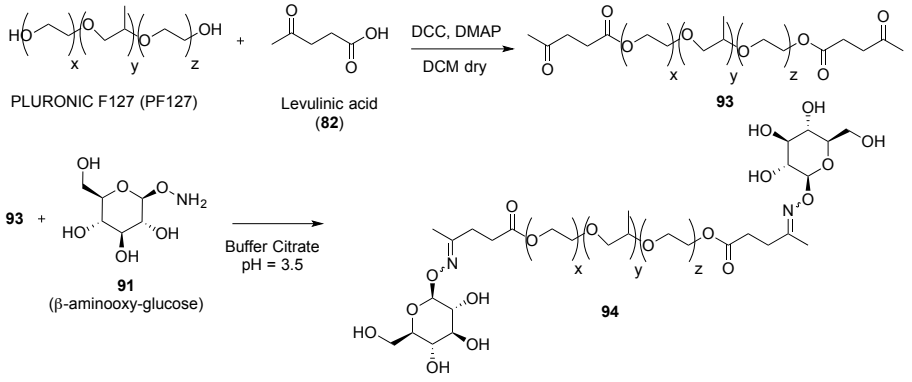

Scheme 12. Synthesis of glycosylated Pluronic block copolymer **94**.

Compound **94** was purified by chromatography and the amount of glycosyl functionalization was calculated by ^{1}H NMR using methyl groups of the polymer as internal standard or added pyridine as external standard. The percentage of glycosylated polymer resulted to be around 74%, really better than the one obtained

with the first synthetic strategy (around 12%). To be sure that the signal of the sugar observed by NMR belonged only to glucose covalently linked to the polymer, compound **94** was analysed by TLC and MS spectrometry (System Applied Biosystems MDS SCIEX instruments: Q TRAP, LC/MS/MS, turbo ion spray and Q STAR elite nano spray). TLC analysis revealed no traces of unreacted β-aminooxy- D-glucose (**91**) and neither unreacted β-aminooxy- D-glucose (**91**) nor its adducts with unlinked levulinic acid were detected by mass spectrometry. Further qualitative analyses were performed by FTIR spectroscopy and NMR. FTIR spectra of levulinic acid, Pluronic F127 and functionalized polymers **93** and **94** were recorded (Figure 31). The FTIR spectra of compounds **93** and **94** displayed an absorption band at 1734 cm^{-1} that indicates the presence of an ester bond (ester C=O stretching is reported at 1735 cm^{-1}). Due to the overlap whit Pluronic F127 absorption bands, unfortunately no carbohydrate peculiar band could be detected by FTIR.

By NMR analysis it was possible to obtain other relevant qualitative informations; in addiction to the signals of the polymer, ^{1}H NMR of **94** displayed the peaks relative to glucose anomeric proton (H-1) and oxime methyl groups. Moreover, ^{13}C NMR showed the signals relative to glucose C-H carbons, carbons of oxime methyl groups and two quaternary signals relative to C=O and C=N double bonds, confirming that the desired glycosylation successfully occurred.

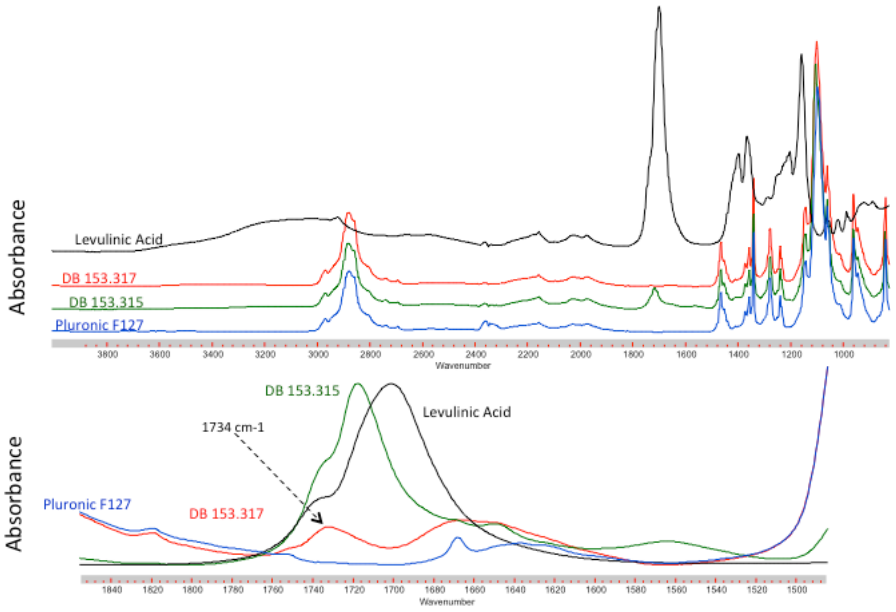

Figure 31. FTIR spectra of Pluronic F127 (in blue), functionalized polymer **93** (in green, sample DB 153.315), glycosylated polymer **94** (in red, sample DB 153.317) and levulinic acid (in black).

Compound **93** was also treated with *O*-β-D-maltosylhydroxylamine (**92**) in citrate buffer (pH = 3.5) to achieve glycosylated Pluronic block copolymer **95** (Scheme 13). Compound **95** was purified by chromatography and the percentage of glycosylated polymer, calculated by ^{1}H NMR as previously discussed, resulted to be around 56%. Glycosylated pluronic block copolymer **95** was characterized with the same techniques used for compound **94**. TLC analysis revealed no traces of unreacted *O*-β-D-maltosylhydroxylamine (**92**) and neither unreacted *O*-β-D-maltosylhydroxylamine (**92**) nor its

adducts with unlinked levulinic acid were detected by mass spectrometry.

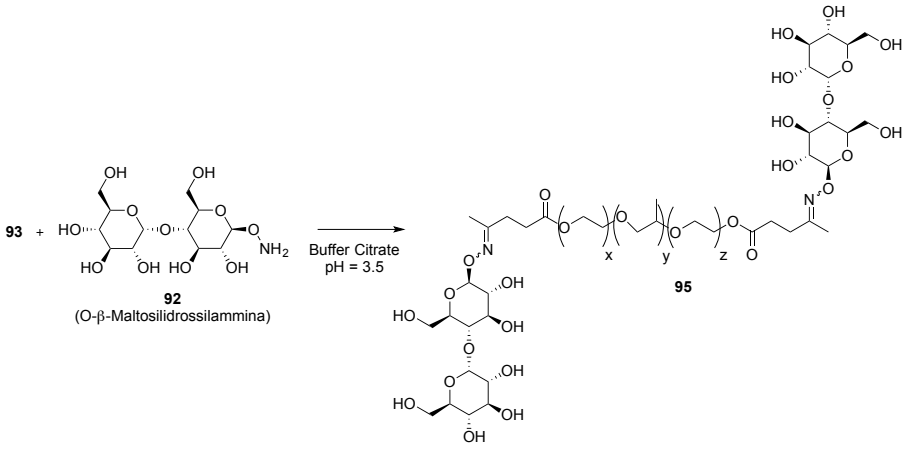

Scheme 13. Synthesis of glycosylated Pluronic block copolymer **95**.

Also the FTIR spectra of compounds **95** displayed an absorption band at 1734 cm^{-1} that indicates the presence of an ester bond; other relevant qualitative informations were obtained by NMR. In addiction to the signals of the polymer, ^{1}H NMR spectrum of **95** displayed the peaks relative to maltose H-1 and H-1' protons, methylenic protons of levulinic acid moiety and oxime methyl groups; from ^{13}C NMR spectrum it was possible to identify the signals relative to maltose C-H carbons, carbons of the oxime methyl groups, methylenic carbons of levulinic acid moiety, and two quaternary signals relative to C=O and C=N double bonds. All these data together confirmed that the desired glycosylation successfully occurred. Synthetized glycosylated pluronic block

copolymers **94** and **95** can potentially be exploited as micellar nanocarriers for antitumor drug delivery providing both passive and active targeting.

6.1. Trehalose mimics as trehalase inhibitors: Conclusion

1) *N-bridged 1-deoxynojirimycin dimers*

In order to obtain new trehalase inhibitors, based on 1-deoxynojirimycin and its *N*-acyl derivatives, that might be specific towards insect trehalase, a small set of *N*-bridged 1-deoxynojirimycin dimers (**29**-**31**, Figure 7) were synthetized. Dimers **29**-**31** have been evaluated as potential inhibitors of insect trehalase from midge larvae of *C. riparius*, porcine trehalase as the mammalian counterpart and α-amylase from human saliva. All the tested compounds (**29**-**31**) resulted inactive against α-amylase, while they were similarly active against *C. riparius* trehalase, with the activity in the low micromolar range. Compound **29** resulted to be the most active derivative of the series (IC_{50} = 6,1 μM); all compounds **29**-**31** showed a slight selectivity towards the insect glycosidase (from 4 to 7 fold), resulting more selective of the parent compound 1-deoxynojirimycin (2 fold more selective towards *C. riparius* trehalase). The obtained biological data confirmed that there are different recognition requirements for the catalytic sites of porcine kidney and insect trehalases. Despite the fact the both trehalase specifically hydrolyze trehalose, they might have significant differences in the catalytic pocket that could be investigated by epitope mapping studies by STD-NMR and exploited for the design and development of specific insect trehalase inhibitors. Of course, further characterizations of the

biological activity of these iminosugar dimers against other relevant glycosidase would be necessary to verify their potential as non-toxic insecticides.

2) *Casuarine derivatives*

In order to identify the simplest pyrrolizidine structure necessary to impart selective insect trehalase inhibition, a series of casuarine analogues (namely (−)-uniflorine A (**36**), 7-deoxycasuarine (**28**), its glucosyl derivative (**25**) and the newly synthesized 7-deoxy uniflorine A (or 7-deoxy-6-*epi*-casuarine, (**37**)) (Figure 9) were evaluated as potential specific inhibitors of insect trehalase from *C. riparius* and *S. littoralis*. Since simple modifications at the C-7 of the B ring of casuarine (OH, H, CH_2OH) are able to influence both potency and specificity of inhibition, it was therefore expected that also modifications at the C-6 of the B ring could disclose interesting results in terms of potency/specificity of trehalase inhibition. Moreover, it is trivially of great importance the obtainment of new specific inhibitors by simple, and low cost synthetic routes in order to investigate them in *in vivo* tests and, if effective, in agri-food industry as non-toxic insecticides and/or fungicides. 7-Deoxy-uniflorine A (**37**), synthesized *ex novo* with a straightforward and simple strategy, and analogues **25**, **28** and **36** were also tested against porcine trehalase as the mammalian counterpart and α-amylase from human saliva as a relevant glucolytic enzyme. None of compounds inhibited α-amylase from human saliva, showing their potential as

non-toxic insecticides/fungicides. Compounds **25** and **28** proved to be active (from micromolar to nanomolar range activity) against both insect and porcine trehalases, with a slight selectivity towards the insect enzyme (from 11 to 17 fold), while compounds **36** and **37** behaved as inhibitors exclusively of insect trehalases (they did not inhibit the mammalian porcine trehalase). Although the glucosylated derivative **25** represents the most active inhibitor in terms of potency of inhibition (IC_{50} = 44 nM towards *C. riparius* trehalase), these biological results demonstrate that the presence of an additional glucosyl moiety is not essential for targeting selective inhibitors of insect trehalase. Indeed, in terms of selectivity, compounds **36** and **37** were identified as the most interesting compounds. The specificity of compounds **36** and **37** suggests that stereochemistry at position 6 of the B ring of casuarine is a key issue in discriminating porcine and insect trehalases. Activity of 7-deoxy uniflorine A (**37**) was also analyzed in preliminary *in vivo* experiments. Effects on larval and pupal weight, larval, pupal and adult morphology and adult emergence, longevity and fertility were monitored, but contrary to what expected, no effects on the analyzed parameters were detected. Due to their selectivity towards insect trehalases, compounds **36** and **37** are the most promising for future development as insecticides and outlined the importance of the stereochemistry at C-6 of the pyrrolizidine nucleus to confer such enzyme specificity. In particular, the straightforward and practical synthesis of **37** (54% yield over 4 steps) will allow further investigation of its

activity for other *in vivo* studies. If its low inhibition of *S. littoralis* trehalase is due to the high *in vivo* trehalose concentrations, it would be of great importance to develop a pure competitive inhibitor based on the structure of **37** and with a lower K_i (as for example, the glucosyl derivative of **37**). Moreover, if the lack of activity is due to the rapid degradation of the inhibitor in *in vivo* conditions, it could be also interesting to test the protected (i.e. acetylated) derivatives of compound **37** to increase its stability.

6.2. Synthesis of multivalent glycoconjugates: Conclusion

1) *Multivalent carbohydrates immobilisation on a biomaterial surface*

We proposed an innovative methodology for the preparation of advanced functional materials exposing on their surface multivalent glycosylated patterns that can be of wide applicability including the development of "smart" biomaterials for tissue engineering. As a model system for the present study, collagen patches were used. The proposed strategy includes thiolation of collagen, chemoselective thiol-ene photoclick-reaction with double-bond terminated heterobifunctional dendrons and finally glycan conjugation by a second chemoselective reaction. The introduction of thiol functional groups on collagen patches was achieved reacting lysine side-chain amino groups with γ-thiobutyrolactone. Derivatization of the thiolated and non-thiolated samples with 5,5'-Dithiobis-(2-Nitrobenzoic Acid) (DTNB) was performed to label and quantify inserted -SH groups by NMR (60% of total lysines bears the thiol group needed for the subsequent coupling to heterobifunctional dendrons). Three new heterobifunctional dendrons (G0, G1, G2, **50**-**52**, Scheme 4) were synthesized in few (2-5) steps from (Boc-aminooxy)acetic acid (**60**) (42%, 29%, 12% overall yield respectively). Dendrons **50**-**52** were immobilized on collagen patches via thiol-ene photoclick reaction, and thus conjugated to lactose (used as model saccharide for multivalent functionalization) by chemoselective

alkoxyamino-carbonyl reaction. XPS, FTIR and ELLA assays confirmed the effectiveness of the collagen multivalent neoglycosylation. In conclusion, we have presented a bio-orthogonal method to functionalize collagen-based biomaterials with multivalent dendrons displaying carbohydrate moieties. The proposed work provides a very innovative approach for the design of smart (cell-responsive) biomaterials, with no precedent in the literature, which improves their potential for tethering bioactive molecules, and enhances the functionality of biomaterial surfaces.

2) Synthesis of multiglycosylated dendrons as ligands of P. aeruginosa LecB

In the search of new high affinity ligands of *P. aeruginosa* LecB, three new dendrons of generation 0, 1 and 2 (**71**-**73**, Figure 22), possessing a double bond at the focal point and carbonyl groups at the termini, have been synthesised. The heterobifunctional dendrons were designed in order to have bio-orthogonal functional groups: in particular, the double bond at the focal point could be useful for further conjugation by thiol-ene chemistry to the desired matrix, whereas carbonyl groups at their termini can be exploited for multivalent carbohydrate functionalization through reductive amination, oxime or hydrazone formation to properly functionalized saccharides. Zero, first and second generation heterobifunctional dendrons (**71**-**73**) were synthesized in few (1-4) steps starting from 9-decen-1-ol (**61**) or

selected building blocks **65** and **69** through esterification reactions with levulinic acid (**82**) (99%, 35%, 18% overall yield respectively). In order to evaluate our glycoconjugates interactions with LecB, α-L-(2-aminoethyl) fucoside (**74**) and α-*O*-L-fucopyranosyl oxyamine (**75**) were synthesized, in 4 and 5 steps, from commercial L-fucopyranose following the procedures already reported in the literature. Compounds **74** and **75** were used as sample monosaccharides for dendron conjugation via reductive amination or alkoxyamine conjugation, respectively. The conjugation of the saccharide via reductive amination resulted scarcely efficient given the large extent of by-products formation (glycosylated dendron (**76**) was obtained in 27 % yield). On the contrary the oxime ligation afforded the glycoconjugated dendrons (**77**, **79** and **81**, Scheme 10) in quantitative yields. The affinity of compounds **77**, **79** and **81** as ligands of *P.aeruginosa* LecB was evaluated studying their binding properties by isothermal titration calorimetry (ITC). All three compounds displayed low- or sub-micromolar affinities. Analysis of the thermodynamic contributions indicates that the divalent compound (**79**) behaves very well with a stoichiometry of 0.5 (compound/lectin monomer) and an affinity 10 times better than the monomeric compound (K_d = 0,128 μM for **79** and 1,18 μM for **77**). The affinity is not huge (Renaudet and co-workers reported a dissociation constant of 28 nM for hexadecavalent glycocluster **49**, Figure 15), but still very good and promising, considering that this glycoconjugate is really easier to synthetize respect to **49**. The

enthalpy of binding is twice the one for the monovalent compound, indicating that both fucose are efficiently recognized. As for the tetravalent compound **81**, it has lower affinity than the divalent (K_d = 0,279 μM for compound **81**). The stoichiometry indicates that all fucose are reaching lectin binding sites, but clearly not very efficiently since the enthalpy is not four times the one of the monovalent compound. It is probable that the molecule is a little bit crowdy and some steric hindrance/constrains prevent all of 4 fucose to be in perfect orientation in binding site. In the next steps of this work, we will try to exploit the glycosylated dendrons **77**, **79** and **81** for further chemoselctive thiol-ene reaction with desired matrices suitably functionalized with thiol groups, i.e. cysteine residues in proteins, and it will be surely interesting to study their binding properties on other biological relevant fucose specific lectins (i.e. AFL from Aspergillus fumigatus).

6.3. Synthesis of glycosylated Pluronic block copolymers as antitumor drugs carriers: Conclusion

Three new functionalized Pluronic block copolymers (**90**, **94** and **95**, Scheme 11–13) were synthetized in order to introduce also active targeting properties on the polymeric carriers. The synthetic strategy involved the introduction of an appropriate linker on the polymer that could be conjugate to the biomolecule of interest. Pluronic F127 was the block copolymer chosen for this project, while glucose was the selected biomolecule for polymer functionalization. Glucose is transported into the cell via facilitative glucose transporters (GLUT) present in all cell types; due to the ubiquity of these transporters, their differential expression is involved in various disease states such as diabetes, ischemia and cancer. Therefore, the introduction of a glucose moiety on the Pluronic block copolymers could potentially increase the tumor cells uptake improving chemoterapic drug cytotoxic activity. Aminooxyacetic acid was used as linker to exploit the aminooxy functionality by reaction with the carbonyl group of D-cellobiose and D-maltose, in order to expose respectively β- and α-glucose on the Pluronic block copolymer. Glycosylated Pluronic block copolymer (**90**), exposing β-glucose, was obtained in few (3) steps, but the amount of the functionalization resulted really poor (around 12% by ^{1}H NMR using both an internal and an external standard). The use of levulinic acid as linker gave much better results. Once inserted on

the polymer, it was exploited for conjugation with β-aminooxy-D-glucose (**91**) and *O*-β-D-maltosylhydroxylamine (**92**), both synthetized following the procedures already reported in the literature. Glycosylated Pluronic block copolymer **94** exposing β-glucose was synthetized in 2 steps and the percentage of glycosylated polymer resulted to be around 74% (calculated by ^{1}H NMR using both an internal and an external standard). Also compound **95**, exposing α-glucose in the presence of a further spacer (the other glucose moiety of maltose), was obtained in 2 steps and the amount of glycosylation resulted around 56% (calculated by ^{1}H NMR using both an internal and an external standard). Both compounds **94** and **95** were characterized using TLC, FTIR, MS, ^{1}H NMR and ^{13}C NMR. All the obtained analytical data confirmed that the desired functionalization successfully occurs. Glycosylated pluronic block copolymers **94** and **95** could be exploited as micellar nanocarriers for antitumor drug delivery, providing to the polymeric micelles both passive and active targeting properties and so probably increasing drug cytotoxic activity. The next steps of this work will include incorporation of Au (III) and Ru (III) antitumor drugs into our glycosylated pluronic block copolymers micelles to evaluate the *in vitro* effect of polymer glycosylation on their cytotoxic activity. Finally, it will be surely interesting to synthetize also α-aminooxy-D-glucose and aminooxy-D-cellobiose to better investigate the consequences of exposing α-or β-glucose on the polymer and to verify if the further

glucose unit present in D-maltose and D-cellobiose is able to modify the behavior of glycosylated Pluronic block copolymers.

7. Experimental Part

7.1. Trehalose mimics as trehalase inhibitors

General methods

Commercial reagents were used as received. Solvents were dried over molecular sieves, for at least 24 h prior to use, when required. When dry conditions were required, the reaction was performed under Ar or N_2 atmosphere. All reactions were carried out under magnetic stirring and monitored by TLC on 0.25 mm silica gel $60F_{254}$ coated glass plates (Merck) with UV detection when possible, or spots were visualized by charring with a conc. H_2SO_4/EtOH/H_2O solution (10:45:45 v/v/v), or with a solution of $(NH_4)_6Mo_7O_{24}$ (21 g), $Ce(SO_4)_2$ (1 g), conc. H_2SO_4 (31 mL) in water (500 mL) and then heating to 110 °C for 5 min. Column chromatographies were carried out on Silica Gel 60 (32-63 μm) or on silica gel (230–400 mesh, Merck). Yields refer to spectroscopically and analytically pure compounds unless otherwise stated. Routine ^1H and ^{13}C NMR spectra were recorded at 25 °C on a Varian Mercury or on a Varian INOVA or on a Varian Gemini instruments at 400 MHz (^1H) and 100.57 or 50 MHz (^{13}C). Chemical shifts are reported in parts per million downfield from TMS (^1H: δ = 0.00 ppm) and $CDCl_3$ (^{13}C: δ = 77.0 ppm) as an internal standard. Integrals are in accordance with assignments; coupling constants (*J*) are given in Hz. For detailed peak assignments 2D spectra were measured (COSY, HSQC, NOESY, and NOE as necessary). IR spectra were recorded with a BX FT-IR Perkin–Elmer System spectrophotometer. ESI-MS spectra were recorded with a System Applied Biosystems MDS SCIEX (Q TRAP, LC/MS/MS, turbo ion spray), or a System Applied Biosystem MDS SCIEX (Q STAR elite nanospray), or a Thermo Scientific™ LCQ Fleet Ion Trap Mass Spectrometer. Elemental analyses were performed with a Perkin-Elmer 2400 analyzer. Optical rotation measurements were performed on a JASCO DIP-370 polarimeter.

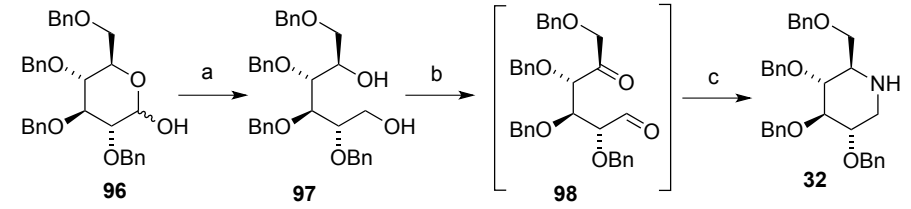

2,3,4,6-Tetra-*O*-benzyl-D-glucopyranose

Scheme 14. Synthesis of 1-deoxynojirimycin (**32**)[100].

Reagents and conditions: (a) $LiAlH_4$, THF, 20 h; (b) 1) DMSO, $(COCl)_2$, CH_2Cl_2, -75 °C, 2 h; 2) Et_3N, -75 to 0 °C, 2 h; (c) $NaBH_3CN$, excess NH_4HCO_2, Na_2SO_4, MeOH, 0 °C to rt, 20 h, 73%, three steps.

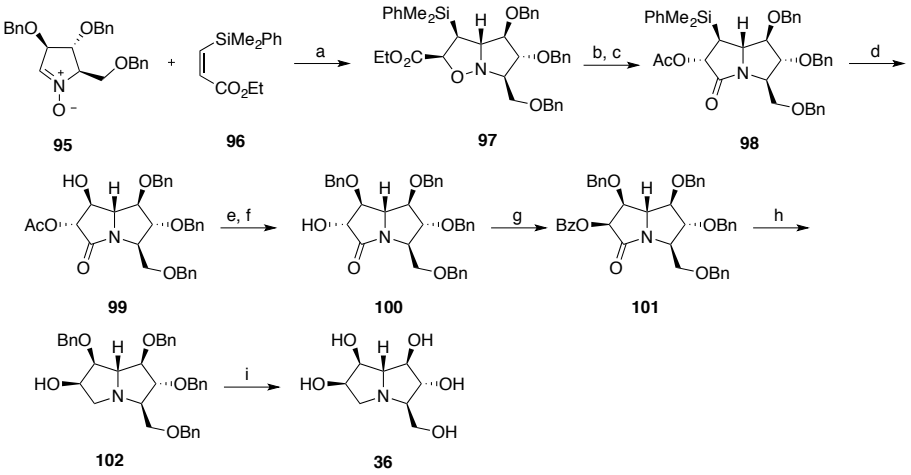

Scheme 15. Synthesis of compound **36**[81, 103].

Reagents and conditions: (a) CH_2Cl_2, rt, 36 h, 79%; (b) Zn, AcOH/H_2O, 60–65 °C, 5 h, 93%; (c) Ac_2O, Py, rt, 15 h, 100%; (d) $Hg(CF_3CO_2)_2$, TFA, AcOH, AcOOH, $CHCl_3$, 82%; (e) $BnOC(=NH)CCl_3$, CF_3SO_3H, Et_2O, rt, 3 h; f) Ambersep 900 OH, MeOH, RT, 15 h, 75% (2 steps); (g) BzOH (1.2 equiv), PPh_3 (1.2 equiv), DIAD (1.2 equiv), THF, rt, 75%; (h) $LiAlH_4$ (4 equiv), THF, reflux, 45%; (i) H_2, 10% Pd/C, MeOH, HCl, rt then Dowex 50WX8, 6% NH_4OH, 71%.

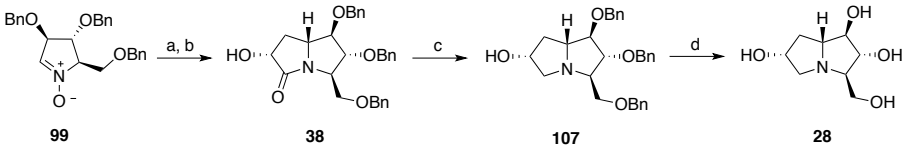

Scheme 16. Synthesis of compound **28**[105].

Reagents and conditions: (a) dimethylacrylamide, CH_2Cl_2, rt, 3 days, 85 %; (b) Zn, AcOH/H_2O, 50 °C, 4 h, 80%; (c) $LiAlH_4$, THF, reflux, 3 h, 75%; (d) H_2, Pd/C, HCl, EtOH, 3 days, 88%.

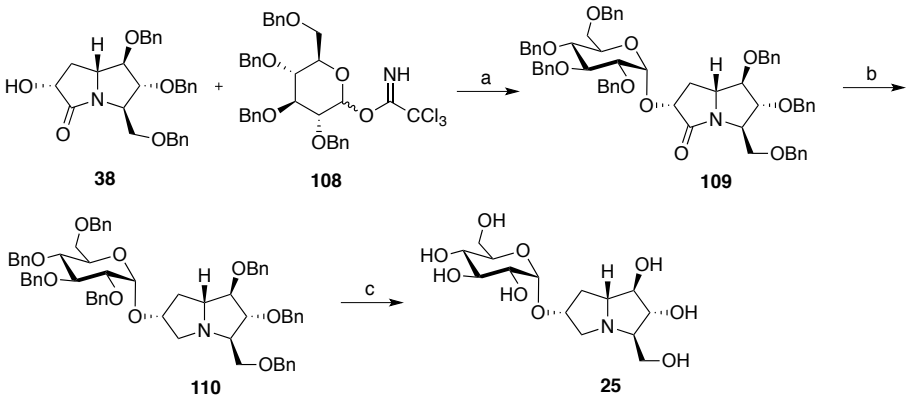

Scheme 17. Synthesis of compound **25**[82].

Reagents and conditions: (a) TMSOTf, Et_2O, rt, 1 h, 88%; (b) $LiAlH_4$, THF, rt, 1 h, 58%; (c) H_2, Pd/C, HCl, MeOH, rt, 18 h, 77%.

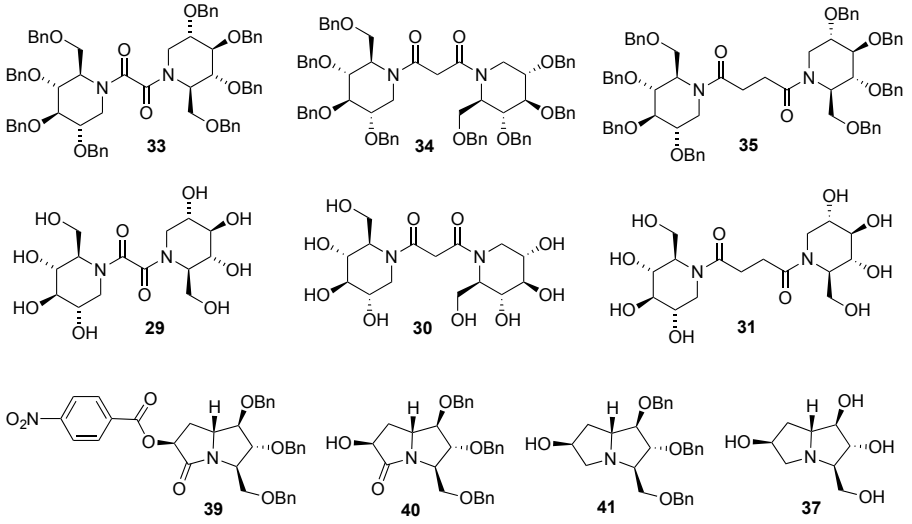

Figure 32. Summary of the synthesised compounds.

General procedure for Diacyl Chloride Condensation (33 and 35)

To a 0.2 M solution of **32** in dry DCM, pyridine (4 eq.) and the appropriate acyl chloride (1 eq.) were added at 0°C. The temperature was slowly increased to r.t. (3 h); the mixture was then concentrated and the residue was purified directly on a silica gel column using a suitable eluent.

1,2-Bis((2*R*,3*R*,4*R*,5*S*)-3,4,5-tris(benzyloxy)-2-((benzyloxy)methyl)piperidin-1-yl)ethane-1,2-dione (33)

Flash column chromatography (petroleum ether/EtOAc, 65:35). ^{1}H NMR (400 MHz, $CDCl_3$): δ = 7.37–7.01 (m, 40H, ArH), 4.77–4.19 (m, 18H, OCH_2Ph, H-5), 3.97–3.54 (m, 12H, H-1a, H-2, H-3, H-4, H-6), 3.14–3.02 (m, 2H, H-1b) ppm. ^{13}C NMR (100.57 MHz, $CDCl_3$): δ = 165.0, 164.7 (C=O), 138.5, 138.5, 138.3, 138.2, 138.2, 138.1, 138.1, 137.9 (C Ar), 128.7–127.6 (CH Ar), 82.4 (C-3), 79.1, 76.1 (C-2, C-4), 73.7–70.1 (OCH_2Ph), 68.9 (C-6), 58.6 (C-5), 43.8 (C-1) ppm. MS (TOF, m/z)**:** $[M + H]^+$ calcd for $C_{70}H_{73}N_2O_{10}$, 1101.5; found 1101.5.

1,3-Bis((2*R*,3*R*,4*R*,5*S*)-3,4,5-tris(benzyloxy)-2-((benzyloxy)methyl)piperidin-1-yl)propane-1,3-dione (34)

Compound **32** (67 mg, 0,123 mmol), malonic acid (6,4 mg, 0,061 mmol), DMAP (3 mg, 0,025 mmol) and p-toluenesulfonic acid (4,7 mg, 0,025 mmol) were dissolved in DCM (1,14 mL). DCC (32 mg, 0,154 mmol) was added and the solution was stirred for 30 minutes at room temperature. Then the DCC-urea was filtered off and washed with a small volume of DCM. The solvent was evaporated, and the residue was purified by flash column chromatography (petroleum ether/EtOAc, 62,5/37,5) giving pure **34** (48 mg, 70%). ^{1}H NMR (400 MHz, $CDCl_3$): δ = 7.34–7.15 (m, 40H, ArH), 4.77–4.59 (m, 6H, H-5, OCH_2Ph), 4.59–4.44 (m, 8H, OCH_2Ph), 4.41–4.25 (m, 4H, OCH_2Ph), 4.03–3.93 (m, 4H, H-2, H-1a), 3.80–3.56 (m, 10H, H-6, H-3, CH_2C=O, H-4), 3.56–3.46 (m, 2H, H-1b) ppm. ^{13}C NMR (100.57 MHz, $CDCl_3$): δ = 166.9 (C=O), 142.7–137.8 (C Ar), 128.4–127.5 (CH Ar), 80.9 (C-3), 78.1, 73.9 (C-2, C-4), 72.9–70.8 (OCH_2Ph), 68.0 (C-6), 54.2 (C-5), 44.4 (C-1), 41.9 (CH_2C=O) ppm. MS (TOF, m/z)**:** $[M + H]^+$ calcd for $C_{71}H_{75}N_2O_{10}$, 1115.5; found 1115.5.

1,4-Bis((2*R*,3*R*,4*R*,5*S*)-3,4,5-tris(benzyloxy)-2-((benzyloxy)methyl)piperidin-1-yl)butane-1,4-dione (35)

Flash column chromatography (petroleum ether/EtOAc, 50:50). ^{1}H NMR (400 MHz, $CDCl_3$): δ = 7.38–7.16 (m, 40H, ArH), 4.82–4.23 (m, 18H, OCH_2Ph, H-5), 4.05–3.41 (m, 12H, H-1a, H-2, H-3, H-4, H-6), 2.97–2.58 (m, 6H, H-1b, CH_2C=O) ppm. ^{13}C NMR (100.57 MHz, $CDCl_3$): δ = 171.8 (C=O), 138.4–137.8 (C Ar), 128.5–127.6 (CH Ar), 82.4 (C-3), 78.9, 74.3 (C-2, C-4), 73.3–71.1 (OCH_2Ph), 68.3 (C-6), 54.5 (C-5), 44.0 (C-1), 32.0 (CH_2C=O) ppm. MS (TOF, m/z)**:** $[M + H]^+$ calcd for $C_{72}H_{77}N_2O_{10}$, 1129.6; found 1129.6.

General Procedure for the Hydrogenolysis Reaction (29-31)

A 0.02 M solution of the appropriate dimer dissolved in EtOAc/EtOH (1:1) was treated with $Pd(OH)_2/C$ (100% in weight). The reaction was stirred for 5 days under a H_2 atmosphere. Palladium was then removed by filtration through a Celite pad followed by washing with EtOH and water. Evaporation of the solvents afforded the corresponding deprotected compounds in quantitative yields.

1,2-Bis((2*R*,3*R*,4*R*,5*S*)-3,4,5-trihydroxy-2-(hydroxymethyl)piperidin-1-yl)ethane-1,2-dione (29)

^{1}H NMR (400 MHz, D_2O): δ = 3.75–3.65 (m, 4H, H-6), 3.60–3.53 (m, 2H, H-2), 3.42–3.26 (m, 6H, H-1a, H-3, H-4), 3.02–2.98 (m, 2H, H-5), 2.82–2.72 (m, 2H, H-1b) ppm. ^{13}C NMR (100.57 MHz, D_2O): δ = 76.2 (C-3), 67.7, 66.9 (C-2, C-4), 60.0 (C-5), 57.6 (C-6), 45.8 (C-1) ppm. MS (TOF, m/z)**:** $[M + H]^+$ calcd for $C_{14}H_{25}N_2O_{10}$, 381.1; found 381.4.

1,3-Bis((2*R*,3*R*,4*R*,5*S*)-3,4,5-trihydroxy-2-(hydroxymethyl)piperidin-1-yl)propane-1,3-dione (30)

^{1}H NMR (400 MHz, D_2O): δ = 4,36 (d, 1H, *J* = 14.4 Hz, CH_2C=O), 3.96–3.52 (m, 16H, H-1, H-2, H-3, H-4, H-5, H-6), 3.20 (d, 1H, *J* = 14.8, CH_2C=O) ppm. ^{13}C NMR (100.57 MHz, D_2O): δ = 74.1 (C-3), 69.3, 68.4 (C-2, C-4), 63.0 (C-5), 59.8 (C-6), 47.7 (C-1), 40.6 (CH_2C=O) ppm. MS (TOF, m/z)**:** $[M + H]^+$ calcd for $C_{15}H_{27}N_2O_{10}$, 395.2; found 395.3.

1,4-Bis((2*R*,3*R*,4*R*,5*S*)-3,4,5-trihydroxy-2-(hydroxymethyl)piperidin-1-yl)butane-1,4-dione (31)

^{1}H NMR (400 MHz, D_2O): δ = 3.82–3.71 (m, 4H, H-6), 3.68–3.61 (m, 2H, H-2), 3.48–3.34 (m, 6H, H-1a, H-3, H-4), 3.09–3.05 (m, 2H, H-5), 2.86–2.80 (m, 2H, H-1b), 2.61–2.50 (m, 4H, CH_2C=O) ppm. ^{13}C NMR (100.57 MHz, D_2O): δ = 76.0 (C-3), 67.5, 66.7 (C-2, C-4), 59.7 (C-5), 57.4 (C-6), 45.6 (C-1), 28.6 (CH_2C=O) ppm. MS (TOF, m/z)**:** $[M + H]^+$ calcd for $C_{16}H_{29}N_2O_{10}$, 409.2; found 409.4.

(1*R*,2*R*,3*R*,6*S*,7a*R*)-1,2-Bis(benzyloxy)-3-[benzyloxy)methyl]-6-*p*-nytrobenzoyl-5*H*-pyrrolizin-5-one (39) *(synthetized by Prof. F. Cardona, Chemistry department, University of Florence)*

To a solution of **38** (108 mg, 0.23 mmol) in dry THF (5 ml) was added triphenylphosphine (181 mg, 0.69 mmol) under nitrogen atmosphere. The reaction mixture was cooled to 0 °C and DIAD (140 mg, 0.69 mmol) was added dropwise. After addition of *p*-nitrobenzoic acid (43 g, 0.26 mmol), the mixture was raised to room temperature and stirred under nitrogen atmosphere for 2 h, until TLC analysis

(AcOEt:EP 3:1) showed the disappearance of the starting material (R_f = 0.35) and the formation of a new product (R_f = 0.66). The solvent was removed under reduced pressure and the crude was purified by flash column chromatography (EP:AcOEt 4:1) affording pure **39** (R_f = 0.14, 138 mg, 0.22 mmol, 96%) as a colorless oil. $[\alpha]_D^{24}$ = -34.4 (*c* = 1.17, $CHCl_3$). ^{1}H NMR (400 MHz, $CDCl_3$): δ = 8.20-8.17 (m, 2H, Ar), 8.13-8.10 (m, 2H, Ar), 7.31-7.19 (m, 15H, Ar), 5.42-5.39 (m, 1H, H-6), 4.56-4.46 (m, 6H, Bn), 4.32 (dd, *J* = 4.9, 3.9 Hz, 1H, H-2), 4.06 (q, *J* = 3.9 Hz, 1H, H-3), 4.02 (q, *J* = 6.6 Hz, 1H, H-7a), 3.69-3.64 (m, 2H, H-1 and Ha-8), 3.55 (dd, *J* = 9.7, 3.9 Hz, 1H, Hb-8), 2.29-2.26 (m, 2H, H-7) ppm. ^{13}C NMR (50 MHz, $CDCl_3$): δ = 169.4 (s, C=O), 164.0 (s, C=O), 150.8 (s, C-Ar), 137.9, 137.6, 137.4 (s, 3C, C-Ar), 134.7 (s, C-Ar), 131.1 (d, 2C, C-Ar), 128.5-127.5 (d, 15C, C-Ar), 123.5 (d, 2C, C-Ar), 88.3 (d, C-1), 87.0 (d, C-2), 75.7 (d, C-6), 73.4 (t, C-Bn) 72.5 (t, C-Bn), 72.4 (t, C-Bn), 69.0 (t, C-8), 62.1 (d, C-7a), 59.5 (d, C-3), 32.8 (t, C-7) ppm. IR ($CDCl_3$) ῡ = 3086, 3060, 3032, 2922, 2866, 1730, 1706, 1530, 1454, 1348, 1269, 1102 cm^{-1}. MS (ESI): *m/z* (%) = 645.37 $[M + Na]^+$. $C_{36}H_{34}N_2O_8$ (622.66): calcd. C 69.44, H 5.50, N 4.50; found C 69.15, H 5.89, N 4.02.

(1*R*,2*R*,3*R*,6*S*,7a*R*)-1,2-Bis(benzyloxy)-3-[(benzyloxy)methyl]-6-hydroxyhexahydro-5*H*-pyrrolizin-5-one (40) *(synthetized by Prof. F. Cardona, Chemistry department, University of Florence)*

A solution of **39** (73 mg, 0.12 mmol) in 12 ml of methanol with ionic exchange resin Ambersep 900 OH (600 mg) was stirred at rt for 15 h then a TLC analysis (AcOEt:EP 3:1) showed the disappearance of starting material (R_f = 0.73) and the formation of a new product (R_f = 0.43). After a filtration through Celite®, the solvent was removed under reduced pressure and the crude was purified by flash column chromatography (AcOEt:EP 2:1) affording pure **40** (R_f = 0.26, 55 mg, 0.12 mmol, 100%) as a colorless oil. $[\alpha]_D^{25}$ = -45.2 (*c* = 1.47, $CHCl_3$). ^{1}H NMR (400 MHz, $CDCl_3$): δ = 7.37-7.25 (m, 15H, Ar), 4.60-4.52 (AB system, *J* = 11.7 Hz, 2H, Bn), 4.59-4.52 (AB system, *J* = 12.2 Hz, 2H, Bn), 4.56-4.48 (AB system, *J* = 11.7 Hz, 2H, Bn), 4.34-4.32 (m, 1H, H-6), 4.31 (dd, *J* = 4.9, 3.9 Hz, 1H, H-2), 4.05 (q, *J* = 7.0 Hz, 1H, H-7a), 4.03-4.00 (m, 1H, H-3), 3.64 (dd, *J* = 7.8, 4.9 Hz, 1H, H-1), 3.61 (dd, *J* = 9.8, 5.9 Hz, 1H, Ha-8), 3.57 (dd, *J* = 9.8, 4.4 Hz, 1H, Hb-8), 3.40 (d, *J* = 2.5

Hz, 1H, OH), 2.21 (ddd, *J* = 14.1, 6.9, 2.5 Hz, 1H, Ha-7), 2.05 (ddd, *J* = 14.1, 6.3, 7.3 Hz, 1H, Hb-7) ppm. ^{13}C NMR (50 MHz, $CDCl_3$): δ = 174.5 (s, C=O), 137.9, 137.8, 137.7 (s, 3C, C-Ar), 128.5-127.7 (d, 15C, C-Ar), 88.7 (d, C-1), 87.5 (d, C-2), 73.4 (t, C-Bn), 73.3 (d, C-6), 72.4 (t, C-Bn), 72.3 (t, C-Bn), 69.0 (t, C-8), 62.1 (d, C-7a), 58.8 (d, C-3), 34.5 (t, C-7) ppm. IR ($CDCl_3$): ϑ = 3365, 3088, 3066, 3032, 2926, 2866, 1688, 1496, 1454, 1308, 1277, 1111, 1103 cm^{-1}. MS (ESI): *m/z* (%) = 496.36 $[M + Na]^+$. $C_{29}H_{31}NO_5$ (473.56): calcd. C 73.55, H 6.60, N 2.96; found C 73.38, H 6.17, N 2.63.

(1*R*,2*R*,3*R*,6*S*,7a*R*)-1,2-Bis(benzyloxy)-3-[(benzyloxy)methyl]-6-hydroxyhexahydro-1*H*-pyrrolizine (41) *(synthetized by Prof. F. Cardona, Chemistry department, University of Florence)*

A solution of **40** (107 mg, 0.23 mmol) in 2 ml of dry THF was stirred under nitrogen atmosphere at 0°C and $LiAlH_4$ (1M solution in THF, 0.92 ml, 0.92 mmol) was added dropwise. The mixture was raised to rt and refluxed for 2 h, until TLC analysis (AcOEt) showed the disappearance of the starting material (R_f = 0.53) and the formation of a new product (R_f = 0.20). Reaction was then quenched with 2 ml of a saturated aqueous solution of Na_2SO_4 at 0°C and after extraction with AcOEt (3x25 ml), the organic layers were dried over Na_2SO_4 and concentrated at reduced pressure. The crude was purified by flash column chromatography (AcOEt), affording pure **41** (R_f = 0.20, 60 mg, 0.13 mmol, 57% yield) as a white solid. M.p. 95-97 °C. $[\alpha]_D^{24}$ = +9.5 (*c* = 1.02, $CHCl_3$). ^{1}H NMR (400 MHz, $CDCl_3$): δ = 7.35-7.23 (m, 15H, Ar), 4.68-4.45 (AB system, *J* = 11.7 Hz, 2H, Bn), 4.56 (d, *J* = 11.7 Hz, 2H, Bn), 4.51 (s, 2H, Bn), 4.48-4.45 (m, 1H, H-6), 4.06 (dd, *J* = 7.0, 5.5 Hz, 1H, H-2), 3.84 (t, *J* = 5.5 Hz, 1H, H-1), 3.72-3.66 (m, 1H, H-7a), 3.57 (dd, *J* = 9.3, 4.7 Hz, 1H, Ha-8), 3.50 (dd, *J* = 9.4, 6.2 Hz, 1H, Hb-8), 3.14-3.11 (m, 1H, Ha-5), 3.00 (td, *J* = 6.6, 5.0 Hz, 1H, H-3), 2.93 (dd, *J* = 11.7, 4.3 Hz, 1H, Hb-5), 2.05 (ddt, *J* = 13.2, 7.0, 1.6 Hz, 1H, Ha-7), 1.95 (bs, 1H, OH), 1.80 (ddd, *J* = 13.7, 9.2, 5.1 Hz, 1H, Hb-7) ppm. ^{13}C NMR (50 MHz, $CDCl_3$): δ = 138.1, 137.9, 137.7 (s, 3C, C-Ar), 128.1-127.1 (d, 15C, C-Ar), 88.3 (d, C-1), 85.8 (d, C-2), 73.7 (d, C-6) 73.0 (t, C-Bn), 72.2 (t, C-Bn), 71.9 (t, C-8), 71.6 (t, C-Bn), 68.7 (d, C-3), 65.9 (d, C-7a), 63.4 (t, C-5), 40.4 (t, C-7) ppm. IR ($CDCl_3$): ϑ = 3390, 3088, 3065, 3031, 2926, 2857,

1496, 1454, 1366, 1260, 1206, 1100, 1076 cm^{-1}. MS (ESI): *m/z* (%) = 460.36 $[M + 1]^+$. $C_{29}H_{33}NO_4$ (459.58): calcd. C 75.79, H 7.24, N 3.05; found C 75.49, H 7.14, N 3.04.

(1*R*,2*R*,3*R*,6*S*,7a*R*)-1,2,6-Trihydroxy-3-(hydroxymethyl)-hexahydro-1*H*-pyrrolizine (37) *(synthetized by Prof. F. Cardona, Chemistry department, University of Florence)*

To a solution of **41** (43 mg, 0.094 mmol) in 10 ml of methanol 22 mg of Pd on activated carbon (10% Pd) and two drops of 37% HCl were added under stirring and nitrogen atmosphere, then the mixture was left under hydrogen atmosphere at rt for 3 days. After TLC analysis (CH_2Cl_2:MeOH 10:1), showing the disappearance of starting material (R_f = 0.43) and the formation of a new product (R_f = 0.00), the mixture was filtered through Celite® and the solvent was removed under reduced pressure affording a crude yellow oil (40 mg). Free amine was obtained by eluting the hydrochloride salt through a Dowex 50WX8 ion-exchange resin. Elution with ammonia 6% afforded the free base **37** (18 mg, 0.094 mmol, 100% yield over two steps) as a white solid. M.p. 159-162 °C. $[\alpha]_D^{21}$ = +25.4 (*c* = 0.31, H_2O). ^1H NMR (400 MHz, D_2O): δ = 4.45 (pseudo q, *J* = 4.2 Hz, 1H, H-6), 3.74-3.68 (m, 2H, H-2 and H-1), 3.65 (dd, *J* = 11.7, 3.9 Hz, 1H, Ha-8), 3.50 (dd, *J* = 11.7, 6.9 Hz, 1H, Hb-8), 3.26 (q, *J* = 7.4 Hz, 1H, H-7a), 2.87 (dd, *J* = 11.7, 3.4 Hz, 1H, Ha-5), 2.81 (dd, *J* = 11.7, 4.4 Hz, 1H, Hb-5), 2.66-2.62 (m, 1H, H-3), 1.94 (ddd, *J* = 13.1, 7.3, 3.9 Hz, 1H, Ha-7), 1.86 (ddd, *J* = 13.2, 7.3, 5.2 Hz, 1H, Hb-7) ppm. ^{13}C NMR (50 MHz, D_2O): δ = 80.6 (d, C-2), 77.8 (d, C-1), 72.2 (d, C-6) 70.1 (d, C-3), 65.3 (d, C-7a), 62.6 (t, C-8), 61.6 (t, C-5), 37.8 (t, C-7) ppm. MS (ESI): *m/z* (%) = 190.1 $[M + 1]^+$. $C_8H_{15}NO_4$ (189.21): calcd. C 50.78, H 7.99, N 7.40; found C 50.97, H 7.89, N 7.59.

Biological assays *were performed in collaboration with Prof. P. Fusi (Biotechnology department, University of Milano-Bicocca), Dr. M. Casartelli and Dr. S. Caccia (Department of Biosciences, University of Milano).*

In vitro assays with different α-glucosidases.

Compounds **29**-**31** were tested for their inhibitory activity against insect trehalase of midge larvae of *C. riparius*[101], porcine trehalase (purchased from Sigma-Aldrich) as the mammalian counterpart and α-amylase from human saliva (purchased from Sigma-Aldrich), as a relevant glucolytic enzyme. The inhibitory activity of compounds **25**, **28**, **36**-**37** was tested also against insect trehalase of *S. littoralis* midgut and Malpighian tubules. *S. littoralis* larvae (first day of sixth instar) were anesthetized with CO_2 prior to dissection. Midgut and Malpighian tubules of *S. littoralis* were isolated in Tris-HCl 20 mM pH 6.8 and homogenized with 5 volumes of the same buffer in a glass and Teflon Potter-Elvehjem, two times 9-strokes at 2,000 rpm, separated by 1 min in ice. The crude homogenate was centrifuged at 13,000g at 4°C for 30 min. The resulting supernatant was used to measure enzyme activities. Proteins were measured according to Bradford using bovine serum albumin as standard[332]. Trehalase activity was measured through a coupled assay with glucose-6-phosphate dehydrogenase and hexokinase according to Wegener et al.[77]. To examine the potential of each compound as a trehalase inhibitor, screening assays of potential inhibitors were carried out at a fixed concentration of 1 mM and dose-response curves were established to determine the IC_{50} values. Experiments were performed at fixed substrate concentration close to the K_m value (0.5 mM for *C. riparius* and *S. littoralis* trehalase and 2.5 mM for porcine trehalase), in the presence of increasing inhibitor concentrations. Initial rates as a function of inhibitor concentration were fitted to the following equation:

$$\frac{v_i}{v} = \frac{1}{1 + \left(\frac{[I]}{IC_{50}} \right)^n}$$

where v_i and v are the initial rate in the presence and in the absence of inhibitor, respectively, $[I]$ is the inhibitor concentration, IC_{50} is the inhibitor concentration producing half-maximal inhibition, and n is the Hill coefficient. The inhibition constant can be calculated using the following Cheng-Prusoff relationship:

$$IC_{50} = K_i \left(1 + \frac{[S]}{K_m}\right)$$

Kinetic experiments were performed using *C. riparius* trehalase measuring enzymatic activity at different trehalose concentrations from 0.25 to 10 mM in the presence of fixed inhibitor concentrations. Kinetic parameters were calculated using a multiparameter, iterative, non-linear regression program based on the Marquardt-Levenberg algorithm (Sigma Plot, Jandel, CA). Data are given ± S.D. of three independent experiments. All enzyme assays were performed in triplicates at 30°C by using sample volumes varying from 5 to 20 µL in 1 mL test and using a Cary3 UV/Vis Spectrophotometer. Enzyme activities were analyzed by Cary Win UV application software for Windows XP. The α-amylase inhibition assay was performed at fixed starch concentration close to the K_m value (0,6% w/v), in the presence of increasing inhibitor concentration. Potential inhibitors were added to 0.5 mL enzyme solution (10 µg/mL). The reaction was initiated by adding 0.5 mL of starch dissolved in 20 mM sodium phosphate pH 6.9 and 6.7 mM sodium chloride and stopped after 3 minutes at room temperature by adding 1 mL of 3,5-dinitrosalicylic acid reagent (43 mM 3,5-dinitrosalicylic acid, 1 M sodium potassium tartrate tetrahydrate and 0.4 M sodium hydroxide in aqueous solution). The mixture was heated at 100°C for 5 minutes. After cooling to room temperature, 10 mL of milliQ water were added and absorbance was recorded at 540 nm using a Cary3 UV/Vis Spectrophotometer[333]. Micromoles maltose released were determined from standard curve and the enzymatic activity was calculated using the following equation:

$$\frac{Units}{mg} = \frac{micromoles\ maltose\ released}{mg\ enzyme\ in\ reaction\ mixture\ x\ 3\ min}$$

All enzymes assays were performed in triplicates at 30°C.

Bioassays with a-glucosidases inhibitor.

S. littoralis larvae (first day of fifth or sixth instars) were intra-hemocoellically injected by an Hamilton syringe (Hamilton, Nevada, USA). Briefly, larvae were anesthetized with CO_2 and injected with a single dose of casuarine derivative **37** (50, 150 and 300 µg/larva and 300 µg/larva in sixth instar and fifth instar respectively). Casuarine derivative **37** in 1:1 H_2O:DMSO. Control larvae were injected with equal amounts of solvent. Larval weight was recorded daily; pupal weight and morphology, adult emergence, fertility and longevity were also monitored.

7.2. Synthesis of multivalent glycoconjugates

General methods

Collagen type I from equine tendon was purchased from OPOCRIN S.p.a.; all other chemicals were purchased from Sigma–Aldrich and used without further purification. All solvents were dried over molecular sieves, for at least 24 h prior to use, when required. When dry conditions were required, the reaction was performed under an Ar or N_2 atmosphere. Thin-layer chromatography (TLC) was performed on silica gel $60F_{254}$ coated glass plates (Merck) with UV detection when possible, or spots were visualized by charring with a conc. H_2SO_4/EtOH/H_2O solution (10:45:45 v/v/v), or with a solution of $(NH_4)_6Mo_7O_{24}$ (21 g), $Ce(SO_4)_2$ (1 g), conc. H_2SO_4 (31 mL) in water (500 mL) and then by heating to 110 °C for 5 min. Flash column chromatography was performed on silica gel 230–400 mesh (Merck) or on a Biotage Isolera One (version 2.0.4, operating system biotage OS 578). Routine ^1H and ^{13}C NMR spectra were recorded on a Varian Mercury instrument at 400 MHz (^1H) and 100.57 MHz (^{13}C). Chemical shifts are reported in parts per million downfield from TMS as an internal standard; *J* values are given in Hz. Mass spectra were recorded on System Applied Biosystems MDS SCIEX instruments: Q TRAP, LC/MS/MS, turbo ion spray and Q STAR elite nanospray. Thiol-ene photo-click reactions were performed on an Applied Photophysics photoreactor (UV lamp, 365 nm). Elemental analyses (C, H, N) were performed with a Perkin–Elmer series II 2400 analyzer. Recombinant LecB was purified from *Escherichia coli* BL21(DE3) containing the plasmid pET25pa2l as previously described[334].

Collagen patches preparation

Type I collagen films from equine tendon (1% collagen gel in acetic acid) were produced by the solvent-casting method as previously described[335]. Briefly, the 1% gel was diluted 1:6 w/v in ultrapure water. The suspension was homogenized at 4°C with a mixer for 2 minutes at maximum speed. After removal of the aggregates, 80 mL of collagen solution was poured into an 8.5 x 12.5 cm plastic plate and the solvent evaporated to dryness in the fume hood for two days.

*Preparation of thiolated-collagen (collagen-SH) (**53**)*

A collagen patch (80 mg, 12 cm x 7 cm) was immersed in 20 mL of 1:1 v/v EtOH:PBS containing 0.025 M γ - thiobutyrolactone for 24 h at room temperature (adapted from Kurimoto et al.[336]). Collagen-SH was washed with 0.1 M HCl (20 mL) for 10 min, than with mQ H_2O (20 mL) for 10 minutes x 3 times, and finally with 20 mL of ethanol for 10 minutes.

Labeling and quantification of thiol groups by NMR

Derivatization of the thiolated and non-thiolated samples with DiThiobis(Nitro Benzoic acid) (DTNB), was performed to label and quantify -SH groups inserted with γ -thiobutyrolactone. Collagen-SH (12 mg) was immersed in an aq. solution (0.035 M) of DTNB and (0.05 M) DIPEA. The reaction was carried out at room temperature for 24 hours. Collagen-S-TNB was thoroughly washed with 20 mL of 0.1 M aq. HCl for 10 min., with 20 mL mQ H_2O for 10 minutes x 3 times, and finally with 20 mL ethanol for 10 minutes. Collagen was dried under vacuum and then dissolved in 0.6 mL of 2 M NaOH in H_2O. ^{1}H-NMR spectra were recorded using a Varian 400 MHz Mercury instrument, operating at a proton frequency equal to 400 MHz, at room temperature. The 5 mm diameter NMR tubes were sealed and kept closed during the full duration of the experiment. The 90º pulse-width (pw90) was calibrated, the number of scans varied depending on the signal-to-noise ratio, and the recycling delay was 5 s.

X-ray Photoelectron Spectroscopy (XPS) *performed by dott. C. Battocchio (Department of Sciences, INSTM, CNISM and CISDiC, University Roma Tre)*

XPS analysis was performed in an instrument of our own design and construction**,** consisting of a preparation and an analysis UHV chamber, equipped with a 150 mm mean radius hemispherical electron analyser with a four-element lens system with a 16-channel detector giving a total instrumental resolution of 1.0 eV as measured at the Ag $3d_{5/2}$ core level. MgKα non-monochromatised X-ray radiation (hν = 1253.6 eV) was used for acquiring core level spectra of all samples (C1s, N1s, S2p and O1s). The spectra were energy referenced to the C1s signal of aliphatic C atoms having a binding energy BE = 285.00 eV. Atomic ratios were calculated from peak

intensities by using Scofield's cross-section values and calculated λ factors[337]. Curve-fitting analysis of the C1s, N1s, S2p and O1s spectra was performed using Gaussian profiles as fitting functions, after subtraction of a Shirley-type background[338]. C1s and O1s signals are extensively discussed in the section 4.2. N1s signals show at least two spectral components associated to amide (-NHCO), amine (-NH-) and O-N=C groups (around 400eV BE) and to O-NH_2 and positively charged amine groups (-NH_3^+) (401.0 eV nearly)[230, 339]. A very similar composition is observed for all samples and, due to the very low number of N atoms in functional molecules structure, the N1s XPS signal is mainly due to the collagen substrate. As for S2p spectra, a single spin-orbit pair is observed at BE values expected for thiol-like sulphur ($S2p_{3/2}$ BE = 163.8 eV)[337].

Infrared spectroscopy *performed by dott. A. Natalello (Biotechnology department, University of Milano-Bicocca)*

The attenuated total reflection (ATR) IR spectra of the collagen patches were collected using a single reflection diamond plate (Golden Gate, Specac, USA) and the FTIR spectrometer Varian 670-IR (Varian Australia Pty Ltd., AU), equipped with a nitrogen-cooled Mercury Cadmium Telluride detector and an air dryer purging system. The following conditions were employed: 2 cm^{-1} spectral resolution, 25 kHz scan speed, 512 scan coadditions, and triangular apodization. ATR/FTIR analyses were performed both on intact collagen patches and on their external layers. To this aim, collagen patches were scraped out on the ATR diamond plate and the spectra of the materials moved out from the film were collected.

Lectin-based assays

Pristine collagen and neoglycosylated collagen samples were treated with a solution of 2% BSA in PBS (100 µL) and shaken (14 h, 5°C), according to manufacturer protocol. The films were then removed and incubated at room temperature with a solution of the lectin from peanut (*Arachis hypogaea*) peroxidase labelled (Sigma-Aldrich, catalogue n° L7759) (0.01 mg/mL, 200 µL) in PBS for 2 h with shaking. The films were then thoroughly washed with PBS to remove unbound lectin and then treated with a solution of OPD (SIGMAFAST™ OPD, Sigma-Aldrich,

catalogue n°P9187) (500 µL, 1 h). The absorbance of an aliquot of this solution (200 µL) was measured at 450 nm.

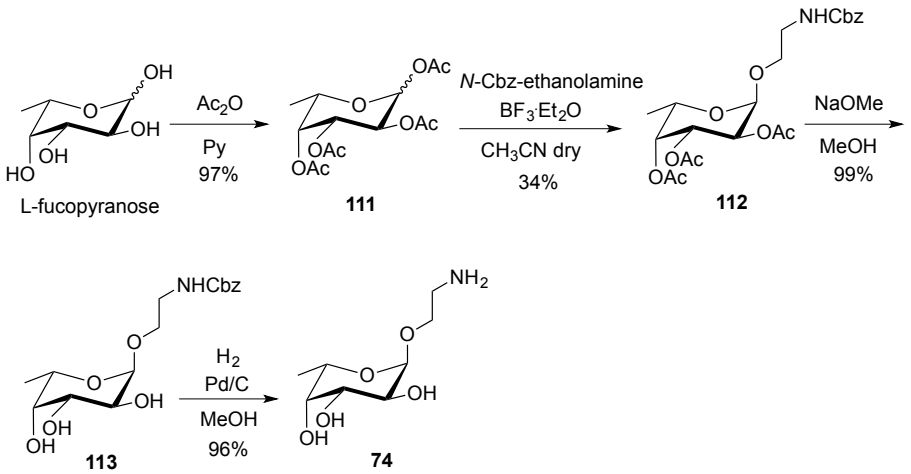

Scheme 18. Synthesis of α-L-(2-aminoethyl) fucopyranoside (**74**)[235].

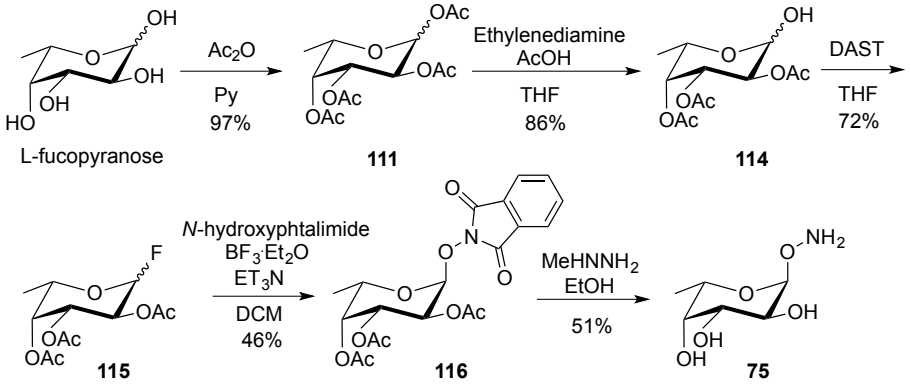

Scheme 19. Synthesis of α-*O*-L-fucopyranosyl oxyamine (**75**)[236].

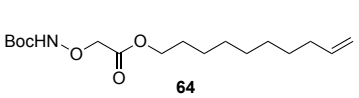

64

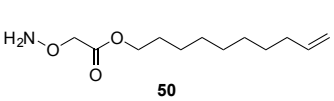

50

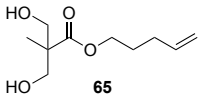

65

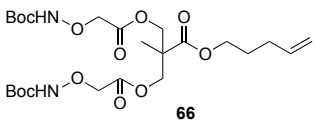

66

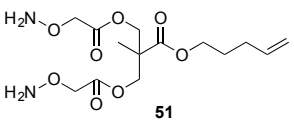

51

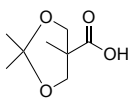

67

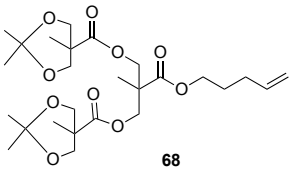

68

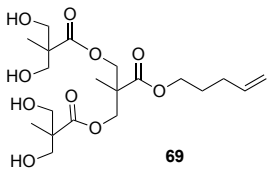

69

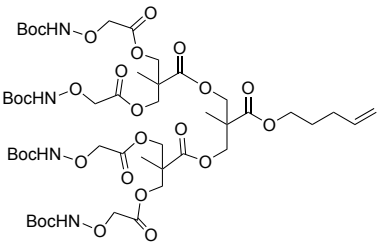

70

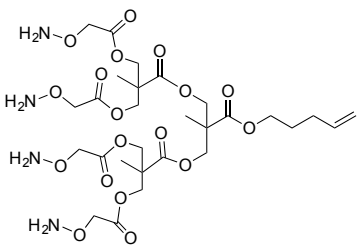

52

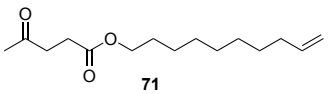

71

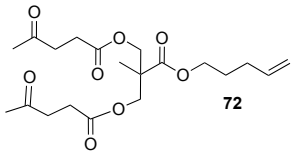

72

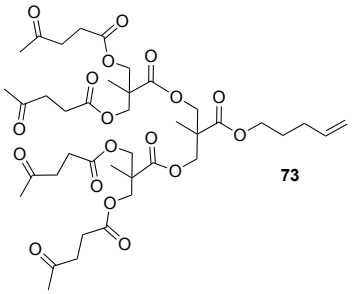

73

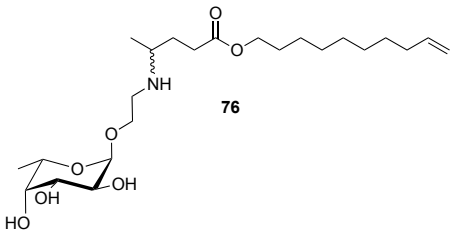

76

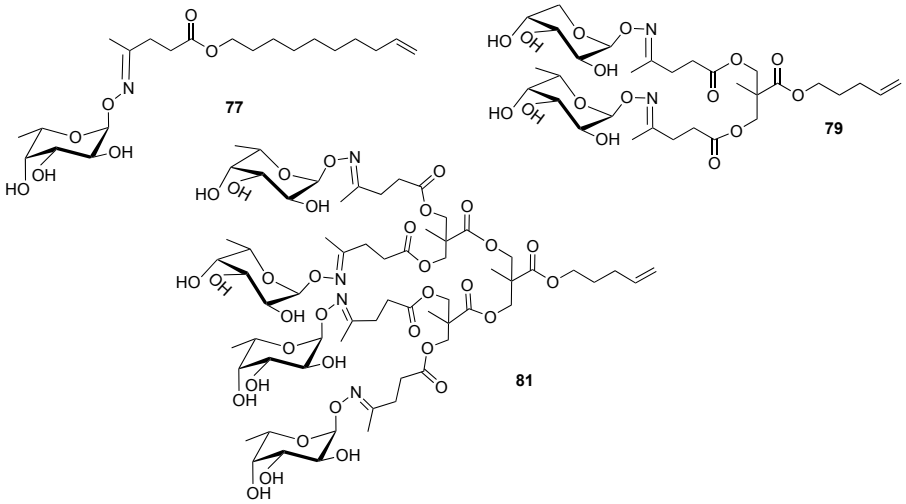

Figure 33. Summary of the synthesized compounds.

Dec-9-en-1-yl 2-(((*tert*-butoxycarbonyl)amino)oxy)acetate (64)

(Boc-aminooxy)acetic acid **60** (499 mg, 2.61 mmol), 9-decen-1-ol **61** (388 mL, 2.17 mmol), DMAP (53 mg, 0.43 mmol) and *p*-toluenesulfonic acid (83 mg, 0.43 mmol) were dissolved in dry CH_2Cl_2 (20 mL). DCC (561 mg, 2.72 mmol) was added and the solution was stirred for 3 h at room temperature. The precipitates were filtered off and washed with CH_2Cl_2. The solvent was evaporated, and the residue was purified by flash column chromatography (petroleum ether/EtOAc, 85:15) affording **64** (522 mg, 73% yield). ^{1}H NMR (400 MHz, $CDCl_3$): δ = 7.96 (s, 1H, NH), 5.73 (ddt, *J* = 16.9, 10.2, 6.7 Hz, 1H, C*H*=CH_2), 4.97 – 4.76 (m, 2H, CH=C*H*$_2$), 4.36 (s, 2H, O-CH_2-C=O), 4.10 (t, *J* = 6.8 Hz, 2H, CH_2-O-C=O), 1.96 (q, *J* = 6.9 Hz, 2H, C*H*$_2$-CH=CH_2), 1.63 – 1.53 (m, 2H, O-CH_2-C*H*$_2$), 1.40 (s, 9H, CH_3), 1.34 – 1.17 (m, 10H, CH_2). ^{13}C NMR (100.57 MHz, $CDCl_3$): δ = 169.65 (O-C=O), 156.24 (NH-C=O), 138.94 (*C*H=CH_2), 114.14 (CH=*C*H$_2$), 81.81 (C Boc), 72.42 (O-*C*H$_2$-C=O), 65.22 (*C*H$_2$-O-C=O), 33.68 (*C*H$_2$-CH=CH_2), 29.23, 29.06, 28.91, 28.77, 28.41, 25.72 (CH_2), 28.07 (CH_3). MS (TOF, m/z): $[M + Na]^+$ calcd for $C_{17}H_{31}NO_5$, 352.2; found 352.3. $C_{17}H_{31}NO_5$ (329.43): calcd. C 61.98, H 9.48, N 4.25; found C 61.85, H 9.50, N 4.26.

Dec-9-en-1-yl 2-(aminooxy)acetate (50)

To a cooled solution (0 °C) of **64** (522 mg, 1.58 mmol) in anhydrous DCM (16 mL), TFA (4.7 mL) was added drop-wise. After 1 h, the reaction mixture was quenched with aq. satd. Na_2CO_3 to neutrality. The mixture was extracted with DCM, the combined organic extracts were dried over anhydrous Na_2SO_4 and concentrated affording compound **50** (211 mg, 58% yield). ^{1}H NMR (400 MHz, $CDCl_3$): δ = 5.85 – 5.61 (m, 3H, NH_2, C*H*=CH_2), 5.01 – 4.75 (m, 2H, CH=C*H*$_2$), 4.17 (s, 2H, O-CH_2-C=O), 4.09 (t, *J* = 6.8 Hz, 2H, CH_2-O-C=O), 1.97 (q, *J* = 6.8 Hz, 2H, C*H*$_2$-CH_2=CH_2), 1.65 – 1.52 (m, 2H, O-CH_2-C*H*$_2$), 1.38 – 1.13 (m, 10H, CH_2). ^{13}C NMR (100.57 MHz, $CDCl_3$): δ = 170.74 (C=O), 139.00 (*C*H=CH_2), 114.13 (CH=*C*H_2), 72.32 (O-*C*H_2-C=O), 64.86 (*C*H_2-O-C=O), 33.70 (*C*H_2-CH_2=CH_2), 29.25, 29.09, 28.94, 28.79, 28.49, 25.77 (CH_2). MS (TOF, m/z): $[M + H]^+$ calcd for $C_{12}H_{23}NO_3$, 230.2; found 230.3. $C_{12}H_{23}NO_3$ (229.32): calcd. C 62.85, H 10.11, N 6.11; found C 62.95, H 10.09, N 6.10.

Pent-4-en-1-yl 3-hydroxy-2-(hydroxymethyl)-2-methylpropanoate (65)

Bis-MPA **62** (2.0 g, 14.9 mmol) and Cs_2CO_3 (5.54 g, 17.0 mmol) were dissolved in anhydrous DMF (11.2 mL) and reacted at 100 °C for 2 h. 5-Bromo-1-pentene **63** (2.2 mL, 17.9 mmol) was added; after 15 h at 100 °C, the solvent was evaporated to dryness. The residue was dissolved in 40 mL of EtOAc and washed twice with water. The organic layer was dried over anhydrous Na_2SO_4 and concentrated. The crude product was purified by flash column chromatography (petroleum ether/EtOAc, 25:75) affording pure **65** (1.266 g, 6.26 mmol, 42 % yield). ^{1}H NMR (400 MHz, $CDCl_3$): δ = 5.80 (ddt, *J* = 13.4, 10.1, 6.7 Hz, 1H, C*H*=CH_2), 5.09 – 4.94 (m, 2H, CH=C*H*$_2$), 4.18 (t, *J* = 6.5 Hz, 2H, CH_2-O-C=O), 3.90 (d, *J* = 11.2 Hz, 2H, C*H*$_2$-OH), 3.71 (d, *J* = 11.2 Hz, 2H, C*H*$_2$-OH), 2.65 (bs, 2H, -OH), 2.14 (dd, *J* = 14.1, 7.0 Hz, 2H, C*H*$_2$-CH=CH_2), 1.83 – 1.72 (m, 2H, O-CH_2-C*H*$_2$), 1.06 (s, 3H, CH_3). ^{13}C NMR (100.57 MHz, $CDCl_3$): δ = 175.95 (C=O), 137.26 (*C*H=CH_2), 115.49 (CH=*C*H_2), 68.01(CH_2OH), 64.41(*C*H_2-O-C=O), 49.12 (*C*-CH_2OH), 29.97 (*C*H_2-CH=CH_2), 27.63 (O-CH_2-*C*H_2), 17.14 (CH_3). MS (TOF, m/z): $[M + Na]^+$ calcd for $C_{10}H_{18}O_4$, 225.1; found 225.2. $C_{10}H_{18}O_4$ (202.25): calcd. C 59.39, H 8.97; found C 59.45, H 8.99.

2-Methyl-2-((pent-4-en-1-yloxy)carbonyl)propane-1,3-diyl bis(2-(((*tert*-butoxycarbonyl)amino)oxy)acetate) (66)

(Boc-aminooxy)acetic acid **60** (340 mg, 1.78 mmol), **65** (150 mg, 0.74 mmol), DMAP (36 mg, 0.30 mmol) and *p*-toluenesulfonic acid (56 mg, 0.30 mmol) were dissolved in dry CH_2Cl_2 (6.9 mL). DCC (382 mg, 1.85 mmol) was added and the solution was stirred for 48 h at room temperature. The solids were filtered off and washed with CH_2Cl_2. The solvent was evaporated, and the residue was purified by flash column chromatography (petroleum ether/EtOAc, 72.5:27.5) to afford pure **66** (393 mg, 0.72 mmol, 97 % yield). ^{1}H NMR (400 MHz, $CDCl_3$): δ = 7.92 (s, 2H, NH), 5.74 (ddt, *J* = 16.9, 10.2, 6.6 Hz, 1H, C*H*=CH_2), 5.04 – 4.92 (m, 2H, CH=C*H*$_2$), 4.40 (s, 4H, O-CH_2-C=O), 4.34 (d, *J* = 11.1 Hz, 2H, C*H*$_2$O-CO-CH_2), 4.28 (d, *J* = 11.1 Hz, 2H, C*H*$_2$O-CO-CH_2), 4.12 (t, *J* = 6.5 Hz, 2H, CH_2-C*H*$_2$-O-C=O), 2.07 (dd, *J* = 14.4, 6.9 Hz, 2H, C*H*$_2$-CH=CH_2), 1.76 – 1.66 (m, 2H, O-CH_2-C*H*$_2$), 1.44 (s, 18H, CH_3 Boc), 1.24 (s, 3H, CH_3). ^{13}C NMR (100.57 MHz, $CDCl_3$): δ = 172.33, 169.13, 156.21 (C=O), 136.96 (*C*H=CH_2), 115.63 (CH=*C*H_2), 82.17 (C Boc), 72.32 (O-*C*H_2-C=O), 65.45 (*C*H_2O-CO-CH_2), 64.86 (CH_2-*C*H_2-O-C=O), 46.29 (*C*-CH_2O-C=O), 29.83 (*C*H_2-CH=CH_2), 28.11 (CH_3 Boc), 27.52 (O-CH_2-*C*H_2), 17.88 (CH_3). MS (TOF, m/z): $[M + Na]^+$ calcd for $C_{24}H_{40}N_2O_{12}$, 571.3; found 571.4. $C_{24}H_{40}N_2O_{12}$ (548.58): calcd. C 52.55, H 7.35, N 5.11; found C 52.63, H 7.37, N 5.10.

2-Methyl-2-((pent-4-en-1-yloxy)carbonyl)propane-1,3-diyl bis(2-(aminooxy)acetate) (51)

To a cooled (0 °C) solution of **66** (142 mg, 0.26 mmol) in anhydrous DCM (2.6 mL) TFA was added dropwise (787 mL). After stirring for 1 h at 0 °C, the reaction mixture was quenched to neutrality with satd. aq. Na_2CO_3. The aqueous layer was extracted with DCM and the combined organic extracts were dried with Na_2SO_4 and concentrated to afford compound **51** (63 mg, 0.18 mmol, 70 % yield). ^{1}H NMR (400 MHz, $CDCl_3$): δ = 5.86 (s, 4H, NH_2), 5.75 (ddt, *J* = 16.9, 10.2, 6.7 Hz, 1H, C*H*=CH_2), 5.02 – 4.96 (m, 2H, CH=C*H*$_2$), 4.35 – 4.26 (m, 4H, C*H*$_2$O-CO-CH_2), 4.21 (s, 4H, O-CH_2-C=O), 4.11 (t, *J* = 6.5 Hz, 2H, CH_2-C*H*$_2$-O-C=O), 2.08 (q, *J* = 7.1 Hz, 2H, C*H*$_2$-CH=CH_2), 1.76 – 1.66 (m, 2H, O-CH_2-C*H*$_2$), 1.24 (s, 3H, CH_3). ^{13}C

NMR (100.57 MHz, $CDCl_3$): δ = 172.47, 170.20 (C=O), 137.12 (*C*H=CH_2), 115.56 (CH=*C*H_2), 72.16 (O-*C*H_2-C=O), 65.45 (*C*H_2O-CO-CH_2), 64.78 (CH_2-*C*H_2-O-C=O), 46.28 (*C*-CH_2O-C=O), 29.88 (*C*H_2-CH=CH_2), 27.56 (O-CH_2-*C*H_2), 17.90 (CH_3). MS (TOF, m/z): $[M + H]^+$ calcd for $C_{14}H_{24}N_2O_8$, 349.2; found 349.4. $C_{14}H_{24}N_2O_8$ (348.35): calcd. C 48.27, H 6.94, N 8.04; found C 48.35, H 6.92, N 8.06.

2,2,5-Trimethyl-1,3-dioxane-5-carboxylic acid (67)

Compound **67** was synthesized and purified following the experimental conditions reported by Ihre et al.[340].

2-Methyl-2-((pent-4-en-1-yloxy)carbonyl)propane-1,3-diyl bis(2,2,5-trimethyl-1,3-dioxane-5-carboxylate) (68)

67 (845 mg, 4.85 mmol), **65** (408 mg, 2.02 mmol), DMAP (99 mg, 0.81 mmol) and *p*-toluenesulfonic acid (154 mg, 0.81 mmol) were dissolved in dry CH_2Cl_2 (19 mL). DCC (1.042 g, 5.05 mmol) was added and the solution was stirred for 24 h at room temperature. The solids were filtered off and washed with a small volume of CH_2Cl_2. The solvent was evaporated, and the residue was purified by flash column chromatography (petroleum ether/EtOAc, 80:20) to afford compound **68** (795 mg, 1.54 mmol, 76 % yield). ^{1}H NMR (400 MHz, $CDCl_3$): δ = 5.74 (ddt, *J* = 16.9, 10.2, 6.6 Hz, 1H, C*H*=CH_2), 5.01 – 4.94 (m, 2H, CH=C*H*$_2$), 4.29 (s, 4H, CH_2O), 4.12 – 4.09 (m, 6H, CH_2O), 3.58 (d, *J* = 12.1 Hz, 4H, CH_2O), 2.08 (dd, *J* = 14.2, 7.0 Hz, 2H, C*H*$_2$-CH=CH_2), 1.74 – 1.67 (m, 2H, O-CH_2-C*H*$_2$), 1.37 (s, 6H, CH_3), 1.32 (s, 6H, CH_3), 1.25 (s, 3H, CH_3), 1.11 (s, 6H, CH_3). ^{13}C NMR (100.57 MHz, $CDCl_3$): δ = 173.53, 172.54 (C=O), 137.12 (*C*H=CH_2), 115.51 (CH=*C*H_2), 98.08 (*C*$(CH_3)_2$), 65.94, 65.31 (CH_2O), 64.69 (CH_2-*C*H_2-O-C=O), 46.70, 42.01 (*C*-CH_2O), 29.94 (*C*H_2-CH=CH_2), 27.62 (O-CH_2-*C*H_2), 24.99, 22.19, 18.52, 17.75 (CH_3). MS (TOF, m/z): $[M + H]^+$ calcd for $C_{26}H_{42}O_{10}$, 515.3; found 515.6. $C_{26}H_{42}O_{10}$ (514.61): calcd. C 60.68, H 8.23; found C 60.74, H 8.21.

2-Methyl-2-((pent-4-en-1-yloxy)carbonyl)propane-1,3-diyl bis(3-hydroxy-2-(hydroxymethyl)-2-methylpropanoate) (69)

Compound **68** (193 mg, 0.37 mmol) was dissolved in 2.5 mL of methanol. Amberlite IR-120 H^+ resin (193 mg) was added, and the reaction mixture was stirred for 15 h at room temperature. After completion of the reaction, the resin was filtered off and thoroughly washed with methanol. The methanol was evaporated to give **69** (163 mg, 0.37 mmol, quant. yield). ^{1}H NMR (400 MHz, $CDCl_3$): δ = 5.78 (ddt, *J* = 16.9, 10.2, 6.6 Hz, 1H, C*H*=CH_2), 5.07 – 4.94 (m, 2H, CH=C*H*$_2$), 4.43 (d, *J* = 11.1 Hz, 2H, CH_2OC=O), 4.25 (d, *J* = 11.1 Hz, 2H, CH_2OC=O), 4.15 (t, *J* = 6.6 Hz, 2H, CH_2-C*H*$_2$-O-C=O), 3.82 (dd, *J* = 11.3, 3.0 Hz, 4H, C*H*$_2$OH), 3.73 – 3.65 (m, 4H, C*H*$_2$OH), 3.24 (bs, 4H, OH), 2.11 (dd, *J* = 14.5, 6.9 Hz, 2H, C*H*$_2$-CH=CH_2), 1.80 – 1.69 (m, 2H, O-CH_2-C*H*$_2$), 1.29 (s, 3H, CH_3), 1.04 (s, 6H, CH_3). ^{13}C NMR (100.57 MHz, $CDCl_3$): δ = 174.97, 173.02 (C=O), 137.04 (*C*H=CH_2), 115.56 (CH=*C*H_2), 66.41, 64.76 (CH_2O), 49.79, 46.22 (*C*-CH_2O), 29.87 (*C*H_2-CH=CH_2), 27.54 (O-CH_2-*C*H_2), 18.11, 17.07 (CH_3). MS (TOF, m/z): $[M + H]^+$ calcd for $C_{20}H_{34}O_{10}$, 435.2; found 435.4. $C_{20}H_{34}O_{10}$ (434.48): calcd. C 55.29, H 7.89; found C 55.37, H 7.88.

(((2-Methyl-2-((pent-4-en-1-yloxy)carbonyl)propane-1,3-diyl)bis(oxy))bis(carbonyl))bis(2-methylpropane-2,1,3-triyl) tetrakis(2-(((tert-butoxycarbonyl)amino)oxy)acetate) (70)

(Boc-aminooxy)acetic acid **60** (450 mg, 2.35 mmol), **69** (213 mg, 0.49 mmol), DMAP (48 mg, 0.39 mmol) and *p*-toluenesulfonic acid (74 mg, 0.39 mmol) were dissolved in dry CH_2Cl_2 (4.5 mL). DCC (505 mg, 2.45 mmol) was added and the solution was stirred for 24 h at room temperature. The solids were filtered off and washed with a small volume of CH_2Cl_2. The solvent was evaporated, and the residue was purified by flash column chromatography (petroleum ether/EtOAc 10:0→1:9) to give **70** (371 mg, 0.33 mmol, 67 % yield). ^{1}H NMR (400 MHz, $CDCl_3$): δ = 8.00 (s, 4H, NH), 5.76 (ddt, *J* = 16.8, 10.2, 6.6 Hz, 1H, C*H*=CH_2), 5.05 – 4.93 (m, 2H, CH=C*H*$_2$), 4.41 (s, 8H, O-CH_2-C=O), 4.33 – 4.19 (m, 12H, CH_2OC=O), 4.13 – 4.06 (m, 2H, CH_2-C*H*$_2$-O-C=O), 2.08 (dd, *J* = 14.2, 7.1 Hz, 2H, C*H*$_2$-CH=CH_2), 1.76 – 1.66 (m, 2H, O-CH_2-C*H*$_2$), 1.44 (s, 36H, CH_3 Boc), 1.22 (s, 9H, CH_3). ^{13}C NMR

(100.57 MHz, $CDCl_3$): δ = 171.65, 169.14, 156.30 (C=O), 137.01 (*C*H=CH_2), 115.61 (CH=*C*H_2), 82.13 (C Boc), 72.31 (O-*C*H_2-C=O), 65.62, 65.24, 64.96 (CH_2O), 46.49, 46.40 (*C*-CH_2O), 29.88 (*C*H_2-CH=CH_2), 28.12 (CH_3 Boc), 27.55 (O-CH_2-*C*H_2), 17.81, 17.60 (CH_3). MS (TOF, m/z): $[M + Na]^+$ calcd for $C_{48}H_{78}N_4O_{26}$, 1149.5; found 1149.5. $C_{48}H_{78}N_4O_{26}$ (1127.14): calcd. C 51.15, H 6.98, N 4.97; found C 51.26, H 6.97, N 4.98.

(((2-methyl-2-((pent-4-en-1-yloxy)carbonyl)propane-1,3-diyl)bis(oxy))bis(carbonyl))bis(2-methylpropane-2,1,3-triyl) tetrakis(2-(aminooxy)acetate) (52)

To a cooled (0 °C) solution of **70** (371 mg, 0.33 mmol) in anhydrous DCM (3.5 mL) TFA was added dropwise (1.0 mL). After stirring for 3 h at 0 °C, the reaction mixture was quenched to neutrality with satd. aq. Na_2CO_3. The aqueous layer was extracted with DCM and the combined organic extracts were dried over Na_2SO_4 and concentrated to afford **52** (134 mg, 0.18 mmol, 56 % yield). ^{1}H NMR (400 MHz, $CDCl_3$): δ = 5.93 – 5.70 (m, 9H, NH_2, C*H*=CH_2), 5.07 – 4.94 (m, 2H, CH=C*H*$_2$), 4.34 – 4.20 (m, 20H, CH_2O), 4.12 (t, *J* = 6.6 Hz, 2H, CH_2-C*H*$_2$-O-C=O), 2.10 (dd, *J* = 14.3, 7.1 Hz, 2H, C*H*$_2$-CH=CH_2), 1.78 – 1.68 (m, 2H, O-CH_2-C*H*$_2$), 1.24 (s, 9H, CH_3). ^{13}C NMR (100.57 MHz, $CDCl_3$): δ = 172.05, 171.82, 170.29 (C=O), 137.11 (*C*H=CH_2), 115.57 (CH=*C*H_2), 72.25 (O-*C*H_2-C=O), 65.68, 65.31, 64.92 (CH_2O), 46.52, 46.44 (*C*-CH_2O), 29.91 (*C*H_2-CH=CH_2), 27.58 (O-CH_2-*C*H_2), 17.78, 17.65 (CH_3). MS (TOF, m/z): $[M + H]^+$ calcd for $C_{28}H_{46}N_4O_{18}$, 727.3; found 727.4. $C_{28}H_{46}N_4O_{18}$ (726.68): calcd. C 46.28, H 6.38, N 7.71; found C 46.34, H 6.39, N 7.70.

Multifunctional collagen patches (collagen-$(ONH_2)_n$)(54)-(56)

Coupling of thiolated collagen (**53**) (12 mg, 5 cm x 2) respectively with mono-, di- and tetra-functional arms (**50-52**, 35 mM) was carried out at room temperature for 1 h in 30 mL of MeOH:H_2O (1:2) mixture by irradiation with a UV-lamp (λ max = 365 nm) using 2,2-dimethoxy-2-phenylacetophenone (DPAP, 14 mM) as a radical initiator. Multifunctional collagens were then washed with 20 mL mQ H_2O for 20 minutes x 3 times, and finally with ethanol (20 mL) for 20 minutes.

Multifunctional collagen glycosylation (collagen-(sugar)$_n$) (57)-(59)

Multifunctional collagen patches **54**-**56** (12 mg, 5 cm x 2) were immersed in acetate buffer (3 mL, pH 4) containing lactose (0.013 M for **54**, 0.027 M for **55** and 0.054 M for **56** respectively) and reacted at room temperature overnight. Glycosylated-collagen was then washed with 20 ml of mQ H_2O for 20 minutes x 3 times, and finally with ethanol (20 mL, 20 min).

General procedure for levulinic acid condensation (71–73)

To a 0.1 M solution of the appropriate compound dissolved in dry DCM, levulinic acid (1.2 equiv), DMAP (0.2 equiv.) and DCC (1.5 equiv.) were added and the reaction mixture was stirred at room temperature (from 1 to 24h, depending on the substrate). The precipitates were filtered off and washed with CH_2Cl_2. The solvent was evaporated, and the residue was purified by on a silica gel column with a suitable eluent.

Dec-9-en-1-yl 4-oxopentanoate (71)

Flash column chromatography (petroleum ether/EtOAc, 85:15). ^{1}H NMR (400 MHz, $CDCl_3$): δ = 5.72 (ddt, *J* = 16.9, 10.2, 6.7 Hz, 1H, C*H*=CH_2), 4.95 – 4.79 (m, 2H, CH=C*H*$_2$), 3.98 (t, *J* = 6.8 Hz, 2H, CH_2O), 2.67 (t, *J* = 6.5 Hz, 2H, CH_3COCH_2), 2.49 (t, *J* = 6.5 Hz, 2H, $CH_2CH_2CO_2$), 2.11 (s, 3H, CH_3CO), 1.96 (q, J = 7.1 Hz, 2H, C*H*$_2$-CH=CH_2), 1.58 – 1.48 (m, 2H, O-CH_2-C*H*$_2$), 1.35 – 1.17 (m, 10H, CH_2) ppm; ^{13}C NMR (100.57 MHz, $CDCl_3$): δ = 206.52, 172.69 (C=O), 138.99 (*C*H=CH_2), 114.09 (CH=*C*H_2), 64.68 (*C*H_2O), 37.84 (CH_3CO*C*H_2), 33.70 (*C*H_2-CH=CH_2), 29.77 (*C*H_3CO), 29.26, 29.10, 28.94, 28.79, 28.48, 27.88, 25.78 (CH_2) ppm; MS (TOF) *m/z*: 277.2 $[M + Na]^+$; found 277.1.

2-Methyl-2-((pent-4-en-1-yloxy)carbonyl)propane-1,3-diyl bis(4-oxopentanoate) (72)

Flash column chromatography (petroleum ether/EtOAc, 55:45). ^{1}H NMR (400 MHz, $CDCl_3$): δ = 5.81 – 5.71 (m, 1H, C*H*=CH_2), 5.05 – 4.92 (m, 2H, CH=C*H*$_2$), 4.24 – 4.15 (m, 4H, C*H*$_2$O-CO-CH_2), 4.11 (t, *J* = 6.4 Hz, 2H, CH_2-C*H*$_2$-O-C=O), 2.71 (t, *J* = 6.4 Hz, 4H, CH_3COCH_2), 2.53 (t, *J* = 6.4 Hz, 4H, $CH_2CH_2CO_2$), 2.15 (s,

6H, CH_3CO), 2.08 (q, *J* = 7.0 Hz, 2H, C*H*$_2$-CH=CH_2), 1.76 – 1.66 (m, 2H, O-CH_2-C*H*$_2$), 1.21 (s, 3H, CH_3) ppm; ^{13}C NMR (100.57 MHz, $CDCl_3$): δ = 206.35, 172.67, 172.16 (C=O), 137.19 (*C*H=CH_2), 115.43 (CH=*C*H_2), 65.41 (C-*C*H_2O), 64.53 (CH_2*C*H_2OCO), 46.22 (*C*-CH_2O), 37.79 (CH_3CO*C*H_2), 29.88 (*C*H_2-CH=CH_2), 29.75 (*C*H_3CO), 27.74, 27.59 (CH_3COCH_2*C*H_2, O-CH_2-*C*H_2), 17.78 (CH_3) ppm; MS (TOF) *m/z*: 421.2 $[M + Na]^+$; found 421.4.

(((2-methyl-2-((pent-4-en-1-yloxy)carbonyl)propane-1,3 diyl)bis(oxy))bis(carbonyl))bis(2-methylpropane-3,2,1-triyl) tetrakis(4-oxopentanoate) (73)

Flash column chromatography (petroleum ether/EtOAc, 25:75). ^{1}H NMR (400 MHz, $CDCl_3$): δ = 5.77 (ddt, *J* = 16.8, 10.2, 6.6 Hz, 1H, C*H*=CH_2), 5.06 – 4.93 (m, 2H, CH=C*H*$_2$), 4.27 – 4.05 (m, 14H, CH_2O), 2.72 (t, *J* = 6.5 Hz, 8H, CH_3COCH_2), 2.54 (t, *J* = 6.4 Hz, 8H, $CH_2CH_2CO_2$), 2.15 (s, 12H, CH_3CO), 2.10 (dd, *J* = 14.3, 7.2 Hz, 2H, C*H*$_2$-CH=CH_2), 1.78 – 1.67 (m, 2H, O-CH_2-C*H*$_2$), 1.23 (s, 9H, CH_3) ppm; ^{13}C NMR (100.57 MHz, $CDCl_3$): δ = 206.41, 172.17, 172.01 (C=O), 137.17 (*C*H=CH_2), 115.48 (CH=*C*H_2), 65.66, 65.21 (C-*C*H_2O), 64.82 (CH_2*C*H_2OCO), 46.54, 46.34 (*C*-CH_2O), 37.79 (CH_3CO*C*H_2), 29.92 (*C*H_2-CH=CH_2), 29.75 (*C*H_3CO), 27.70, 27.59 (CH_3COCH_2*C*H_2, O-CH_2-*C*H_2), 17.72, 17.58 (CH_3) ppm; MS (TOF) *m/z*: 894.4 $[M + Na]^+$; found 894.4.

General procedure for reductive amination reaction (76 and 78):

The appropriate dendron (1 equiv.) and α-L-(2-aminoethyl) fucoside (**74**, 1 equiv.) were dissolved in EtOH (0.1 M in respect to **74**). AcOH (1 equiv.) and 3 M Na_2SO_4 (1% of solvent volume) were added and the mixture was heated under reflux for 2 h. $NaCNBH_3$ (1.5 equiv) was then added and the reaction was heated under reflux for other 4 h.

Dec-9-en-1-yl 4-((2-((3,4,5-trihydroxy-6-methyltetrahydro-2H-pyran-2-yl)oxy)ethyl)amino)pentanoate (76)

The mixture obtained as described in the general procedure was concentrated and the residue was purified by flash column chromatography (i-PrOH/NH_3, 95:5). ^{1}H

NMR (400 MHz, CD_3OD): δ = 5.80 (ddt, *J* = 16.9, 10.0, 6.7 Hz, 1H, C*H*=CH_2), 5.02 – 4.90 (m, 2H, CH=C*H*$_2$), 4.77 (bs, 1H, H-1), 4.07 (t, *J* = 6.6 Hz, 2H, CH_2OC=O), 3.94 (dd, *J* = 13.2, 6.5 Hz, 1H, H-5), 3.85 – 3.79 (m, 1H, OC*H*$_2$$CH_2$NH), 3.77– 3.62 (m, 3H, H-2, H-3, H-4), 3.56 – 3.46 (m, 1H, OC*H*$_2$$CH_2$NH), 2.92 – 2.83 (m, 2H, C*H*$_2$NH), 2.78 (dd, *J* = 12.0, 6.5 Hz, 1H, CH_2C*H*CH_3), 2.40 (dd, *J* = 15.7, 8.7 Hz, 2H, CH_2C=O), 2.04 (dd, *J* = 15.4, 8.6 Hz, 2H, C*H*$_2$-CH=CH_2), 1.66 – 1.59 (m, 4H, CH_2C*H*$_2$$CO_2$, O-$CH_2$-C*H*$_2$- CH_2), 1.45 – 1.24 (m, 10H, CH_2), 1.21 (d, *J* = 6.6 Hz, 3H, CH_3-6), 1.12 (d, *J* = 6.3 Hz, 3H, C*H*$_3$-CH-NH) ppm; MS (TOF) *m/z*: 446.3 $[M + H]^+$; found 446.5.

General procedure for dendron/alkoxyamine conjugation (77, 79 and 81)

The appropriate dendron (1 equiv.) and α-*O*-L-fucopyranosyl oxyamine (**75**, 1 equiv.) were dissolved in citrate buffer (pH=3.5, 0.1 M in respect to **75**) and stirred at room temperature overnight. The mixture was concentrated and the product recovered.

(E/Z)-glycodendron (77)

^{1}H NMR (400 MHz, D_2O, major isomer): δ = 5.61 (dt, *J* = 17.4, 7.2 Hz, 1H, C*H*=CH_2), 5.26 (bs, 1H, H-1), 4.87 – 4.71 (m, 2H, CH=C*H*$_2$), 3.95 – 3.85 (m, 2H, CH_2O), 3.82 – 3.69 (m, 3H, H-2, H-4, H-5), 3.65 (bs, 1H, H-3) 2.49 – 2.35 (m, 4H, CH_2C=O, CH_2C=N), 1.90 – 1.84 (m, 2H, C*H*$_2$-CH=CH_2), 1.78 (s, 3H, CH_3C=N), 1.50 – 1.43 (m, 2H, O-CH_2-C*H*$_2$), 1.24 – 1.12 (m, 10H, CH_2), 1.01 (d, *J* = 6.1 Hz, 3H, CH_3-6) ppm; MS (TOF) *m/z*: 438.2 $[M + Na]^+$; found 438.2.

(E/Z,E/Z)-glycodendron (79)

^{1}H NMR (400 MHz, D_2O, major isomer): δ = 5.74 (dt, *J* = 16.4, 6.8 Hz, 1H, C*H*=CH_2), 5.26 (bs, 2H, H-1), 4.94 – 4.87 (m, 2H, CH=C*H*$_2$), 4.19 – 4.10 (m, 4H, CH_2O), 4.04 (t, *J* = 5.8 Hz, 2H, CH_2C*H*$_2$O), 3.84 (q, *J* = 6.2 Hz, 2H, H-5), 3.79 – 3.71 (m, 4H, H-2, H-4), 3.67 (bs, 2H, H-3), 2.56 – 2.35 (m, 8H, CH_2C=O, CH_2C=N), 1.99 (dd, *J* = 13.7, 6.7 Hz, 2H, C*H*$_2$-CH=CH_2), 1.80 (s, 6H, CH_3C=N), 1.61 (dt, *J* = 13.3, 6.8 Hz, 2H, O-CH_2-C*H*$_2$), 1.13 (s, 3H, CH_3), 1.03 (d, *J* = 6.5 Hz, 6H, CH_3-6) ppm; ^{13}C NMR (100.57 MHz, D_2O, major isomer): δ = 174.98, 174.43,

174.34 (C=O), 161.95 (C=N), 138.05 (*C*H=CH_2), 115.04 (CH=*C*H_2), 99.68 (C-1), 71.68 (C-3), 69.60 (C-4), 67.44 (C-2), 66.90 (C-5), 66.06 (C-*C*H_2O), 65.44 (CH_2*C*H_2OCO), 46.34 (*C*-CH_2O), 30.12, 30.06 (*C*H_2-C=O, *C*H_2-C=N), 29.34 (*C*H_2-CH=CH_2), 26.83 (O-CH_2-*C*H_2), 16.78 (CH_3), 15.24 (CH_3-6), 13.93 (*C*H_3-C=N) ppm; MS (TOF) *m/z*: 743.3 $[M + Na]^+$; found 743.3.

(E/Z,E/Z,E/Z,E/Z)-glycodendron (81)

^{1}H NMR (400 MHz, D_2O, major isomer): δ = 5.73 (ddt, *J* = 17.1, 10.3, 6.6 Hz, 1H, C*H*=CH_2), 5.26 (d, *J* = 2.7 Hz, 4H, H-1), 5.01 – 4.83 (m, 2H, CH=C*H*$_2$), 4.24 – 4.07 (m, 12H, CH_2O), 4.03 (t, *J* = 6.2 Hz, 2H, CH_2C*H*$_2$O), 3.83 (dd, *J* = 12.1, 5.8 Hz, 4H, H-5), 3.79 – 3.71 (m, 8H, H-2, H-4), 3.67 (bs, 4H, H-3), 2.55 – 2.37 (m, 16H, CH_2C=O, CH_2C=N), 2.00 (dd, *J* = 13.9, 7.1 Hz, 2H, C*H*$_2$-CH=CH_2), 1.80 (s, 12H, CH_3C=N), 1.64 (dd, *J* = 13.6, 6.8 Hz, 2H, O-CH_2-C*H*$_2$), 1.16 (s, 3H, CH_3), 1.12 (s, 6H, CH_3), 1.03 (d, *J* = 6.7 Hz, 12H, CH_3-6) ppm; ^{13}C NMR (100.57 MHz, D_2O, major isomer): δ = 174.35, 174.20, 173.72 (C=O), 161.68 (C=N), 137.94 (*C*H=CH_2), 115.19 (CH=*C*H_2), 99.78 (C-1), 71.71 (C-3), 69.67 (C-4), 67.49 (C-2), 66.91 (C-5), 66.08 (C-*C*H_2O), 65.51 (CH_2*C*H_2OCO), 46.42 (*C*-CH_2O), 30.17, 30.07 (*C*H_2-C=O, *C*H_2-C=N), 29.50 (*C*H_2-CH=CH_2), 26.94 (O-CH_2-*C*H_2), 16.86 (CH_3), 15.30 (CH_3-6), 14.00 (*C*H_3-C=N) ppm; MS (TOF) *m/z*: 758.3 $[M + 2Na]^{2+}$; found 758.1.

Isothermal Titration Calorimetry spectroscopy *performed by Prof. A. Imberty (CERMAV-CNRS, University of Grenoble)*

ITC experiments were performed with a VP-ITC isothermal titration calorimeter (Microcal). The experiments were carried out at 25 °C. Glycoconjugates **77**, **79**, and **81** and LecB were dissolved in the same buffer composed of 20 mM Tris with 100 mM NaCl, 0.1 mM $CaCl_2$ and 5% DMSO at pH 7.5. The glycoclusters were placed in the microcalorimeter cell (1.447 mL) at concentrations varying from 0.3 to 1 mM. A total of 30 injections of 10 μL of LecB (0.1 mM) were added at intervals of 3.5 or 5 min while stirring at 310 rpm. Control experiments performed by injection of buffer into the protein solution yielded insignificant heats of dilution. The experimental data were fitted to a theoretical titration curve using Origin software supplied by

Microcal, with ΔH (enthalpy change), K_a (association constant), and N (number of binding sites per monomer) as adjustable parameters. Dissociation constant (K_d), free energy change (ΔG), and entropy contributions ($T\Delta S$) were derived from the previous ones. Two or three independent titrations were performed for each ligand tested.

7.3. Synthesis of glycosylated Pluronic block copolymers as antitumor drugs carriers

General methods

Chemicals were purchased from Sigma–Aldrich and used without further purification. All solvents were dried over molecular sieves, for at least 24 h prior to use, when required. When dry conditions were required, the reaction was performed under an Ar or N_2 atmosphere. Thin-layer chromatography (TLC) was performed on silica gel $60F_{254}$ coated glass plates (Merck) with UV detection when possible, or spots were visualized by charring with a conc. H_2SO_4/EtOH/H_2O solution (10:45:45 v/v/v), or with a solution of $(NH_4)_6Mo_7O_{24}$ (21 g), $Ce(SO_4)_2$ (1 g), conc. H_2SO_4 (31 mL) in water (500 mL) and then by heating to 110 °C for 5 min. TLC spots were visualized also using a solution of $BiO(NO_3)*H_2O$ (0.1122 g), KI (2.64 g), $BaCl_2$ (7.75 g), CH_3COOH (14.6 mL) in water (85 mL). Flash column chromatography was performed on silica gel 230–400 mesh (Merck). Routine ^1H and ^{13}C NMR spectra were recorded on a Varian Mercury instrument at 400 MHz (^1H) and 100.57 MHz (^{13}C). Chemical shifts are reported in parts per million downfield from TMS as an internal standard; *J* values are given in Hz. Mass spectra were recorded on System Applied Biosystems MDS SCIEX instruments: Q TRAP, LC/MS/MS, turbo ion spray and Q STAR elite nanospray.

Infrared spectroscopy *performed by dott. A. Natalello (Biotechnology department, University of Milano-Bicocca)*

The attenuated total reflection (ATR) IR spectra were collected using a single reflection diamond plate (Golden Gate, Specac, USA) and the FTIR spectrometer Varian 670-IR (Varian Australia Pty Ltd., AU), equipped with a nitrogen-cooled Mercury Cadmium Telluride detector and an air dryer purging system. The following conditions were employed: 2 cm^{-1} spectral resolution, 25 kHz scan speed, 512 scan coadditions, and triangular apodization.

Analysis of Pluronic F127 block copolymer composition by ^{1}H-NMR

Pluronic F127 was purchased by Sigma-Aldrich and used without any further purification. The composition of the block copolymer was analysed by ^{1}H NMR ($CDCl_3$). The peak relative to the methyl groups of the propylene oxide units (1.18–1.07 ppm) was easily identified and resulted isolated by all the others peaks of the copolymer. Comparing the integral value of this signal with the one relative to all CH_2- and CH- protons (3.85–3.25 ppm) we established that there were present 3.5 ethylene oxide units for each propylene oxide unit. ^{1}H-NMR spectra were recorded using a Varian 400 MHz Mercury instrument, operating at a proton frequency equal to 400 MHz, at room temperature. The 5 mm diameter NMR tubes were sealed and kept closed during the full duration of the experiment. The 90º pulse-width (pw90) was calibrated, the number of scans varied depending on the signal-to-noise ratio, and the recycling delay was 5 s.

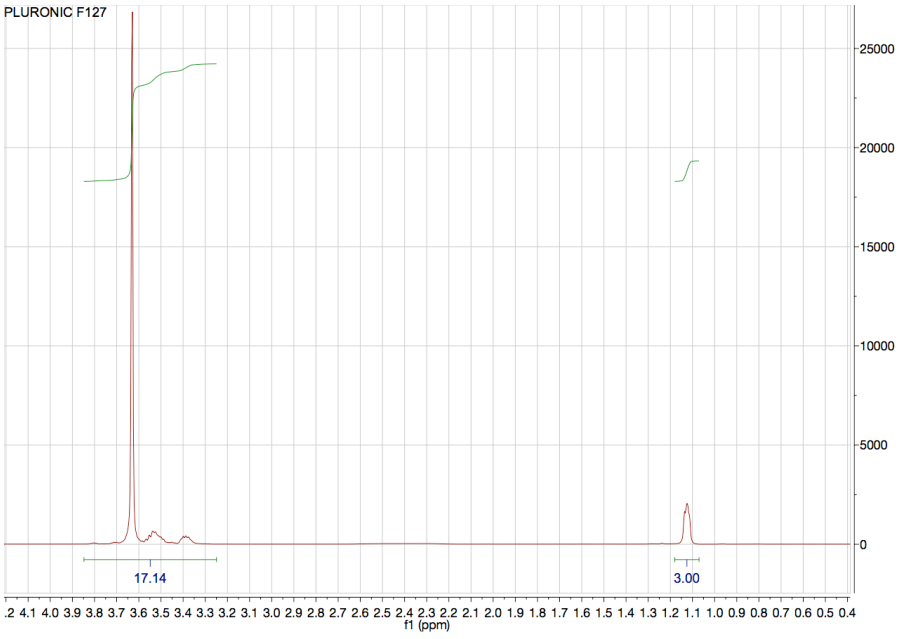

Figure 34. ^{1}H NMR ($CDCl_3$) spectra of Pluronic F127.

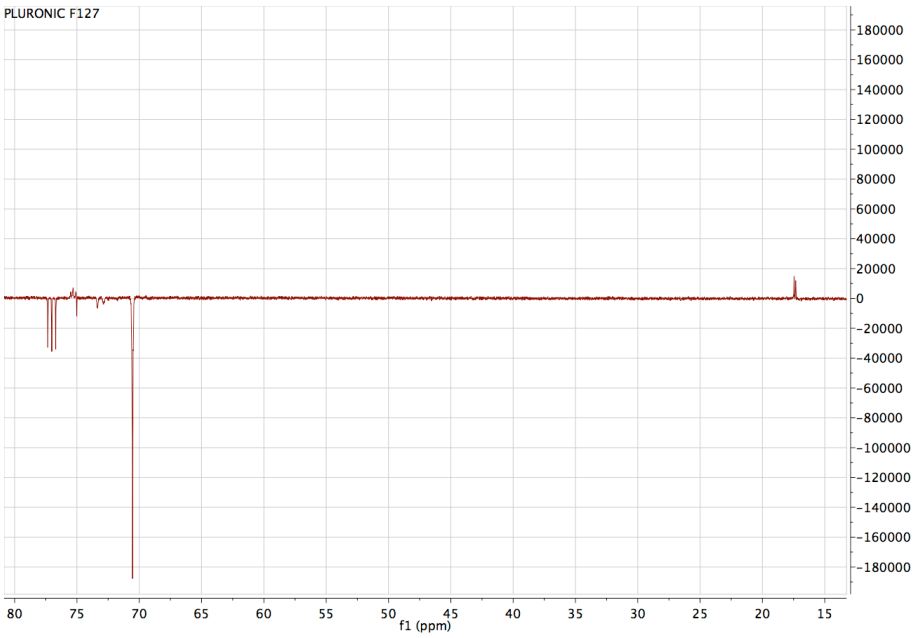

Figure 35. ^{13}C NMR ($CDCl_3$) spectra of Pluronic F127.

Quantification of Pluronic F127 functionalization by ^{1}H-NMR

Knowing the average molecular weight of Pluronic F127, reported by Sigma-Aldrich (MW≈12600 Da), and the ratio between ethylene oxide/propylene oxide units, we could calculated the average number of propylene oxide units in the copolymer (**59.28 units**). This value was used to quantify the Pluronic block copolymer functionalization using the propylene oxide methyl groups as internal standard. Quantification of the copolymer functionalization was performed also using added pyridine as an external standard, according to the following procedure: 20 mg of the proper functionalized copolymer were dissolved in 700 μL of D_2O or $CDCl_3$ and 0.00304 mmol of pyridine were added from a mother solution of pyridine in D_2O (1:50, 500 μL). ^{1}H-NMR spectra were recorded using a Varian 400 MHz Mercury instrument, operating at a proton frequency equal to 400 MHz, at room temperature. The 5 mm diameter NMR tubes were sealed and kept closed during the full duration of the experiment. The 90º pulse-width (pw90) was

calibrated, the number of scans varied depending on the signal-to-noise ratio, and the recycling delay was 5 s.

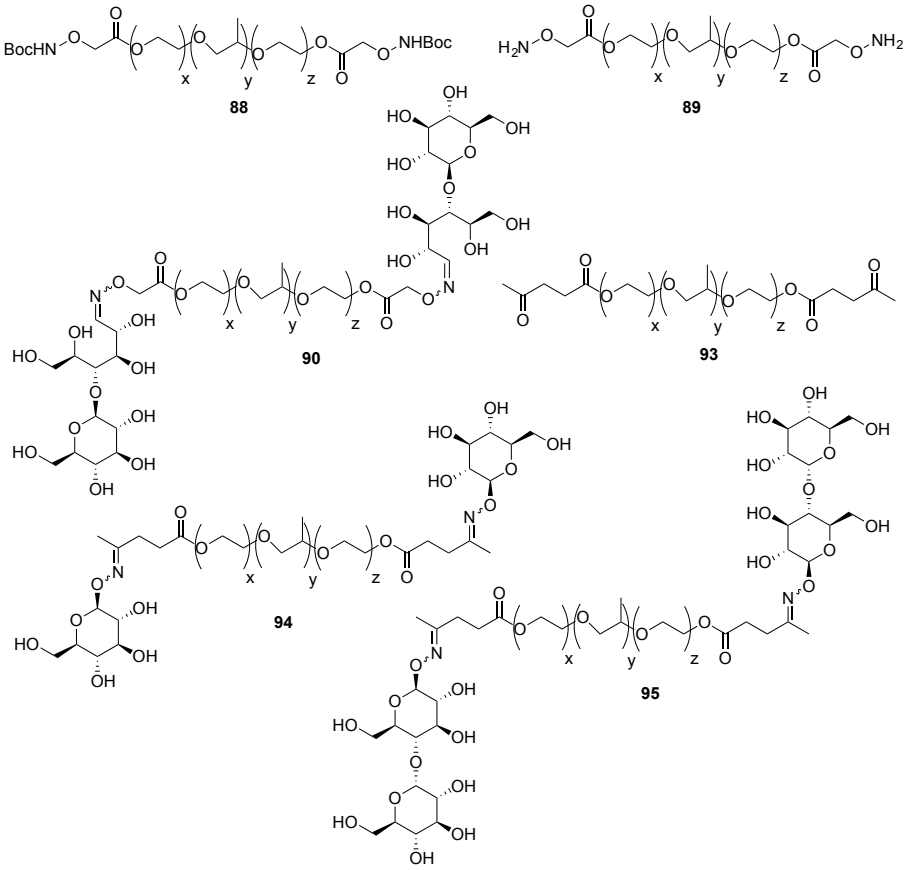

Figure 36. Summary of the synthesised compounds.

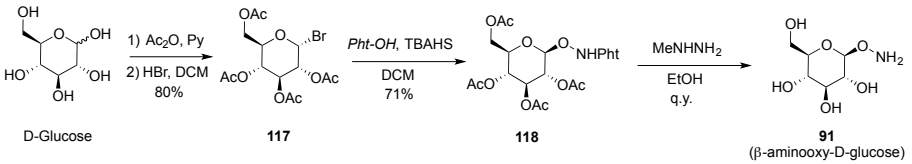

Scheme 20. Synthesis of β-aminooxy-D-glucose (**91**)[330].

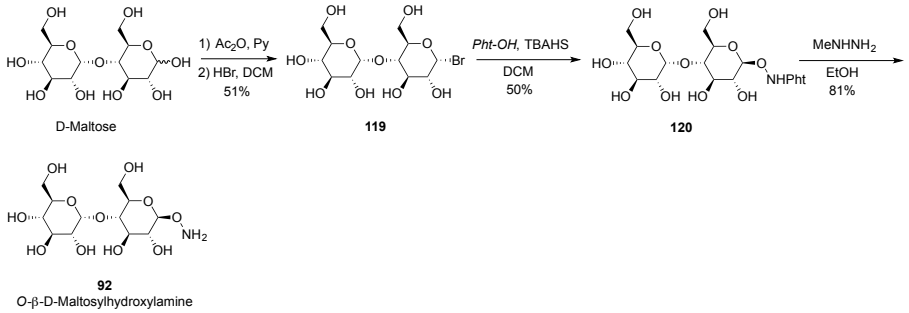

Scheme 21. Synthesis of *O*-β-D-maltosylhydroxylamine (**92**)[331].

Boc-aminooxy-functionalized Pluronic F127 (88)

(Boc-aminooxy)acetic acid **60** (760 mg, 3.98 mmol), Pluronic F127 (2.1 g, 0.166 mmol), DMAP (160 mg, 1.33 mmol) and *p*-toluenesulfonic acid (250 mg, 1.33 mmol) were dissolved in dry CH_2Cl_2 (15 mL). DCC (850 mg, 4.15 mmol) was added and the solution was stirred for 48h at room temperature. The precipitates were filtered off and washed with CH_2Cl_2. The solvent was evaporated, and the residue was purified by flash column chromatography (2-propanol/NH_3 95:5→85:15) affording **88** (1.95 g, average functionalization around 74% by ^{1}H NMR). ^{1}H NMR (400 MHz, $CDCl_3$): δ = 4.30 – 2.40 (m, C*H*$_2$-CH$_2$, CH$_3$-C*H*-CH$_2$, CH$_3$-CH-C*H*$_2$, O-CH$_2$-C=O), 1.30 (s, C(CH$_3$)$_3$), 0.96 (bs, C*H*$_3$-CH-CH$_2$) ppm; ^{13}C NMR (100.57 MHz, $CDCl_3$): δ = 75.30, 75.13, 74.94 (CH$_3$-*C*H-CH$_2$), 73.18, 72.75, 70.39 (*C*H$_2$-CH$_2$, CH$_3$-CH-*C*H$_2$, O-*C*H$_2$-C=O), 28.11 (C(*C*H$_3$)$_3$), 17.33, 17.22 (*C*H$_3$-CH-CH$_2$) ppm.

Aminooxy-functionalized Pluronic F127 (89)

To a cooled (0 °C) solution of **88** (1.95 g, 0.150 mmol) in anhydrous DCM (6 mL) TFA was added dropwise (3.0 mL). After stirring for 3 h at 0 °C, the reaction mixture was stirred overnight at room temperature and then quenched to neutrality with satd. aq. Na_2CO_3. The aqueous layer was extracted with DCM and the combined organic extracts were dried over Na_2SO_4 and concentrated to afford **89** (1.7 g, 100% of conversion by ^{1}H NMR). ^{1}H NMR (400 MHz, $CDCl_3$): δ = 3.85 –

3.25 (m, C*H*$_2$-CH$_2$, CH$_3$-C*H*-CH$_2$, CH$_3$-CH-C*H*$_2$, O-CH$_2$-C=O), 1.15 – 1.00 (m, C*H*$_3$-CH-CH$_2$) ppm; ^{13}C NMR (100.57 MHz, CDCl$_3$): δ = 75.44, 75.24, 75.03 (CH$_3$-*C*H-CH$_2$), 73.31, 72.79, 70.49 (*C*H$_2$-CH$_2$, CH$_3$-CH-*C*H$_2$, O-*C*H$_2$-C=O), 17.42, 17.30 (*C*H$_3$-CH-CH$_2$) ppm.

(E/Z)-Glycosylated Pluronic F127 (90)

To a solution of **89** (163 mg, 0.013 mmol) in H$_2$O/MeOH (1:1, 2 mL) D-cellobiose (89 mg, 0.260 mmol) and acetic acid (15 μL, 0.260 mmol) were added. The reaction mixture was stirred at room temperature for 6 days. The solvent was evaporated, and the residue was purified by flash column chromatography (2-propanol/NH$_3$ 95:5→85:15) affording **90** (140 mg, average functionalization around 12% by ^{1}H NMR). ^{1}H NMR (400 MHz, CDCl$_3$): δ = 5.25 – 5.02 (m, H-1') 3.98 – 2.61 (m, C*H*$_2$-CH$_2$, CH$_3$-C*H*-CH$_2$, CH$_3$-CH-C*H*$_2$, O-CH$_2$-C=O, H-2, H-3, H-4, H-5, H-6, H-2', H-3', H-4', H-5', H-6'), 1.39 – 0.62 (m, C*H*$_3$-CH-CH$_2$) ppm.

Ketone-functionalized Pluronic F127 (93)

To a solution of Pluronic F127 (2.0 g, 0.164 mmol) dissolved in dry DCM (15 mL), levulinic acid **82** (457 mg, 3.936 mmol), DMAP (80 mg, 0.656 mmol) and DCC (1.0 g, 4.92 mmol) were added and the reaction mixture was stirred at room temperature for 48h. The precipitates were filtered off and washed with CH$_2$Cl$_2$ and the solvent was evaporated. Crude **93** was used for the next reaction without any further purification.

(E/Z)-β-Glucose-functionalized Pluronic F127 (94)

93 (1.410 g, 0.110 mmol) and β-aminooxy-D-glucose (**91**, 215 mg, 1.102 mmol) were dissolved in citrate buffer (9.6 mL, pH=3.5) and stirred at room temperature for 48h. The mixture was concentrated and the residue was purified by flash column chromatography (2-propanol/NH$_3$ 95:5→80:20) affording **94** (1.288 g, average functionalization around 74% by ^{1}H NMR). ^{1}H NMR (400 MHz, D$_2$O): δ = 4.93 – 4.72 (m, H-1), 4.05 – 2.94 (m, O-C*H*$_2$-CH$_2$-O, CH$_3$-C*H*-CH$_2$, CH$_3$-CH-C*H*$_2$, H-2, H-3, H-4, H-5, H-6), 1.82 – 1.69 (m, CH$_3$C=N), 1.29 – 0.69 (m, C*H*$_3$-CH-CH$_2$) ppm; ^{13}C NMR (100.57 MHz, D$_2$O): δ = 165.43, 162.67 (C=O, C=N), 102.63 (C-1),

76.03, 75.55, 75.32, 75.20, 75.09 71.37, (CH_3-*C*H-CH_2, C-2, C-3, C-4, C-5), 72.17, 71.81, 71.58, 69.85, 69.45, 67.40, 60.20 (O-*C*H_2-CH_2-O, CH_3-CH-*C*H_2), 60.54, (C-6), 23.56, 20.62 (*C*H_3-C=N), 15.91 (*C*H_3-CH-CH_2) ppm.

(E/Z)-β-Maltose-functionalized Pluronic F127 (95)

93 (419 mg, 0.0327 mmol) and *O*-β-D-maltosylhydroxylamine (**92**, 117 mg, 0.327 mmol) were dissolved in citrate buffer (2.85 mL, pH=3.5) and stirred at room temperature for 3 days. The mixture was concentrated and the residue was purified by flash column chromatography (2-propanol/NH_3 95:5→80:20) affording **95** (335 mg, average functionalization around 56% by ^{1}H NMR). ^{1}H NMR (400 MHz, D_2O): δ = 5.24 (d, *J* = 3.8 Hz, H-1'), 4.86 (d, *J* = 8.8 Hz, H-1), 4.27 – 2.80 (m, O-C*H*$_2$-CH2-O, CH_3-C*H*-CH_2, CH_3-CH-C*H*$_2$, H-2, H-3, H-4, H-5, H-6, H-2', H-3', H-4', H-5', H-6'), 2.68 (t, *J* = 6.4 Hz, CH_2-C=N), 2.37 (t, *J* = 6.4 Hz, CH_2-C=O), 2.06 (s, CH_3C=N), 1.55 – 0.63 (m, C*H*$_3$-CH-CH_2) ppm; ^{13}C NMR (100.57 MHz, D_2O): δ = 191.00 (C=O), 150.51 (C=N), 106.87 (C-1), 99.52 (C-1'), 81.37, 76.68, 75.33, 75.22, 75.12, 73.05, 72.71, 72.62, 71.22, 70.55, 70.40, 65.98 (CH_3-*C*H-CH_2, C-2, C-3, C-4, C-5, C-2', C-3', C-4', C-5'), 72.12, 71.82, 71.62, 69.88, 69.57, 69.48, 69.34, 68.27, 67.40, 64.46, 60.23 (O-*C*H_2-CH_2-O, CH_3-CH-*C*H_2), 62.44 , 62.35 (C-6, C-6'), 38.16 (*C*H_2-C=O, *C*H_2-C=N), 29.03, 19.57 (*C*H_3-C=N), 15.88 (*C*H_3-CH-CH_2) ppm.

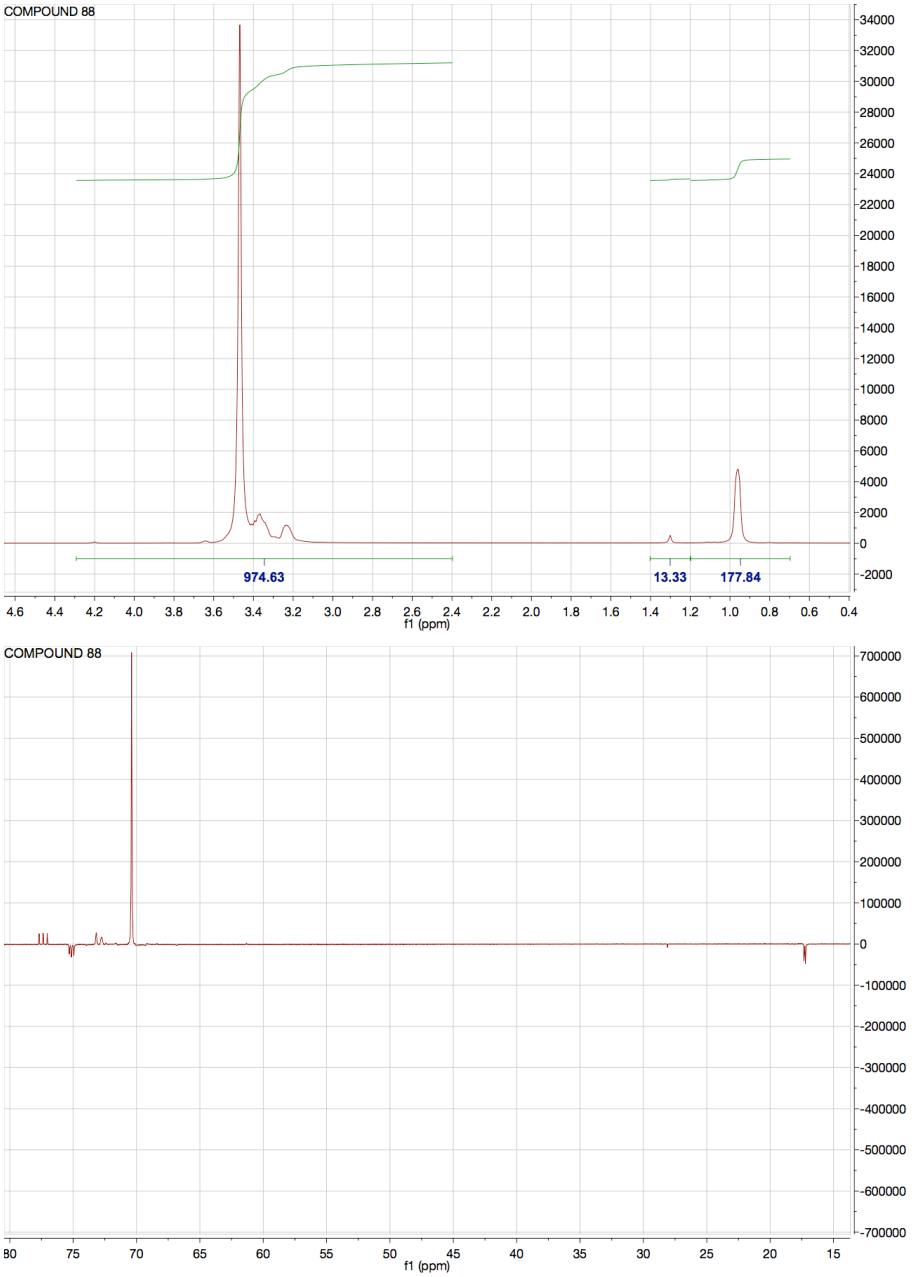

Figure 37. ^{1}H NMR (top) and ^{13}C NMR (bottom) spectra of **88** ($CDCl_3$).

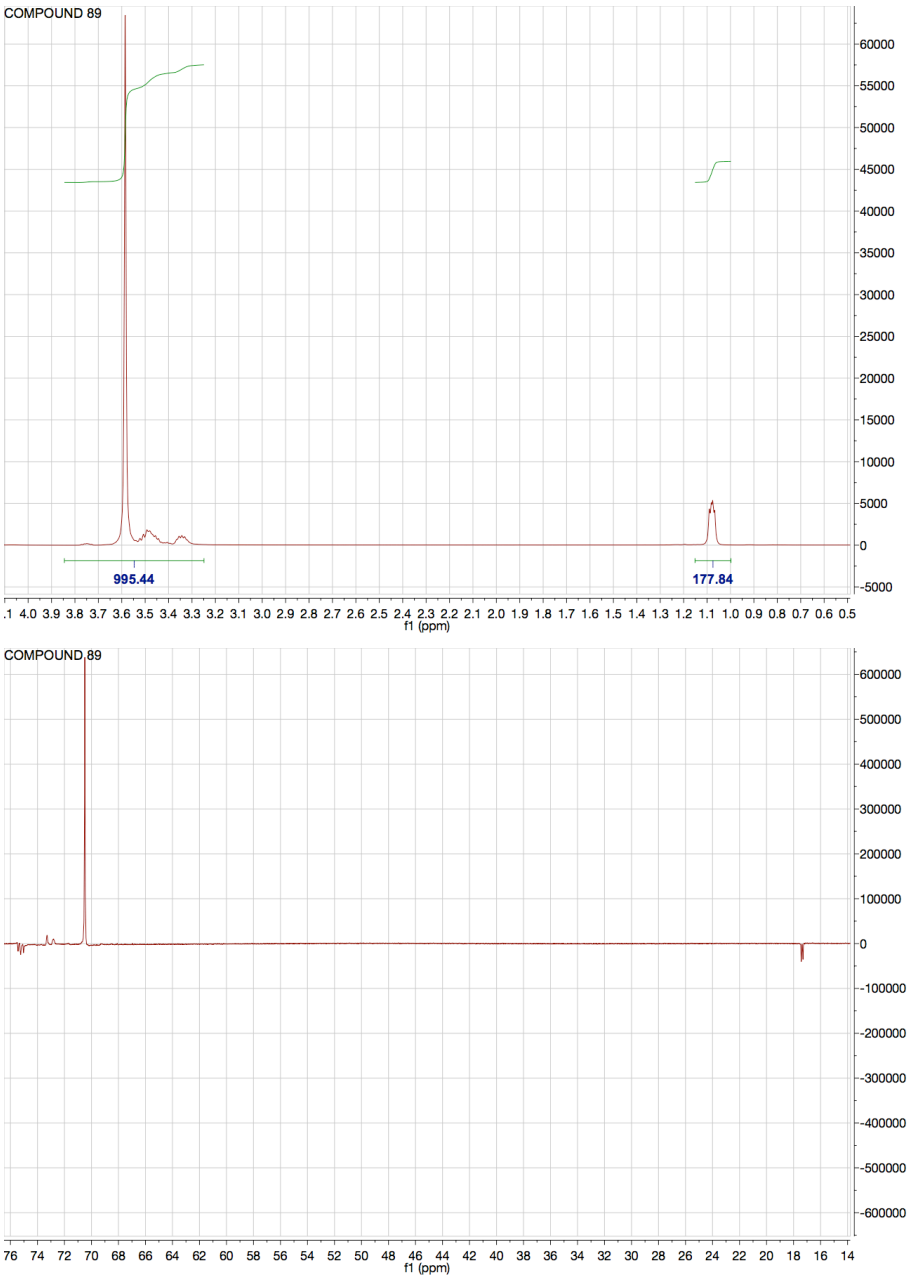

Figure 38. ^{1}H NMR (top) and ^{13}C NMR (bottom) spectra of **89** ($CDCl_3$).

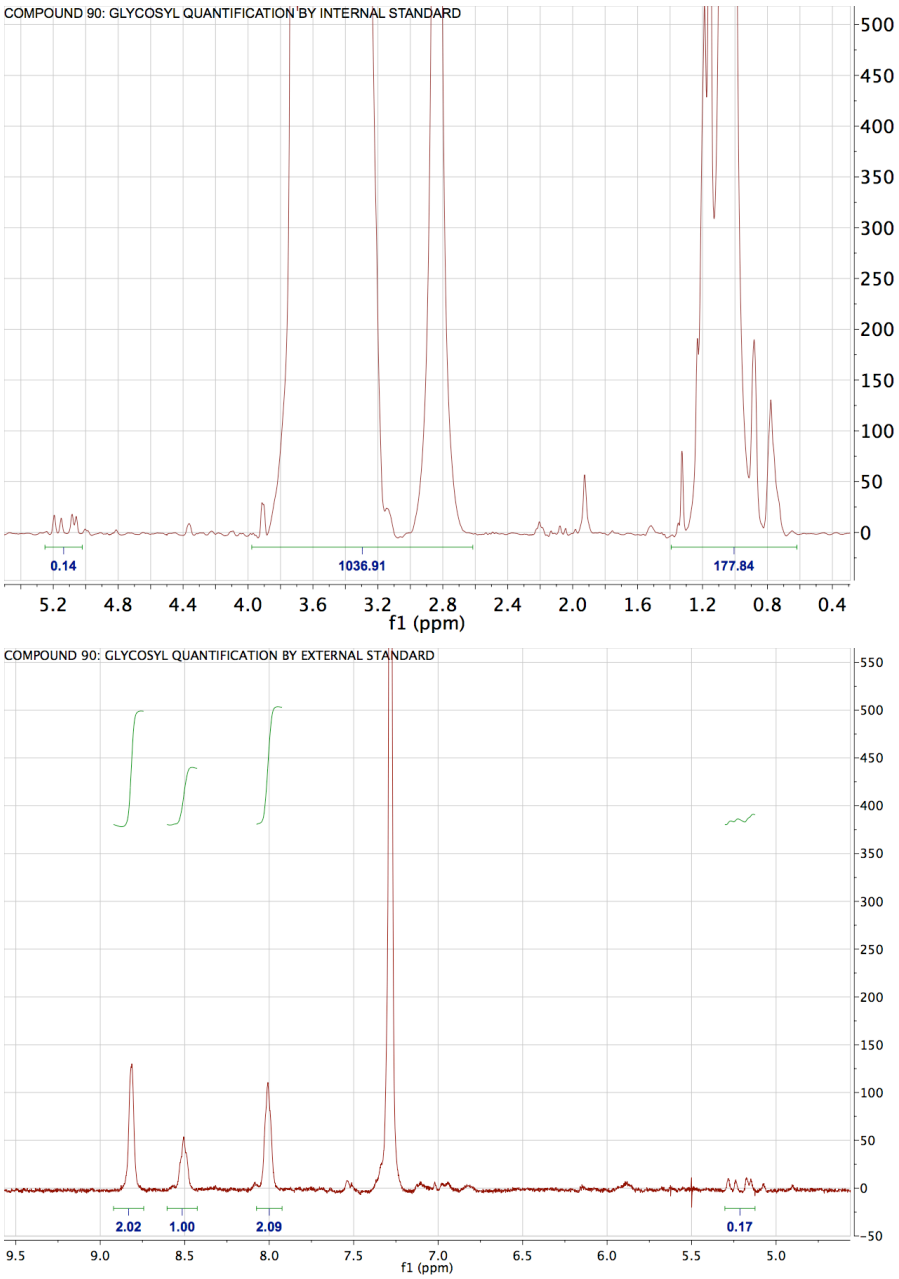

Figure 39. ^{1}H NMR of **90** ($CDCl_3$). Glycosyl quantification by internal (top) and external standard (bottom).

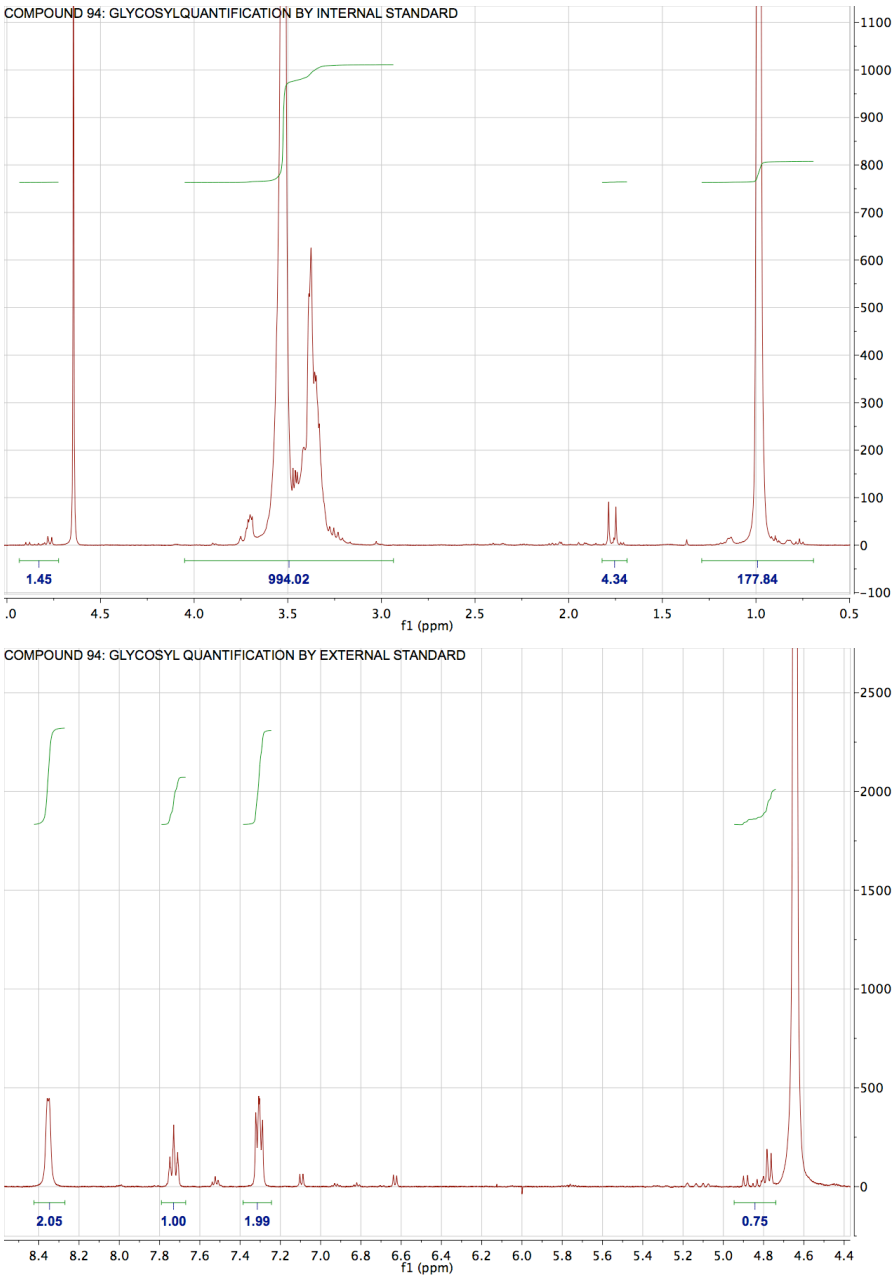

Figure 40. ^{1}H NMR of **94** (D_2O). Glycosyl quantification by internal (top) and external standard (bottom).

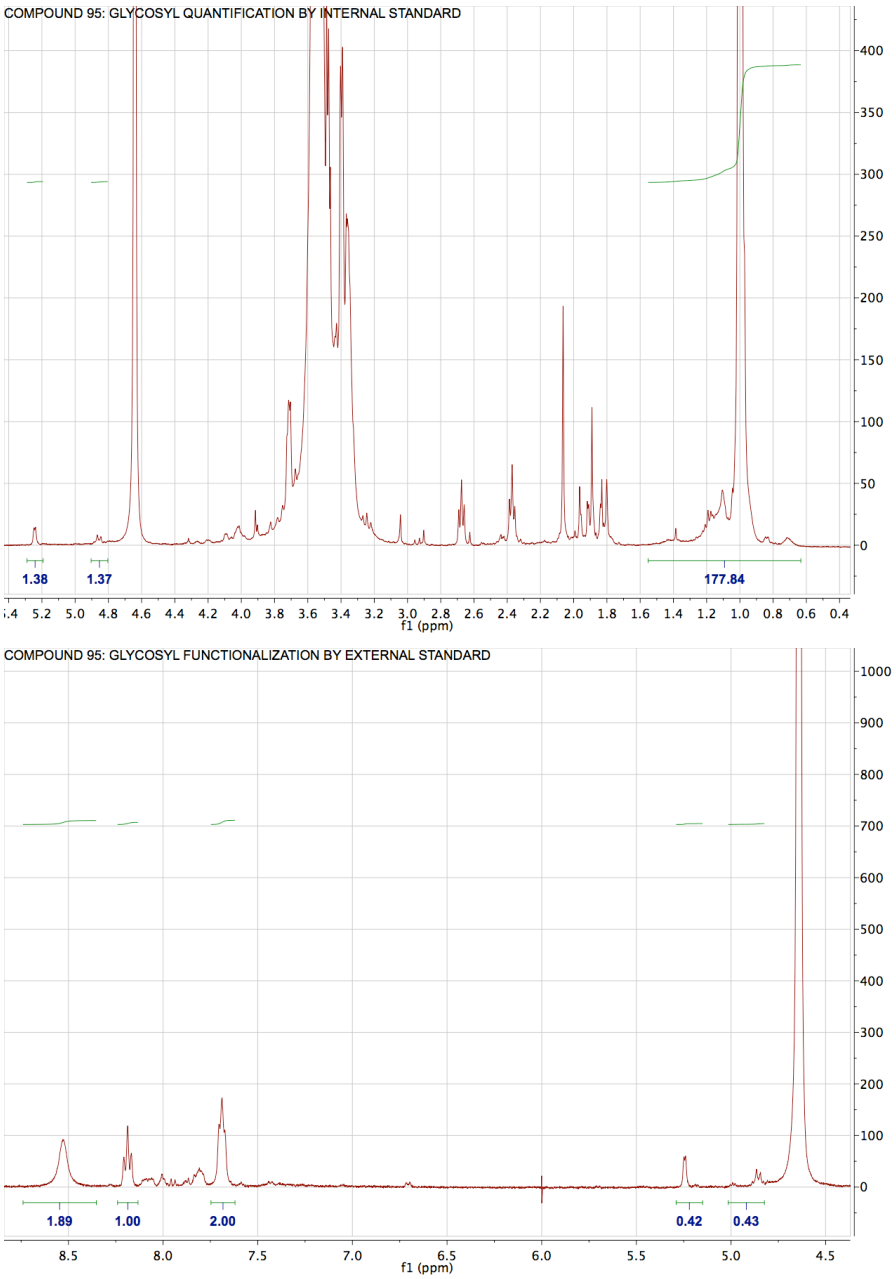

Figure 41. ^{1}H NMR of **95** (D_2O). Glycosyl quantification by internal (top) and external standard (bottom).

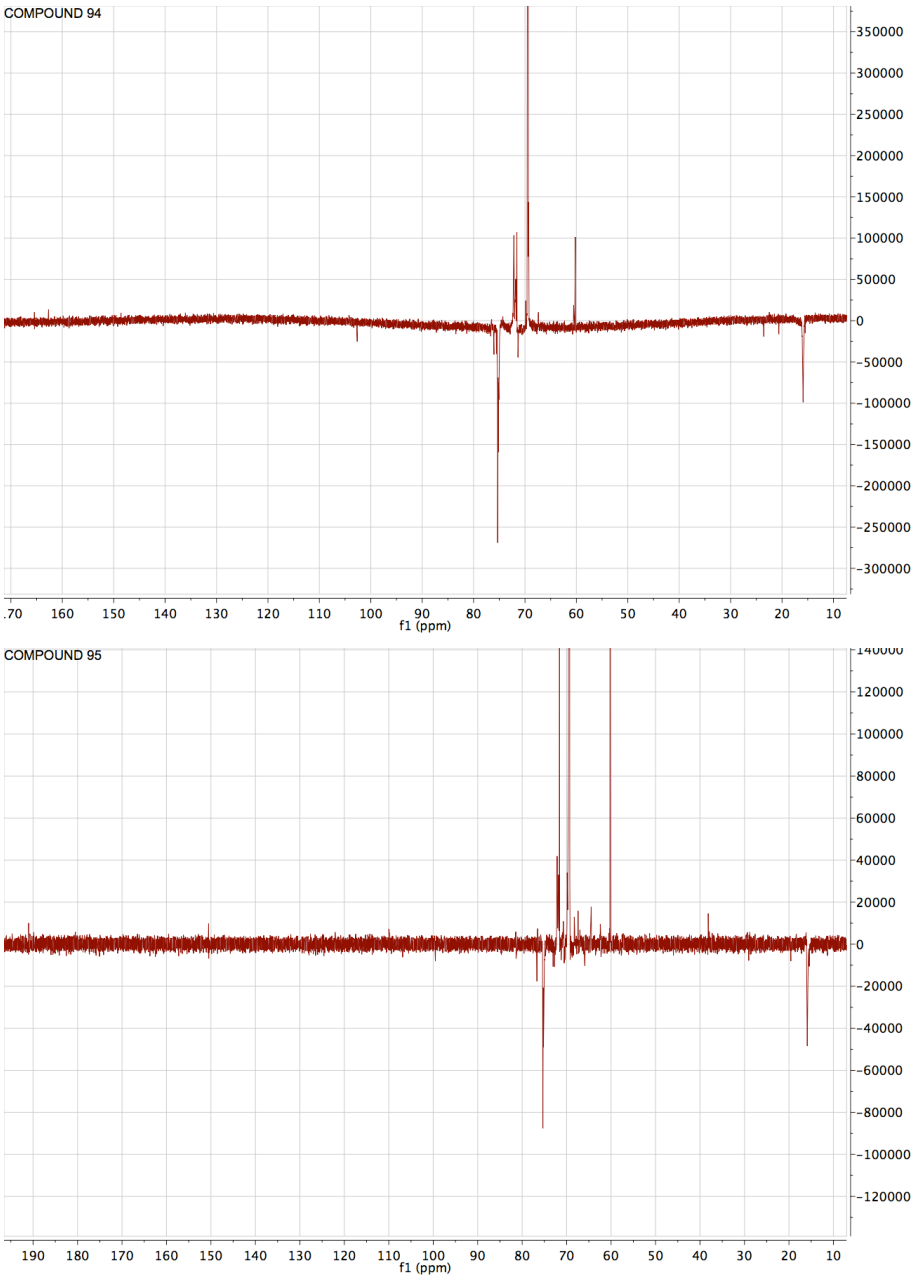

Figure 42. ^{13}C NMR (D_2O) spectra of **94** (top) and **95** (bottom).

References

1 Stern, R. et al. (2008) Chem. Rev., 108, 5061–5085.
2 Del Valle, E. M. M. (2004) Process. Biochem., 39, 1033–1046.
3 Gagneux, P. et al. (1999) Glycobiology, 9, 747–755.
4 Varki, A. et al. (2009) Essentials of Glycobiology, Cold Spring Harbour, New York, 2nd edn.
5 Varki, A. (2011) Evolutionary forces shaping the Golgi glycosylation machinery: why cell surface glycans are universal to living cells. Cold Spring Harb. Perspect. Biol. 3, a005462.
6 Misevic, G. N. et al. (1993) J. Biol. Chem., 268, 4922–4929.
7 Sachs, J. L. (2008) Trends Ecol. Evol., 23, 245–248.
8 Hynes, R. O. (2012) JCB, 196, 671–679.
9 Hynes, R. O. (2009) Science, 326, 1216–1219.
10 Hynes, R. O. et al. (2012) Overview of the matrisome–an inventory of extracellular matrix constituents and functions. Cold Spring Harb. Perspect. Biol. 4, a004903.
11 Simonetti, N. et al. (1974) Nature, 250, 344–346.
12 Naseem, S. et al. (2012) Commun. Integr. Biol., 5, 156–159.
13 Rana, N. A. et al. (2011) Curr. Opin. Struct. Biol., 21, 583–589.
14 Walt, D. et al. (2012) Transforming glycoscience: a roadmap for the future. Washington: National Academies Press.
15 Zielinska, D. F. et al. (2010) Cell, 141, 897–907.
16 Marek, K. W. et al. (1999) Glycobiology, 9, 1263–1271.
17 Freeze, H. H. (2006) Nat. Rev. Genet., 7, 537–551.
18 Nairn, A. V. et al. (2008) J. Biol. Chem., 283, 17298–17313.
19 Lauc, G. et al. (2010) PLoS Genet., 6, e1001256.
20 Lauc, G. et al. (2010) Mol. Biosyst., 6, 329–335.
21 Kneževic´, A. et al. (2009) J. Proteome Res., 8, 694–701.
22 Pucic, M. et al. (2011) Mol. Cell. Proteomics, 10, M111 0 10090.
23 Menni, C. et al. (2013) PLoS ONE, 8, e82558.
24 Lauc, G. et al. (2013) PLoS Genet., 9, e1003225.
25 Marchalonis, J. J. et al. (2002) J. Mol. Recogn., 15, 260–271.
26 Nimmerjahn, F. et al (2008) Nat. Rev. Immunol., 8, 34–47.
27 Mihai, S. et al. (2012) Autoimmun. Rev., 12, 657–660.

28 Iida, S. et al. (2006) Clin. Cancer Res., 12, 2879–2887.
29 Masuda, K. et al. (2007) Mol. Immunol., 44, 3122–3131.
30 Scanlan, C. N. et al. (2008) Proc. Natl. Acad. Sci. U.S.A., 105, 4081–4082.
31 Shinkawa, T. et al. (2003) J. Biol. Chem., 278, 3466–3473.
32 Preithner, S. et al. (2006) Mol. Immunol. 43, 1183–1193.
33 Kaneko, Y. et al. (2006) Science, 313, 670–673.
34 Debre, M. et al. (1993) Lancet, 342, 945–949.
35 Anthony, R. M. et al. (2011) Nature, 475, 110–113.
36 Karsten, C. M. et al. (2012) Nat. Med., 18, 1401–1406.
37 Ackerman, M. E. et al. (2013) J. Clin. Invest., 123, 2183–2192.
38 Gornik, O. et al. (2012) Biochim. Biophys. Acta, 1820, 1318–1326.
39 Walcheck, B. et al. (1996) Nature, 380, 720–723.
40 Sperandio, M. et al. (2009) Immunol. Rev., 230, 97–113.
41 Stanley, P. (2007) Curr. Opin. Struct. Biol., 17, 530–535.
42 Hicks, C. et al. (2000) Nat. Cell Biol., 2, 515–520.
43 Schier, A. F. et al. (2000) Nature, 403, 385–389.
44 Yan, Y. T. et al. (2002) Mol. Cell. Biol., 22, 4439–4449.
45 Lauc, G. et al. (2010) Mol. Biosyst., 6, 2373–2379.
46 Lauc, G. et al. (2013) Biochim. Biophys. Acta, 1840, 65–70.
47 Pierce, J. G. et al. (1981) Annu. Rev. Biochem., 50, 465–495.
48 Bush, C. A. et al. (1999) Annu. Rev. Biophys. Biomol. Struct., 28, 269–293.
49 Ma, F. et al. (2012) J. Biol. Chem., 287, 38073–38079.
50 Koropatkin, N. M. et al. (2012) Nat. Rev. Microbiol., 10, 323–335.
51 Wacklin, P. et al. (2011) PLoS ONE, 6, e20113.
52 Coyne, M. J. et al. (2005) Science, 307, 1778–1781.
53 Pacheco, A. R. et al. (2012) Nature, 492, 113–117.
54 Elbein, A. D. (1974) Adv. Carbohydr. Chem. Biochem., 30, 227.
55 Thevelein, J. M. (1996) Regulation Of Trehalose Metabolism And Its Relevance To Cell Growth And Function, In The Mycota, ed.by Brambl R, Marzluf GA. Springer, Berlin Heidelberg New York, pp 395–414.
56 Strom, A.R. et al. (1993) Mol. Microbiol., 8, 205.
57 Wingler, A. (2002) Phytochemistry, 60, 437.
58 Singer, M. A. et al. (1998) Trends Biotechnol., 16, 460.
59 Benaroudj, N. et al. (2001) J. Biol. Chem., 276, 24261.
60 Richards, A. B. et al. (2002) Food Chem. Toxicol., 40, 871.
61 Takayama, K. et al. (1976) Biochemistry, 15, 441.
62 Crowe, J.H. et al. (1987) Biochem. J., 242, 1.

63 Adams, R. P. et al. (1990) Biochem. Syst. Ecol, 18, 107.
64 Roser, B. (1991) Trends Food Sci. Tech., 2, 166.
65 Crowe, J. H. et al. (1988) Biochim. Biophys. Acta, 947, 367.
66 Wyatt, G.R. et al. (1956) Fed. Proc., 15, 388.
67 Howden, G.F. et al. (1956) Chem. Ind., 1453.
68 Thompson S. N. (2003) Adv. Insect. Physiol., 31, 206.
69 Mullins, D. E. (1985) Chemistry and Physiology Of The Hemolymph. In: Comparative Insect Physiology, Biochemistry And Pharmacology, Vol. 3 (Eds. Kerkut, G. A., And Gilbert, L. I.), Pp. 355–400. New York: Pergamon Press.
70 Bourquelot, E. (1983) Bull. Soc. Mycol. Fr., 9:189.
71 Coutinho, P.M. et al. (1999). Recent Advances In Carbohydrate Bioengineering. Royal Society Of Chemistry, Cambridge, pp. 3.
72 Yonemaya, Y. et al (1987) J. Cell. Physiol., 131, 330.
73 Dahlqvist, A. (1968) Anal. Biochem., 22, 99.
74 Ruf, J. et al. (1990) J. Biol. Chem., 265, 15034.
75 Defaye, J. et al. (1983) Carbohydr. Res., 124, 265.
76 Gibson, R.P. et al. (2007) Angew. Chem. Int. Ed., 46, 4115.
77 Wegener, G. et al. (2003) J. Exp. Biol., 206, 1233.
78 Asano, N. et al (1990) J. Antibiot., 43, 722-726.
79 Kyosseva, S. V. et al. (1995) Arch. Biochem. Biophys., 316, 821-826.
80 Kato, A. et al. (2003) Tetrahedron: Asymmetry, 14, 325-331.
81 Cardona, F. et al. (2009) Chem. Eur. J., 15, 1627-1636.
82 Cardona, F. et al. (2010) Chem. Commun., 46, 2629-2631.
83 Forcella, M. et al. (2010) Glycobiology, 20, 1186-1195.
84 Bini, D. et al. (2011) Eur. J. Org. Chem., 3995–4000.
85 Bini, D. et al. (2012) Beilstein J. Org. Chem., 8, 514–521.
86 Bini, D. et al. Trehalose mimetics as inhibitors of trehalose processing enzymes. In Specialist of Periodical Reports, SPR Carbohydrate Chemistry; Vol. 37, cap 10. Publisher: Royal Society of Chemistry (31 Dec 2011), 1-44.
87 Asano, N. (2003) Glycobiology, 13, 93R.
88 Compain P, Martin O. Iminosugars: from synthesis to therapeutic applications. John Wiley & Sons Ltd. The Atrium Southern Gate: England 2007.
89 Rhinehart, B. L. et al. (1987) J. Pharmacol. Exp. Ther., 241, 915–920.
90 Wormald, M. R. et al. (1996) Carbohydr. Lett., 2, 169.
91 a) Chopra, R. N. et al., Glossary of Indian Medicinal Plants, Council of Scientific and Industrial Research (India), New Dehli, 1956, 55; b) Nair, R. B. et al. (1986) Ancient Science of Life: Journal of International Institute of Ayurveda, 6, 80–84.

92 Nash, R. J. et al. (1994) Tetrahedron Lett., 35, 7849.
93 Grover, J. K. et al.(2002) J. Ethnopharmacol., 81, 81.
94 Mentreddy, S. R. (2007) J. Sci. Food Agric., 87, 743.
95 Bell, A. A. et al. (1997) Tetrahedron Lett., 38,5869.
96 Denmark, S. E. et al. (2000) J. Org. Chem., 65, 2875.
97 Asano, N. et al. (1996) Eur. J. Biochem., 240, 692.
98 Silva, M.C.P. et al. (2004) Insect Biochem. Mol. Biol., 34, 1089.
99 Asano, N. et al. (1987) J. Antibiot., 40, 526.
100 Wennekes, T. et al. (2007) J. Org. Chem., 72, 1088-1097.
101 Forcella, M. et al. (2012) Arch. Insect Biochem. Physiol., 81(2), 77-89.
102 Matsumura, T. et al. (2000) Pharm. Biol., 38, 302.
103 Parmeggiani, C. et al. (2009) J. Nat. Prod., 72, 2058.
104 Brandi, A. et al. (2009) Chem. Eur. J., 15, 7808.
105 Bonaccini, C. et al. (2010) Eur. J. Org. Chem., 5574.
106 The enantiomer of **41** was previously reported: Podolan, G. et al. (2011) Synlett, 1668.
107 Behr, J.-B. et al. (2002) Eur. J. Org. Chem., 1256.
108 The inhibition of chitin synthase by **37** was reported: Behr, J.-B. et al. (2007) Nat. Prod. Res., 21, 76.
109 For the activity of compounds **25**, **28** and **37** against a panel of commercially available glycosidases see: D'Adamio, G. et al. (2014) Org. Biomol. Chem., 12, 6250 and Ref. 105.
110 González Tanarro, C. M. et al. (2011) J. Enz. Inhib. & Med. Chem., 26, 350.
111 Calculated using the Baici equation: Baici, A. (1981) Eur. J. Biochem., 119, 9.
112 Ando, O. et al. (1995) Bioscience, Biotechnology and Biochemistry, 59, 711.
113 Pennacchio, F. et al. (2012) in Parasitoid viruses: symbionts and pathogens, ed. N. E. Beckage, J.-M. Drezen, Elsevier, p. 269.
114 Bonnin, B. C. et al. (2014) Trends in Biotech., 32, 91.
115 Schaffer, C et al. (2003) Prog. Chem .Org. Nat. Prod., 85, 51.
116 Gabius, H. J. et al. (2012) Trends Biochem. Sci., 36, 298–313.
117 Lis, H. et al. (1998) Chem. Rev., 98, 637–674.
118 Kiessling, L. L. et al. (2000) Curr. Opin. Chem. Biol., 4, 696–703.
119 Lee Y. C. et al. (1995) Acc. Chem. Res., 28, 321–327.
120 Lundquist, J. J. et al. (2002) Chem. Rev., 102, 555–578.
121 Mammen, M. et al. (1998) Angew. Chem., Int. Ed., 37, 2754–2794.
122 Gabius, H.-J. (2004) Adv. Drug Delivery Rev., 56, 421 – 424.
123 Gabius, H.-J. et al. (2002) Biochim. Biophys. Acta Gen. Subj., 1572, 165 –177.
124 Ambrosi, M. et al. (2005) Org. Biomol. Chem., 3, 1593 –1608.
125 Dyukova, V. I. et al. (2006) Biochim. Biophys. Acta, 1760, 603–609.
126 Horlacher, T. et al. (2008) Chem. Soc. Rev., 37, 1414–1422.

127 Oyelaran, O. et al. (2009) Curr. Opin. Chem. Biol., 13, 406–413.
128 Song E. H. et al. (2009) Curr. Opin. Chem. Biol., 13, 626–632.
129 Rillahan C. D. et al. (2011) Annu. Rev. Biochem., 80, 797–823.
130 Feizi T, et al (2003) Curr. Opin. Struct. Biol., 13, 637.
131 Paulson J. C. et al. (2006) Nat. Chem. Biol., 2, 238.
132 Dam, T. K. et al. (2010) Adv. Carbohydr. Chem. Biochem., 63, 139–164.
133 Dam, T. K. et al. (2009) Biochemistry, 48, 3822–3827.
134 Gestwicki, J. E. et al. (2002) J. Am. Chem. Soc., 124, 14922–14933.
135 Reynolds, M. et al. (2011) C. R. Chim., 14, 74–95.
136 Chabre, Y. M. et al. (2010) Adv. Carbohydr. Chem. Biochem., 63, 165–393.
137 Deniaud, D. et al. (2011) Org. Biomol. Chem., 9, 966–979.
138 Pieters, R. J. (2009) Org. Biomol. Chem., 7, 2013–2025.
139 Darbre, T. et al. (2008) Curr. Top. Med. Chem., 8, 1286–1293.
140 Doores, K. J. et al. (2006) Chem.–Eur. J., 12, 656–665.
141 Imberty, A. et al. (2008) Chem.–Eur. J., 14, 7490–7499.
142 Kitov, P. I. et al. (2000) Nature, 403, 669–672.
143 Imberty, A. et al. (2008) Curr. Opin. Struct. Biol., 18, 567–576.
144 Karlsson, K. A. (2001) Adv. Exp. Med. Biol., 491, 431–443.
145 Pieters, R. J. (2011) Adv. Exp. Med. Biol., 715, 227–240.
146 Sharon, N. (1996) Adv. Exp. Med. Biol., 408, 1–8.
147 Davis, B. G. (2002) Chem. Rev., 102, 579–602.
148 Payne, R. J. et al. (2010) Chem. Commun., 46, 21–43.
149 Rendle, P. M. et al. (2004) J. Am. Chem. Soc., 126, 4750–4751.
150 Bes, L. et al. (2003) Macromolecules, 36, 2493–2499.
151 Otsuka, I. et al. (2010) ChemBioChem, 11, 2399–2408.
152 Ponader, D. et al. (2012) Biomacromolecules, 13, 1845–1852.
153 Rieger, J. et al. (2007) Biomacromolecules, 8, 2717–2725.
154 Baldini, L. et al. (2007) Chem. Soc. Rev., 36, 254–266.
155 Cecioni, S. et al. (2009) Chem.–Eur. J., 15, 13232–13240.
156 Dondoni, A. et al. (2010) Chem. Rev., 110, 4949–4977.
157 Andre, S. et al. (2011) Chem. Commun., 47, 6126–6128.
158 Andre, S. et al. (2001) ChemBioChem, 2, 822–830.
159 Heidecke, C. et al. (2007) Chem.–Eur. J., 13, 9056–9067.
160 Mintzer, M. A. et al. (2012) Mol. Pharm., 9, 342–354.
161 Touaibia, M. et al. (2007) Mini–Rev. Med. Chem., 7, 1270–1283.
162 Turnbull, W. B. et al. (2002) J. Biotechnol., 90, 231–255.
163 Fulton, D. A. et al. (2001) Bioconjugate Chem., 12, 655–672.

164 Gomez-Garcia, M. et al. (2012) J. Org. Chem., 77, 1273–1288.
165 Krauss, I. J. et al. (2007) J. Am. Chem. Soc., 129, 11042–11044.
166 Ohta, T. et al. (2003) Angew. Chem., Int. Ed., 42, 5186–5189.
167 Pujol, A. M. et al. (2011) J. Am. Chem. Soc., 133, 286–296.
168 Cecioni, S. et al. (2011) Chem.–Eur. J., 17, 3252–3261.
169 Nierengarten, J.-F. et al. (2010) Chem. Commun., 46, 3860–3862.
170 Marradi, M. et al. (2010) Adv. Carbohydr. Chem. Biochem., 64, 211–290.
171 Wang, X. et al. (2011) Chem. Commun., 47, 8620–8622.
172 Kikkeri, R. et al. (2010) Angew. Chem., Int. Ed., 49, 2054–2057.
173 Robinson, A. et al. (2005) ChemBioChem, 6, 1899–1905.
174 Yang, Y. et al. (2010) Bioorg. Med. Chem., 18, 5234–5240.
175 Astronomo R. D. et al. (2010) Nat. Rev. Drug Discovery, 9, 308–324.
176 Verez-Bencomo, V. et al. (2004) Science, 305, 522–525.
177 Mager, M. D. et al (2011) Nature Chem., 3, 582−589.
178 Place, N. S. et al. (2009) Nature Mater., 8, 457−470.
179 a) Cipolla, L. et al. (2012) Smart biomaterials: the contribution of Glycoscience. In Specialist Periodical Reports-Carbohydrate Chemistry; A. P. Rauter, T. Lindhorst, Eds.; Royal Society of Chemistry: London; Vol. 38, pp. 416−445; b) Chawla, K. et al. (2012) Biomaterials, 33, 6052−6060; c) Sapsford, K. E. et al. (2013) Chem. Rev., 113, 1904−2074; d) Koepsel, J. T. et al. (2012) ChemBioChem, 13, 1717−1724; e) Slaney, A. M. et al. (2011) ACS Appl. Mater. Interfaces, 3, 1601−1612; f) Santoyo-Gonzalez, F. et al. (2009) Chem. Soc. Rev., 38, 3449−3462.
180 Parenteu-Bareil, R. et al. (2010) Materials, 3, 1863.
181 Patterson, J. et al. (2010) Mater. Today, 13, 14.
182 Piez, K.A. (1985) Collagen, in: Encyclopediaofpolymer scienceandengineering, J.I. Kroschwitz (ed), John Wiley and Sons, New York, p 699.
183 Friess, W. (1998) Eur. J. Pharm. Biopharm., 45, 113.
184 Engel, J. et al. (2005) Top.Curr. Chem., 247, 7.
185 Fields, G.B. (2010) Org. Biomol. Chem., 6, 1237.
186 Fields, G.B. et al. (1996) Biopolymers, 40, 345.
187 Puxkandl, R. et al. (2002) Philos. Trans. R. Soc. Ser. B., 357, 191.
188 Glowacki, J. et al. (2008) Biopolymers, 89, 338.
189 Lefebvre, F. et al. (1996) Biomaterials, 17, 1813.
190 Lefebvre, F. et al. (1992) Biomaterials, 13, 28.
191 Kojima, C. et al. (2009) J. Am. Chem. Soc., 131, 6052.
192 Kotch, F.W. et al. (2006) Proc. Natl. Acad. Sci. U. S. A., 103, 3028.
193 Kaufman, H.E. et al. (1994) J. Ocul. Pharmacol., 10, 17.
194 Fonseca, M.J. et al. (1996) Biochem. Biophys. Acta., 279, 259.

195 a) Masand, S. N. et al. (2012) Biomaterials, 33, 790–797; b) Sricholpech, M. et al. (2012) J. Biol. Chem., 287, 22998–23009; c) Andrés-Bergós, J. et al. (2012) Biol. Chem., 287, 33615–33628; d) Jürgensen, H. J. et al. (2011) J. Biol. Chem., 286, 32736–32748; e) Taga, Y. et al. (2013) J. Proteome Res., 12, 2225−2232.
196 Gilboa-Garber, N. (1982) Methods Enzymol., 83, 378–385.
197 Chemani, C. et al. (2009) Infect. Immun., 77, 2065–2075.
198 Hauber, H. P. et al. (2008) Int. J. Med. Sci., 5, 371–376.
199 Gustke, H. et al. (2012) Eur. J. Clin. Microbiol. Infect. Dis., 31, 207–215.
200 Imberty, A. et al. (2004) Microbes Infect., 6, 222–229.
201 Mitchell, E. et al. (2002) Nat. Struct. Biol., 9, 918–921.
202 Tielker, D. et al. (2005) Microbiology, 151, 1313–1323.
203 Bartels, K. M. et al. (2011) J. Bacteriol., 193, 1107–1113.
204 Consoli, G. M. L. et al. (2011) Tetrahedron Lett., 52, 5831–5834.
205 Morvan, F. et al. (2007) Bioconjugate Chem., 18, 1637–1643.
206 Marotte, K. et al. (2007) Org. Biomol. Chem., 5, 2953–2961.
207 Andreini, M. et al. (2010) Carbohydr. Res., 345, 1400–1407.
208 Clouet, A. et al. (2004) Angew. Chem., Int. Ed., 43, 4612–4615.
209 Maillard, N. et al. (2009) Nat. Protocols, 4, 132–142.
210 Reymond, J.-L. et al. (2012) Org. Biomol. Chem., 10, 1483–1492.
211 Johansson, E. M. V. et al. (2007) New J. Chem., 31, 1291–1299.
212 Kolomiets, E. et al. (2007) Org. Lett., 9, 1465–1468.
213 Sabin, C. et al. (2006) FEBS Lett., 580, 982–987.
214 Johansson, E. M. V. et al (2011) MedChemComm, 2, 418–420.
215 Johansson, E. M. V. et al. (2008) Chem. Biol., 15, 1249–1257.
216 Kolomiets, E. et al. (2009) ChemMedChem, 4, 562–569.
217 Berthet, N. et al. (2013) Bioconjugate Chem., 24, 1598−1611.
218 a) Kleene, R. et al. (2004) Nature Rev. Neurosci., 5, 195−208; b) Moremen, K. W. et al. (2012) Nature Rev., 13, 448−462; c) Johnson, J. L. et al. (2013) Trends Immunol., 34, 290−298; d) Hakomori, S. (2001) Adv. Exp. Med. Biol., 491, 369−402; e) Hart, G. W. et al. (2010) Cell, 143, 672−676.
219 Bishop J. R. et al. (2007) Glycobiology, 17, 23R.
220 Ohtsubo, K. et al. (2006) Cell, 126, 855.
221 Van Kooyk, Y et al. (2008) Nature Immunol., 9, 593.
222 a) Taylor, M. E. et al. (2009) Glycobiology, 19, 1155−1162; b) Sharon, N. et al. (2004) Glycobiology, 14, 53R−62R.
223 Bertozzi, C. R. et al. (2001) Science, 291, 2357−2364.
224 a) Boyd, S. E. et al. (1996) Chem. Eur. J., 2, 1115-1128; b) Ledin, P. A. et al. (2011) Chem. Eur. J., 17, 839–846.

225 a) Irure, A. et al. (2013) Biomater. Sci., 1, 658−668; b) Stevens, J. et al. (2006) Nat. Rev. Microbiol., 4, 857−864; c) de la Fuente, J. M. et al. (2006) Biochim. Biophys. Acta, 1760, 636−651; d) Pieters, R. J. (2007) Med. Res. Rev., 27, 796−816; e) Lim, Y.-b. et al. (2007) Org. Biomol. Chem., 5, 401−405; f) Kiessling, L. L. et al (2006) Angew. Chem. Int. Ed., 45, 2348−2368; g) Barnard, A. et al. (2012) Angew. Chem. Int. Ed., 51, 6572−6581.
226 a) Paez, J. I. et al. (2012) Polymers, 4, 355−395; b) Röglin, L. et al. (2011) Angew. Chem. Int. Ed., 50, 102−112.
227 Miller, E. J. (1976) Mol. Cell. Biochem., 13, 165–192.
228 Kalia, J. et al. (2008) Angew. Chem. Int. Ed., 47, 7523–7526.
229 Wojdyr, M. J. (2010) Appl. Cryst., 43, 1126–1128.
230 NIST X-ray Photoelectron Spectroscopy Database, Version 4.1. http://srdata.nist.gov/xps/
231 a) Battocchio, C. et al. (2010) Mater. Sci. Eng. B, 169, 36–42; b) Iucci, G. et al. (2007) Mater. Sci. Eng. C, 27, 1201–1206.
232 Beamson, G. et al. (1992) High Resolution XPS for Organic Polymers: The Scienta ESCA300 Database.
233 Barth, A. (2007) Biochim. Biophys. Acta, 1767, 1073-1101.
234 a) Guilbert, M. et al. (2013) Biochim. Biophys. Acta, 1830, 3525–3531; b) Natalello, A. et al. (2005) Biochem. J., 385, 511–517.
235 Šardzík, R. et al. (2010) Beilstein J. Org. Chem., 6, 699–703.
236 Duléry, V. er al. (2007) Carbohydr. Res., 342, 894–900.
237 St. Hilaire, P.M. et al. (1998) Rapid Commun. Mass Specrom., 12, 1475-1484.
238 Hudak, J.E. et al. (2011) J. Am. Chem. Soc., 133, 16127- 16135.
239 Lippert, B. (1999) Coord. Chem. Rev., 182, 263 –295.
240 Boulikas, T. et al. (2007) Cancer Ther., 5, 537 – 583.
241 a) Kelland, L. (2007) Nat. Rev. Cancer, 7, 573 –584; b) Reedijk, J. (2008) Platinum Met. Rev., 52, 2 – 11.
242 Dorr, R. T. (1996) In Platinum and Other Metal Coordination Compounds in Cancer Chemotherapy 2; Pinedo, H. M., Schornagel, J. H., Eds.; Plenum Press: New York; pp 131-154.
243 Allardyce, C. S. et al. (2001) Platinum Met. Rev., 45, 62 –69.
244 Keppler, B. K. et al. (1996) In Platinum and Other Metal Coordination Compounds in Cancer Chemotherapy 2; Pinedo, H. M., Schornagel, J. H., Eds.; Plenum Press: New York; pp 253-268.
245 Farrell, N. (1989) In Catalysis by Metal Complexes; James, B. R., van Leeuwen, P. W. N. M., Eds.; Kluwer Academic Publishers: Dordrecht, The Netherlands; Vol. 11, pp 44-46.
246 Guo, Z. et al. (1999) Angew. Chem., Int. Ed., 38, 1512-1531.
247 van Rijt, S. H. et al. (2009) Drug Discovery Today, 14, 1089 – 1097.
248 Kostova, I. (2006) Anticancer Agents Med. Chem., 6, 19–32.
249 Ott, I. (2009) Coord. Chem. Rev., 253, 1670–81.

250 Ward, J. R. (1988) Am. J. Med., 85, 39-44.
251 Mirabelli, C. K. et al. (1985) Cancer Res., 4, 32-39.
252 Puddephat, R. J. (1978) The Chemistry of Gold; Elsevier: Amsterdam.
253 Tiekink, E. R. T. (2008) Inflammopharmacology,16, 138–42.
254 Gabbiani, C. et al. (2007) Gold Bull., 40, 73–88.
255 Nobili, S. et al. (2010) Med. Chem. Res., 30, 550–80.
256 Tiekink, E. R. T. (2002) Crit. ReV. Oncol. Hematol., 42, 225-248.
257 Dhubhghail, O. M. N. et al. (1993) In Metal Complexes in Cancer Chemotherapy; Keppler, B. K., Ed.; VCH: Weinheim, Germany; pp 221-248.
258 Sadler, P. J. et al. (1994) Met.-Based Drugs, 2-3, 107-144.
259 Calamai, P. et al. (1998) Anti-Cancer Drug Des., 13, 67-80.
260 Messori, L. et al. (2000) Med. Chem., 43, 3541-3548.
261 Marcon, G. et al. (2002) Med. Chem., 45, 1672-1677.
262 Kostova, I. (2006) Curr. Med. Chem., 13, 1085 –1107.
263 Heffeter, P. et al. (2008) Drug Resist. Updates, 11, 1– 16.
264 a) Levina, A. et al. (2009) Metallomics, 1, 458 – 470; b) Antonarakis, E. S. et al. (2010) Cancer Chemother. Pharmacol., 66, 1–9.
265 Ang, W. H. et al. (2011) J. Organomet. Chem., 696, 989 –998.
266 Pacor, S. et al. (2004) J. Pharmacol. Exp. Ther., 310, 737 – 744.
267 Hartinger, C. G. et al. (2006) J. Inorg. Biochem., 100, 891 –904.
268 Alessio, E. et al. (2004) Curr. Top. Med. Chem., 4, 1525 – 1535.
269 Ramalingam, S. et al. (2008) Oncologist, 13, 5 –13.
270 Dempke, W. C. M. et al. (2010) Lung Cancer, 57, 257 – 274.
271 a) Ihde, D. C. et al. (1992) J. Med., 327, 1434 –1441; b) Bunn, P. A. Jr. (1989) Semin. Oncol., 16, 10– 21; c) Bunn, P. A. Jr. (1989) Semin. Oncol., 16, 27– 33.
272 a) Cocchietto, M. et al. (2003) Invest. New Drugs, 21, 55– 62; b) Vacca, A. et al. (2002) Br. J. Cancer, 86, 993 –998.
273 Kapitza, S. et al. (2005) J. Cancer Res. Clin. Oncol., 131, 101 –110.
274 a) Pongratz, M. et al. (2004) J. Anal. At. Spectrom., 19, 46– 51; b) Ang, W. H. et al. (2006) Eur. J. Inorg. Chem., 4003 – 4018.
275 Sava, G. et al. (2000) Int. J. Oncol., 17, 353 – 365.
276 Reisner, E. et al. (2008) Inorg. Chim. Acta, 361, 1569 –1583.
277 Wang, X. et al. (2007) Anti-Cancer Agents Med. Chem., 7, 19– 34.
278 Borch, R. F. et al. (1988) in Platinum and Other Metal Coordination Compounds in Cancer Chemotherapy (Ed.: M. Nicolini), Martinus Nijoff Publishing, Boston, pp. 216 –281.
279 Kabanov, A. V. et al. (1995) Bioconjug. Chem., 6, 639–643.
280 Savic, R. et al. (2003) Science, 300, 615–618.

281 Kwon, G. S. (2003) Crit. Rev. Ther. Drug Carrier Syst., 20, 357–403.
282 Torchilin, V. P. et al. (2003) Proc. Natl. Acad. Sci. U S A, 100, 6039–6044.
283 Trentin, D. et al. (2005) J. Control. Release, 102, 263–275.
284Missirlis, D. et al. (2005) Langmuir, 21, 2605–2613.
285 Kabanov, A. V. et al. (2004) Curr. Pharm. Des., 10, 1355–1363.
286 Salem, A. K. et al. (2003) Nat. Mater., 2, 668–671.
287 Nayak, S. et al. (2005) Angew. Chem. Int. Ed. Engl., 44, 7686–7708.
288 Croy, S. R. et al. (2006) Curr. Pharm. Des., 12, 4669–4684.
289 Escorcia, F. E. et al. (2007) Nanomed., 2, 805–815.
290 Hall, J. B. et al. (2007) Nanomed, 2, 789–803.
291 Suri, S. S. et al. (2007) J. Occup. Med. Toxicol., 2, 16.
292 Kabanov, A. et al. (1995) Macromolecules, 28, 2303–2314.
293 Kozlov, M. et al. (2000) Macromolecules, 33, 3305–3313.
294 Kabanov, A. V. et al. (2003) Adv. Drug. Deliv. Rev., 55, 151–164.
295 Spitzenberger, T. J. et al. (2007) J. Cereb. Blood Flow Metab., 27, 1033–1042.
296 Batrakova, E. et al. (1998) Pharm. Res., 15, 1525–1532.
297 Batrakova, E. et al. (1998) Pharm. Res., 15, 850–855.
298 Kwon, S. H. et al. (2007) Arch. Pharm. Res., 30, 1138–1143.
299 Alakhov, V. et al. (1999) Colloids Surf. B: Biointerfaces, 16, 113–134.
300 Kabanov, A. et al. (2002) Crit. Rev. Ther. Drug Carrier Syst., 19, 1–72.
301 Krupka, T. M. et al. (2007) Exp. Biol. Med. (Maywood), 232, 950–957.
302 Kabanov, A. V. et al. (1989) FEBS Lett., 258, 343–345.
303 Saski, W. et al. (1995) J. Pharm. Sci., 54, 277–280.
304 Saski, W. et al. (1965) J. Pharm. Sci., 54, 71–74.
305 Croy, S. R. et al. (2004) J. Control. Release, 95, 161–171.
306 Croy, S. R. et al. (2005) J. Pharm. Sci., 94, 2345–2354.
307 Valle, J. W. et al. (2004) J. Clin. Oncol.; ASCO Annual Meeting Proceedings (Post-Meeting Edition), p. 4195.
308 Alakhov, V. et al. (1996) Bioconjug. Chem., 7, 209–216.
309 Venne, A. et al. (1996) Cancer Res., 56, 3626–3629.
310 Batrakova, E. V. et al. (1996) Br. J. Cancer, 74, 1545–1552.
311 Krupka, T. M. et al. (2006) Invest. Radiol., 41, 890–897.
312 Kabanov, A. V. et al. (2005) J. Control. Release, 101, 259–271.
313 Kabanov, A. et al. (2005) Adv. Genet., 53PA, 231–261.
314 Kabanov, A. V. (2006) Adv. Drug Deliv. Rev., 58, 1597–1621.
315 Kabanov, A. et al. (2002) Adv. Drug Deliv. Rev., 54, 759–779.
316 Kabanov, A. et al. (2002) J. Control. Release, 82, 189–212.

317 Batrakova, E. et al. (2001) J. Pharmacol. Exp. Ther., 296, 551–557.
318 Batrakova, E. et al. (2001) J. Pharmacol. Exp. Ther., 299, 483–493.
319 Szakacs, G. et al. (2006) Nat. Rev. Drug Discov., 5, 219–234.
320 Regev, R. et al. (2007) Febs J., 274, 6204–6214.
321 Batrakova, E. V. et al. (2003) Pharm. Res., 20, 1581–1590.
322 Yamagata, T. et al. (2007) J. Control. Release, 124, 1–5.
323 Yamagata, T. et al. (2007) Drug Metab. Dispos., 35, 1142–1148.
324 Minko, T. et al. (2005) J. Control. Release, 105, 269–278.
325 Batrakova, E. et al. (1999) Pharm. Res., 16, 1373–1379.
326 Miller, D. et al. (1997) Bioconjugate Chem., 8, 649–657.
327 Batrakova, E. V. et al. (2001) Br. J. Cancer, 85, 1987–1997.
328 Batrakova, E. V. et al. (2006) Mol. Pharm., 3, 113–123.
329 Medina, R. A. et al. (2002) Biol. Res., 35, 9-26.
330 Renaudet, O. et al. (2001) Tetrahedron Letters, 42, 7575–7578.
331 Brunner, H. et al. (2005) Z. Anorg. Allg. Chem., 631, 2555–2562.
332 Bradford, M. M. (1976) Anal. Biochem., 72, 248.
333 Bernfeld, P. (1995) Method. Enzymol., 1, 149-158.
334 Mitchell, E. P. et al. (2005) Proteins: Struct. Funct. Bioinf., 58, 735−746.
335 Taraballi, F. et al. (2013) J. Colloid Interface Sci., 394, 590–597.
336 Kurimoto, A. et al. (2001) J. Biotechnol., 86, 1–8.
337 Swift, P. et al. (1983) in Practical Surface Analysis by Auger and X-ray Photoelectron Spectroscopy,(Eds: D. Briggs and M. P. Seah), J. Wiley & Sons, Chichester, UK, Ch. 2 and appendix 3.
338 Shirley, D. A. (1972) Phys. Rev. B., 5, 4709-4714.
339 Burger, K. et al. (1974) Inorg. Chim. Acta, 11, 25.
340 Ihre, H. et al. (1998) Macromolecules, 31, 4061–4068.